

# Magnetic and Electric Field Meters Developed for the U.S. Department of Energy

H. Kirkham  
A. Johnston

January 1988

Prepared for

Office of Energy Storage and Distribution  
United States Department of Energy

Through an agreement with

National Aeronautics and  
Space Administration

by

Jet Propulsion Laboratory  
California Institute of Technology  
Pasadena, California

Prepared by the Jet Propulsion Laboratory, California Institute of Technology,  
for the U.S. Department of Energy through an agreement with the National  
Aeronautics and Space Administration.

This report was prepared as an account of work sponsored by an agency of the  
United States Government. Neither the United States Government nor any agency  
thereof, nor any of their employees, makes any warranty, express or implied, or  
assumes any legal liability or responsibility for the accuracy, completeness,  
or usefulness of any information, apparatus, product, or process disclosed, or  
represents that its use would not infringe privately owned rights.

Reference herein to any specific commercial product, process, or service by  
trade name, trademark, manufacturer, or otherwise, does not necessarily  
constitute or imply its endorsement, recommendation, or favoring by the United  
States Government or any agency thereof.

This publication reports on work performed under NASA Task RE-152, Amendment  
203 and sponsored through DOE/NASA Interagency Agreement No. DE-AI01-79ET 29372  
(Mod. A009).

## ABSTRACT

This report describes work done at the Jet Propulsion Laboratory for the Office of Energy Storage and Distribution of the U.S. Department of Energy on the measurement of power line fields. A magnetic field meter is discussed that uses fiber optics to couple a small measuring probe to a remote readout device. The use of fiber optics minimizes electric field perturbation due to the presence of the probe and provides electrical isolation for the probe, so that it could be used in a high field or high voltage environment. Power to operate the sensor electronics is transferred via an optical fiber, and converted to electrical form by a small photodiode array. The fundamental, the second and third harmonics of the field are filtered and separately measured, as well as the broadband rms level of the field. The design of the meter is described in detail and data from laboratory tests are presented. The report also describes work done to improve the performance of a dc electric field meter. Measurements made of a high voltage dc bushing in a Swedish laboratory, using the improved meter, are discussed. DC electric fields are measured with synchronous detection to provide field magnitude data in two component directions.

## ACKNOWLEDGEMENTS

The field meters described in this report could not have been built without the contributions of a large number of people. First among these is Ken Klein, Director of the Office of Energy Storage and Distribution of the United States Department of Energy, whose financial support began the whole effort, and whose moral support over the last few years helped us maintain momentum.

The authors would also like to acknowledge the help of Shannon Jackson at JPL. Shannon played a major role in building the hardware described here, and in optimizing the designs in a number of ways. He was also responsible for performing the tests that characterized the various instruments. Also at JPL, Eddie Hsu continued to be an asset to the project. His skill with computers translated into both circuit board designs and a number of useful programs. Heather Friend deserves thanks for her contributions to this report, not the least of which are the elegant circuit diagrams to be found throughout. Finally, the authors thank Charlotte Marsh and Ermine van der Wyk, our editors at JPL, for their careful and prompt reviews of the manuscript.

## PREFACE

This report describes the work performed at the Jet Propulsion Laboratory on the measurement of electric and magnetic fields near high voltage transmission lines. The work was sponsored by the Office of Energy Storage and Distribution of the United States Department of Energy.

Throughout the 1970s and early 1980s there was continuing public interest in the possible biological issues associated with the transmission of electrical power. Responding to this, the Department of Energy, as well as some electric utilities, sponsored research to investigate the effects (if any) that electric fields had on animals, both large and small. At first, the biological work concentrated on ac fields, since ac lines are far more common than dc ones. However, some investigations were carried out into dc field effects, and the measurement of dc fields became necessary.

DC electric field measurement is also of interest in the development of equipment for handling high voltage dc power. An example of this application is discussed in the section on insulator tests at ASEA, Appendix A.

My group at the Jet Propulsion Laboratory was charged with the application of the technology of fiber optics to the problems of power system measurements. Our first development was the free-body dc electric field meter, which made possible the measurement of the electric field due to a dc power line in air, close to a distorting object. This allowed dc fields to be treated experimentally for the first time in the same way as ac fields. Some improvements to that field meter, and some new experimental results obtained with it are described in this report.

Most of this report deals with a meter built to measure ac magnetic fields. The instrument was developed partly in response to the findings of the New York State Power Lines Project, a \$5 million study undertaken to research and review the literature of possible health hazards of power lines, which created renewed interest in magnetic fields when it was published in 1987.

There are two problems faced by this kind of study: it is difficult to establish a causal connection from what are often barely significant statistics; and it is hard to reconcile epidemiological evidence with laboratory work that seems to show that fields much higher than those associated with power lines have no biological effects. In spite of these difficulties, one effect that the authors of the 153-page report believe warrants further investigation is a possible link between leukemia and power line magnetic fields. Only two of four studies of this topic showed any connection at all, and they were from the same geographical area.

Nevertheless, this finding will stimulate further experimental investigations, and a very small, electrically isolated measurement probe, like the one described here, might be useful.

HAROLD KIRKHAM

*Pasadena, California  
January, 1988*

PAGE \_\_\_\_\_

# CONTENTS

ABSTRACT . . . . .	iii
ACKNOWLEDGEMENTS . . . . .	iv
PREFACE . . . . .	v
PART ONE. EXECUTIVE SUMMARY	
Introduction . . . . .	1
Magnetic Field Meter System . . . . .	2
Modifications to Electric Field Meters . . . . .	5
Visit to Sweden November 10-17, 1987 . . . . .	7
Concluding Remarks . . . . .	10
PART TWO. MAGNETIC AND ELECTRIC FIELD METERS DEVELOPED FOR THE U.S. DEPARTMENT OF ENERGY	
1. INTRODUCTION: FROM ELECTRIC TO MAGNETIC FIELDS . . . . .	1-1
1.1. The Measurement of Electric Fields in the Transmission Line Environment . . . . .	1-1
1.2. Design Approach, Magnetic Field Meter . . . . .	1-2
1.3. Organization of Report . . . . .	1-4
2. MAGNETIC FIELD METER SYSTEM . . . . .	2-1
2.1. Design Approach . . . . .	2-1
2.2. Design Details . . . . .	2-3
2.2.1. Probe . . . . .	2-3
2.2.2. Laser Power Supply . . . . .	2-5
2.2.3. Data Board . . . . .	2-8
2.2.4. Measurement Board . . . . .	2-8
2.2.5. Mechanical Construction . . . . .	2-12
2.3. Calibration . . . . .	2-14
2.3.1. Calibration from First Principles . . . . .	2-14
2.3.2. Experimental Calibration . . . . .	2-15
2.3.3. Uncertainties in Calibration . . . . .	2-15
2.4. Experimental Results . . . . .	2-16
2.4.1. Frequency Response . . . . .	2-16
2.4.1.1. Probe Frequency Response . . . . .	2-16
2.4.1.2. Link Frequency Response . . . . .	2-17
2.4.1.3. Choice of Phase Detector . . . . .	2-18
2.4.1.4. Broadband Filter Frequency Response . . . . .	2-20
2.4.1.5. Overall Frequency Response . . . . .	2-20
2.4.1.6. Single-Frequency Bandpass Filters . . . . .	2-21
2.4.2. Photodiode Array . . . . .	2-23
2.4.3. Light Sensitivity of Hybrid . . . . .	2-23
2.4.4. Dynamic Range . . . . .	2-24
2.4.4.1. Probe Saturation . . . . .	2-24
2.4.4.2. Noise Floor . . . . .	2-25
2.4.4.3. Experimental Results . . . . .	2-25
2.4.5. Calibration Accuracy . . . . .	2-26
2.4.6. Example of Field Measurement . . . . .	2-27

3.	MODIFICATIONS TO ELECTRIC FIELD METERS . . . . .	3-1
3.1.	AC Field Meter . . . . .	3-1
3.1.1.	Synchronous Detector . . . . .	3-1
3.2.	DC Field Meter . . . . .	3-3
3.2.1.	Data Channel . . . . .	3-3
3.2.2.	Synchronous Detector . . . . .	3-3
3.3.	Considerations of Probe Shape . . . . .	3-6
3.4.	Suggestions for Future Work . . . . .	3-8
4.	CONCLUSIONS . . . . .	4-1
4.1.	DC Field Meter . . . . .	4-1
4.1.1.	Significance of the DC Field Meter . . . . .	4-2
4.2.	AC Field Meter . . . . .	4-3
4.3.	Magnetic Field Meter . . . . .	4-5
4.4.	Field Meter Receiver . . . . .	4-7
4.5.	Summary of Field Meter Results . . . . .	4-8
4.6.	Concluding Remarks . . . . .	4-9
APPENDIX A.	REPORT ON VISIT TO ASEA, SWEDEN . . . . .	A-1
A.1.	Background Information . . . . .	A-1
A.2.	Initial Tests in Västerås . . . . .	A-4
A.3.	Tests at Ludvika . . . . .	A-7
A.4.	The Effect of Incomplete Wetting of the Bushing . . . . .	A-12
A.5.	Further Tests in Västerås . . . . .	A-14
A.6.	Suggestions For Future Work . . . . .	A-16
A.7.	Conclusions . . . . .	A-17
APPENDIX B.	THE HELMHOLTZ COIL . . . . .	B-1
APPENDIX C.	GRAPHICAL PRESENTATION PROGRAM . . . . .	C-1
C.1.	Overview . . . . .	C-1
C.2.	Program Description . . . . .	C-2
C.2.1.	TRANS.PAS . . . . .	C-2
C.2.2.	INTER.PAS . . . . .	C-2
C.2.3.	GR.FOR . . . . .	C-3
C.3.	Data File Format . . . . .	C-4
C.4.	Graphics Routines . . . . .	C-5
C.5.	Program Listings . . . . .	C-6
C.5.1.	TRANS.PAS Listing . . . . .	C-6
C.5.2.	INTER.PAS Listing . . . . .	C-13
C.5.3.	GR.FOR Listing . . . . .	C-25
APPENDIX D.	REFERENCES . . . . .	D-1

# LIST OF FIGURES

1.	Circuit of hybrid IC in magnetic probe . . . . .	2
2.	Block diagram of receiver system . . . . .	3
3.	Completed probe and the receiver . . . . .	4
4.	60-Hz magnetic field around hair dryer . . . . .	5
5.	Cutaway views of dc field meter probe . . . . .	6
6.	Field meter probes, before and after modification . . . . .	7
7.	Bushing inside high voltage hall . . . . .	8
8.	Composite of bushing test results . . . . .	9
2-1.	Comparison of electric and magnetic field meter systems . . . . .	2-2
2-2.	Circuit of hybrid IC in magnetic probe . . . . .	2-3
2-3.	Parts layout, magnetic field hybrid . . . . .	2-5
2-4.	Photograph of hybrid IC for magnetic field probe . . . . .	2-6
2-5.	Laser power supply circuit . . . . .	2-7
2-6.	Magnetic field meter data board . . . . .	2-9
2-7.	Block diagram of measurement board . . . . .	2-10
2-8.	State variable filter circuit . . . . .	2-10
2-9.	RMS detector circuit . . . . .	2-11
2-10.	Cross-section through magnetic field meter probe . . . . .	2-12
2-11.	Photodiode array, mounted on ceramic substrate . . . . .	2-13
2-12.	Magnetic field meter probe . . . . .	2-13
2-13.	Probe frequency response . . . . .	2-16
2-14.	Probe deviation from ideal integrator . . . . .	2-17
2-15.	Link frequency response . . . . .	2-18
2-16.	Broadband filter characteristic . . . . .	2-20
2-17.	Overall system response . . . . .	2-21
2-18.	Filter characteristic, 60-Hz filter . . . . .	2-21
2-19.	Filter characteristic, 120-Hz filter . . . . .	2-22
2-20.	Filter characteristic, 180-Hz filter . . . . .	2-22
2-21.	Diode array characteristic . . . . .	2-23
2-22.	Performance of laser/array combination . . . . .	2-24
2-23.	Dynamic range of field meter . . . . .	2-26
2-24.	60-Hz magnetic field around hair dryer . . . . .	2-27
2-25.	120-Hz magnetic field around hair dryer . . . . .	2-28
2-26.	180-Hz magnetic field around hair dryer . . . . .	2-29
2-27.	Wideband magnetic field around hair dryer . . . . .	2-29
3-1.	Synchronous detector circuit, revised . . . . .	3-2
3-2.	DC field meter, data channel . . . . .	3-4
3-3.	DC synchronous detector board . . . . .	3-5
3-4.	Exploded view of probes . . . . .	3-7
3-5.	Cutaway isometric views of probe . . . . .	3-9
3-6.	Photograph of assembled probes . . . . .	3-10
3-7.	Modified position pulse system . . . . .	3-11
4-1.	DC electric field meter probe . . . . .	4-4
4-2.	AC electric field meter probe . . . . .	4-5
4-3.	AC magnetic field meter probe . . . . .	4-7
4-4.	Multi-purpose field meter receiver . . . . .	4-8

A-1.	Cross sections through wall penetration . . . . .	A-2
A-2.	Grading cylinders inside bushing . . . . .	A-3
A-3.	Equipotential lines of electric field along graded bushing . . . . .	A-4
A-4.	Results obtained with DOE/JPL meter . . . . .	A-5
A-5.	Results obtained with DOE/JPL meter . . . . .	A-6
A-6.	Calculated field near toroidal electrode (ACE output) . . . . .	A-6
A-7.	Linearity tests of DOE/JPL meter . . . . .	A-7
A-8.	Ludvika, and the high voltage test facility of the ASEA company . . . . .	A-8
A-9.	Test arrangement inside high voltage hall . . . . .	A-9
A-10.	Electric field scan, dry bushing . . . . .	A-10
A-11.	Scan of de-energized bushing . . . . .	A-11
A-12.	Data at 500 kV, showing field meter failure . . . . .	A-11
A-13.	Discharge of de-energized bushing . . . . .	A-12
A-14.	Composite of results from wet and dry tests . . . . .	A-13
A-15.	Calibration curve for high-field saturation . . . . .	A-16
B-1.	Field due to a circular current-carrying wire . . . . .	B-1
B-2.	Two circular current-carrying coils . . . . .	B-2
C-1.	Flowchart of graphical presentation routines . . . . .	C-1

PART ONE

EXECUTIVE SUMMARY

PAGE \_\_\_\_\_ INTERSECTIONALLY BLANK

## EXECUTIVE SUMMARY

### Introduction

Between 1984 and the present, the Communications and Control for Electric Power Systems Project at the Jet Propulsion Laboratory has been developing for its sponsor, the U.S. Department of Energy, a series of novel field meters. The first of these instruments was a device capable of measuring the electric field due to a direct current power line, without any reference to the ground. For the first time a truly isolated measurement of such an electric field was possible.

Following this, a version of the electric field meter was made to measure the 60 Hz ac fields due to the more commonplace ac power lines. This device too, was electrically isolated. It was powered optically, rather than by batteries. The small size of the optical power diode array, combined with the use of hybrid electronics, helped to create one of the smallest active-probe field meter systems ever constructed.

In this report, the last in the series of field meters is described. This instrument measures the magnetic field due to alternating current power lines, and was developed because of renewed interest in the possible biological effects of magnetic fields.

It is worthwhile to say a few words to put the issue of magnetic fields into perspective. The recently renewed interest in power line electric and magnetic fields has been caused largely by one report in particular. Biological Effects of Power Line Fields, the final report of the Scientific Advisory Panel of the New York State Power Lines Project, suggested that further investigation of a possible link between leukemia and power line magnetic fields was warranted. This report, of a series of studies undertaken to research and review the literature of possible health hazards of power lines, was published in 1987. While most of the studies in the report found no connection between power line fields and biological effects, two of the four studies investigating a link between magnetic fields and cancer did find a possible link of statistical significance. It happens that these two studies were from the same geographical area.

There are two problems faced by this kind of study. First, it is difficult to establish a causal connection from such barely significant statistics. Second, it is very hard to reconcile epidemiological evidence of this kind with laboratory work that has been undertaken over the last two decades which appears to show no biological effects from fields that are even stronger than those experienced near real power lines.

Nevertheless, if further investigations are to be carried out, methods of making measurements of the fields will be needed, and there may be applications where an electrically isolated measurement of the magnetic field is justified. Such a measurement can be made using the meter described in this report.

During 1987 some improvements were also made to the existing electric field meters designed and built at the Jet Propulsion Laboratory. These too are described in this report.

## Magnetic Field Meter System

The magnetic field meter system was made by modifying the electric field meter system built earlier. In modifying the electric field meter to measure magnetic fields, it was desired to retain the features of small size, spherical shape and the capability of calibration from first principles. Another goal in the design was to retain, as far as possible, the electronics that had already been developed for the electric field meter.

Two principal differences may be noted between the measurement of electric field and the measurement of magnetic field. First, the electric field can be measured with an electrometer amplifier with zero input impedance, whereas the magnetic field can be measured best with a coil of wire going into an amplifier whose input impedance is infinitely high. Second, the waveform of the electric field is a rather pure 60 Hz, whereas the waveform of the magnetic field can be expected to be rich in harmonics. The first of these two factors means a slight redesign in the probe. The second factor means that the signal must be handled differently in the receiver.

Figure 1 shows the circuit of the hybrid integrated circuit in the probe of the magnetic meter.

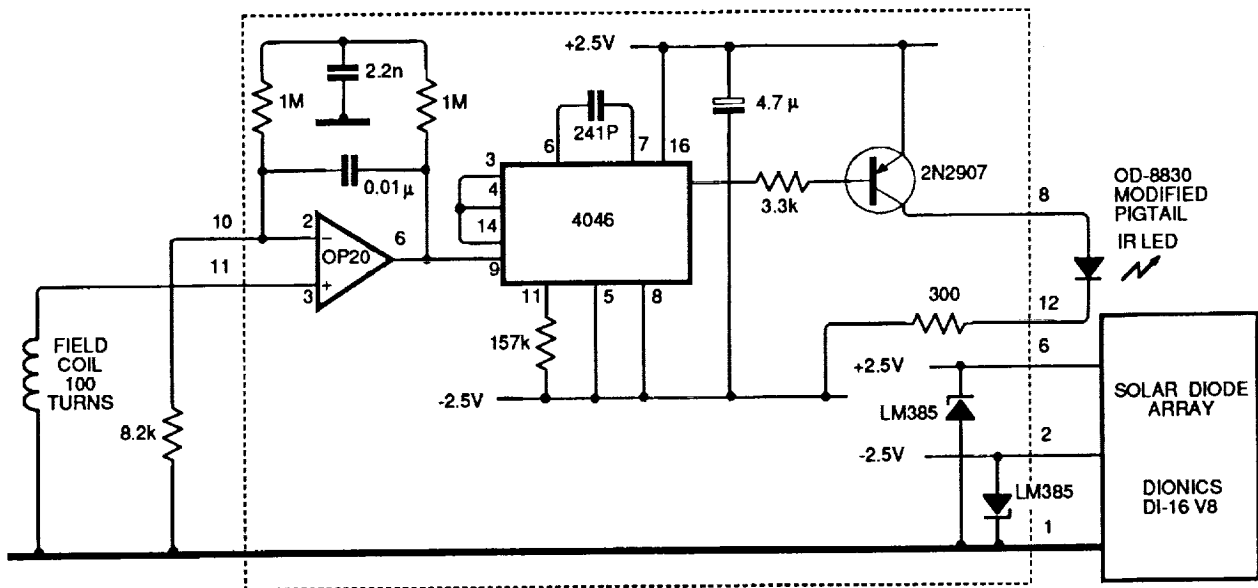


Figure 1. Circuit of hybrid IC in magnetic probe

A pickup coil is connected to the non-inverting input of the first stage. This ensures that the coil sees a high impedance, and this makes possible a calibration from first principles. This amplifier has an integrating characteristic, which compensates for the derivative relationship between the voltage induced in the coil and the flux through it.

No range switch is built into the probe. The system was designed principally to measure fields of the magnitudes of interest in biological work, from about

0.1  $\mu\text{T}$  up to about 1 mT. Higher fields may be experienced in the neighborhood of electrical equipment; their measurement with our system would require a less sensitive probe.

The output of the first stage modulates a voltage controlled oscillator. A train of very short optical pulses at the frequency of this oscillator is used to bring the information representing the magnetic field to the receiver.

Power for the probe is furnished from a laser, and converted to electrical form in the probe by a small photodiode array. While in previous years we have developed our own photodiode array for this purpose, a range of commercially available arrays was brought to our attention during 1987. These were made in silicon with dielectric isolation. Continued problems with producing our own gallium arsenide photodiode arrays made use of the commercial silicon components the obvious choice. In spite of the use of theoretically poorer material, their efficiency has been found to be comparable with our own devices. The manufacturer is Dionics Inc. of Westbury, New York.

In the receiver, the modulating waveform is reconstructed in a phase locked loop, and filters are used to separate various components of the waveform. The fundamental, second, and third harmonics are separately measured, as well as the broadband energy in the signal. The block diagram (Figure 2) shows how this is accomplished.

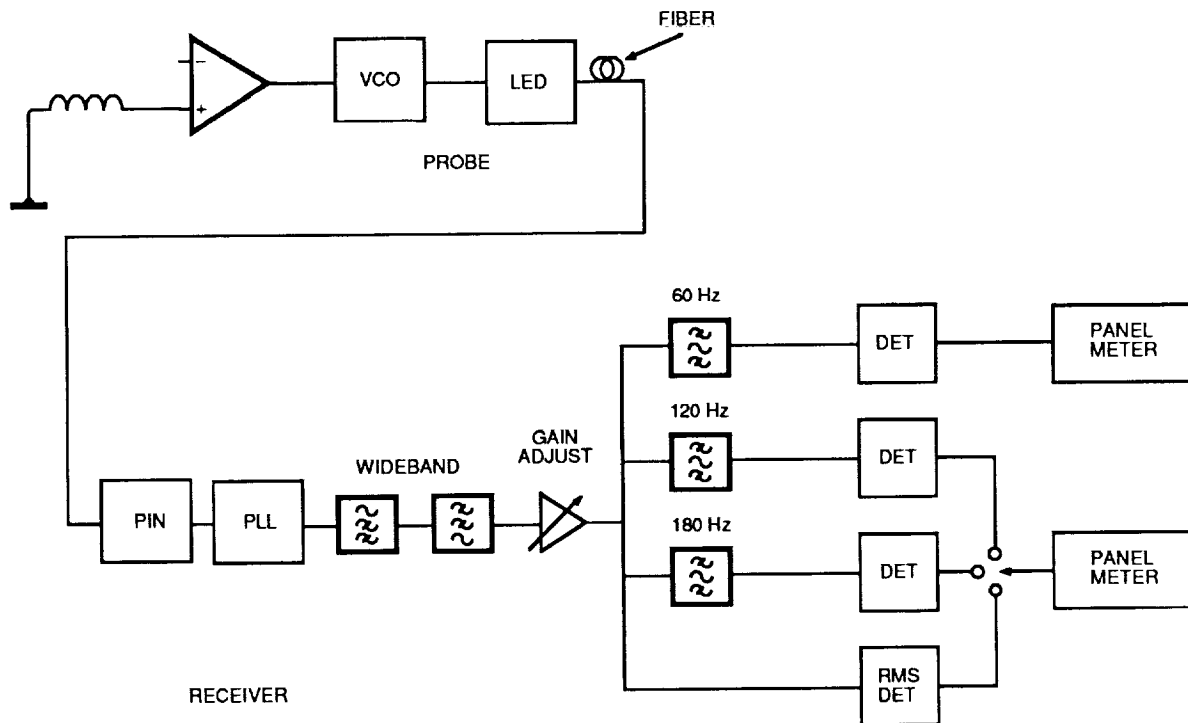


Figure 2. Block diagram of receiver system

Figure 3 shows the completed probe and the receiver. The probe is 2 cm in diameter (the same as the earlier electric field meter probe) and contained within a spun-brass housing. Two optical fibers connect the probe to the receiver. One brings optical power from the laser in the receiver to energize the probe electronics, the other returns the data. The fibers are contained inside the fiberglass support pole.

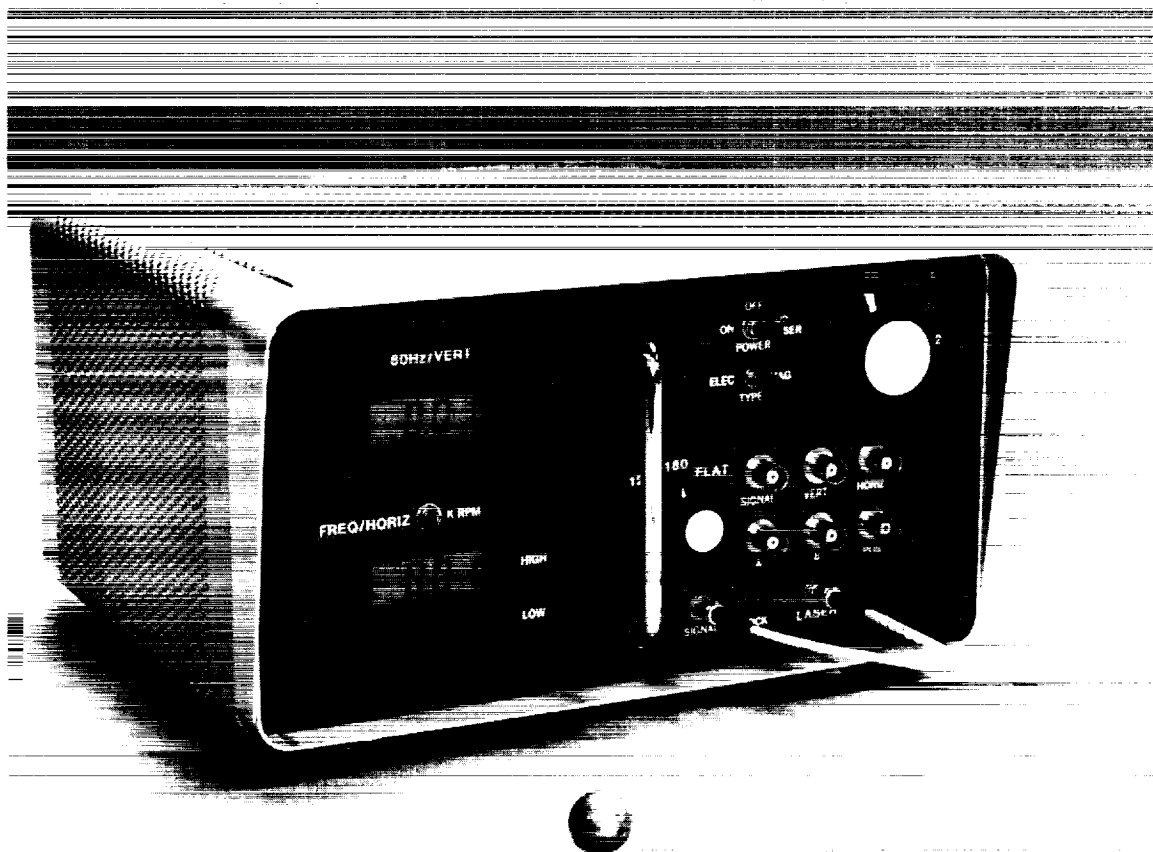


Figure 3. Completed probe and the receiver

For demonstration purposes measurements were made, using this system, of the magnetic field near a small hair dryer. In the past we have presented measurements of this kind in the form of lines representing the vectors of the field. On this occasion it was thought to be more useful to show the field as contours of equal field magnitude. In order to develop such a contour map from the measured data, a computer program was written. The output of this program, showing the contours of the fundamental-frequency magnetic field is shown in Figure 4.

It may be estimated from the figure that the peak field near the hair dryer was in the order of  $20 \mu\text{T}$  (200 mG). Slightly higher values were observed at 120 Hz, in a circular shape, evidently centered on the motor.

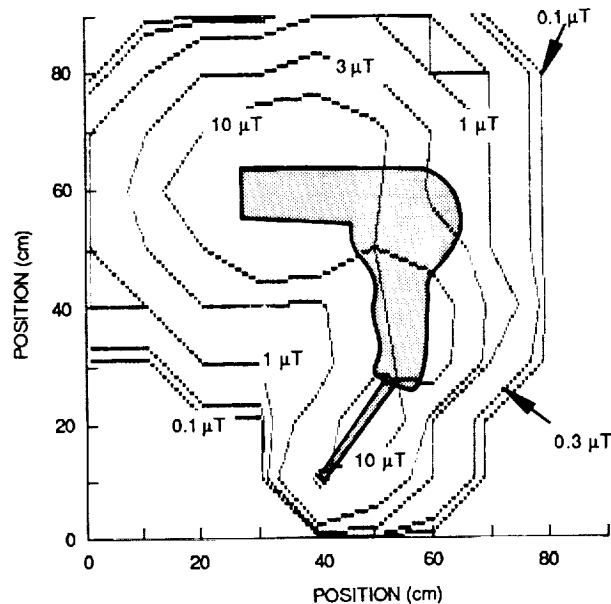


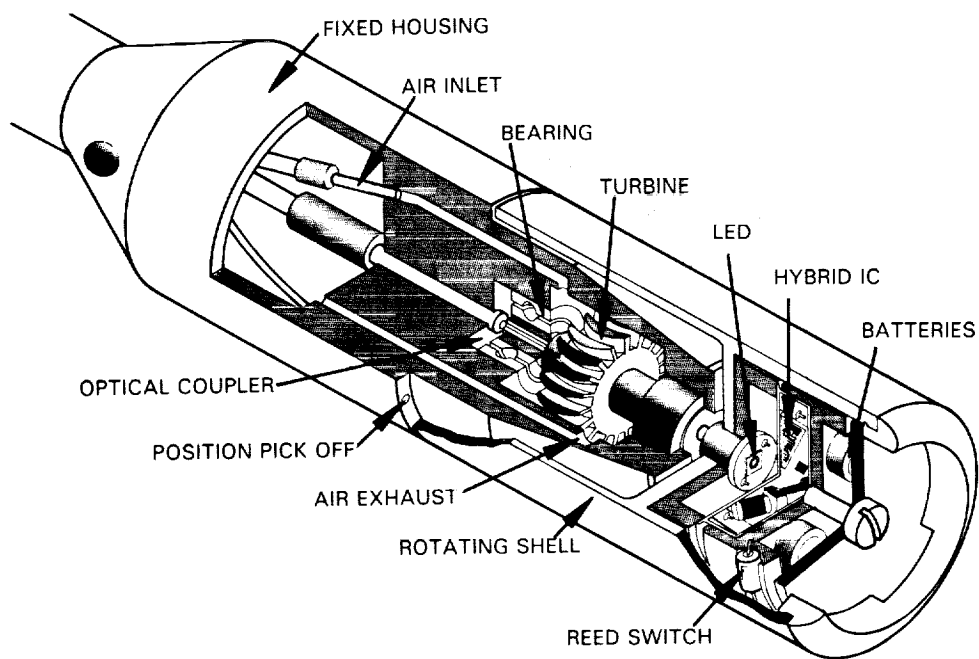
Figure 4. 60-Hz magnetic field around hair dryer

#### Modifications to Electric Field Meters

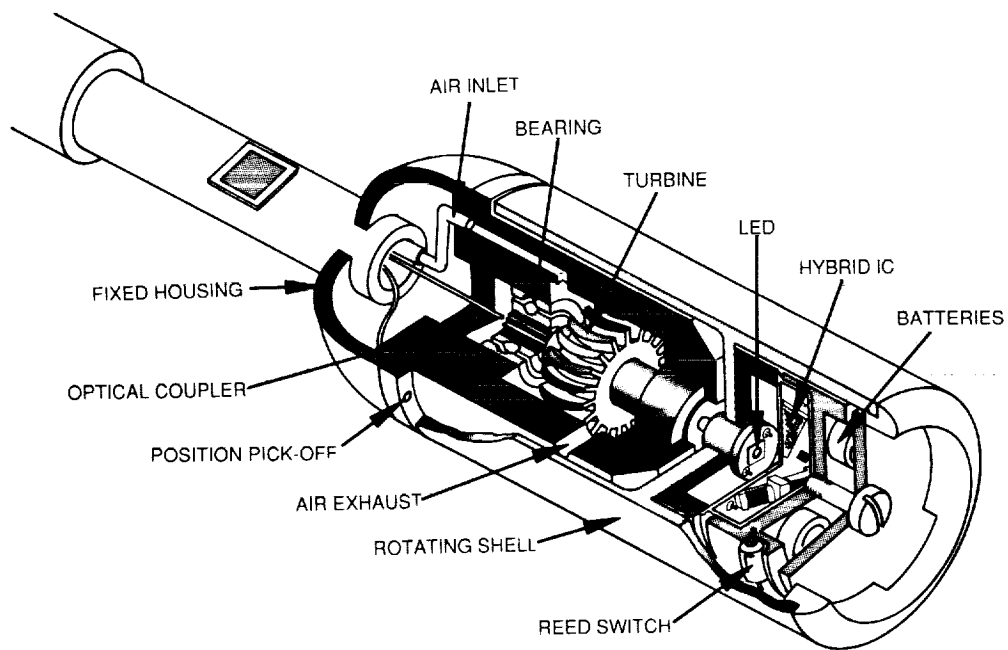
While most of our efforts during 1987 were on the development of the magnetic field meter, we did spend some time improving both the dc electric field meter and its ac counterpart. The improvements to the ac meter consisted of relatively minor modifications to the circuit boards in the receiver, and will not be discussed here. However, the dc meter probe was improved considerably by a redesign of its mechanical structure.

The changes were made in order to reduce the length of the probe. In the original version, the probe was 10 cm long, more than half of which was merely support for the rotating measurement section. This support area, which housed the air supply for the turbine driving the probe and contained two fiber couplers, was completely redesigned. The rotating section, which contained the hybrid integrated circuit that measured the field, and its battery power supply, was not changed.

Figure 5 shows cut-away views of the original field meter probe and the revised version. The simplification in construction is evident. As a result of the improvements in the support for the rotating part of the field meter, the overall length of the device was reduced from 10 cm to 5 cm, see Figure 6.



(a) Before modification



(b) After shortening the housing

Figure 5. Cutaway views of dc field meter probe

ORIGINAL PAGE IS  
OF POOR QUALITY

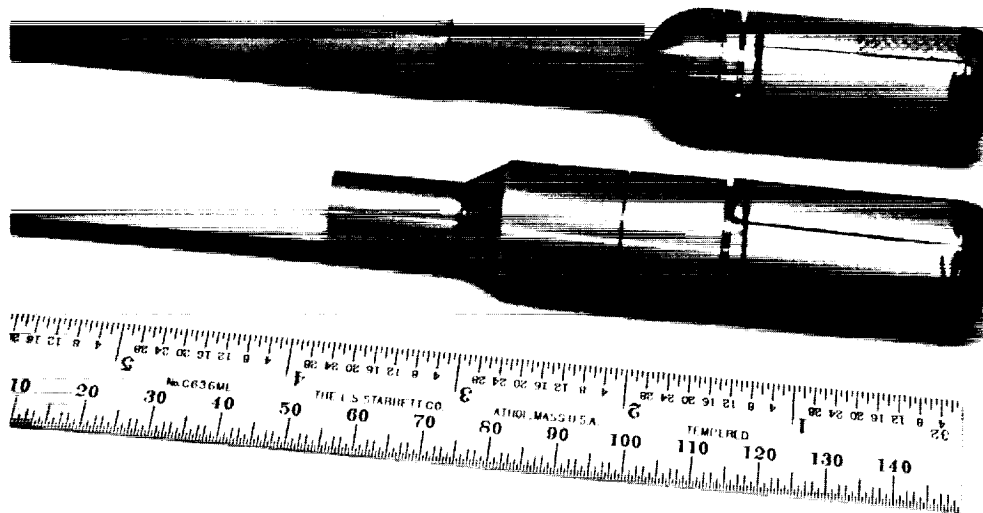


Figure 6. Field meter probes, before and after modification

Visit to Sweden November 10-17, 1987

In an attempt to understand the mechanism of anomalous flashovers which have occurred on ac/dc bushings from time to time, the Swedish manufacturer ASEA scheduled a series of tests of a high voltage bushing under dry and artificial rain conditions in their high voltage hall in Ludvika, Sweden. Because of the work done by the Communications and Control Project on the measurement of dc electric fields, task manager Kirkham was invited to participate in these tests. In November 1987 two prototypes of the revised dc electric field meter were taken to Sweden to measure the electric field in the vicinity of a test bushing.

The tests performed at ASEA were of a bushing similar to the ones used on operating  $\pm 600$  kV (dc) systems. Altogether this device is 15 m long, approximately 9 m of which are on the outside of the converter station. The overall configuration of the bushing and the test arrangement is shown in Figure 7.

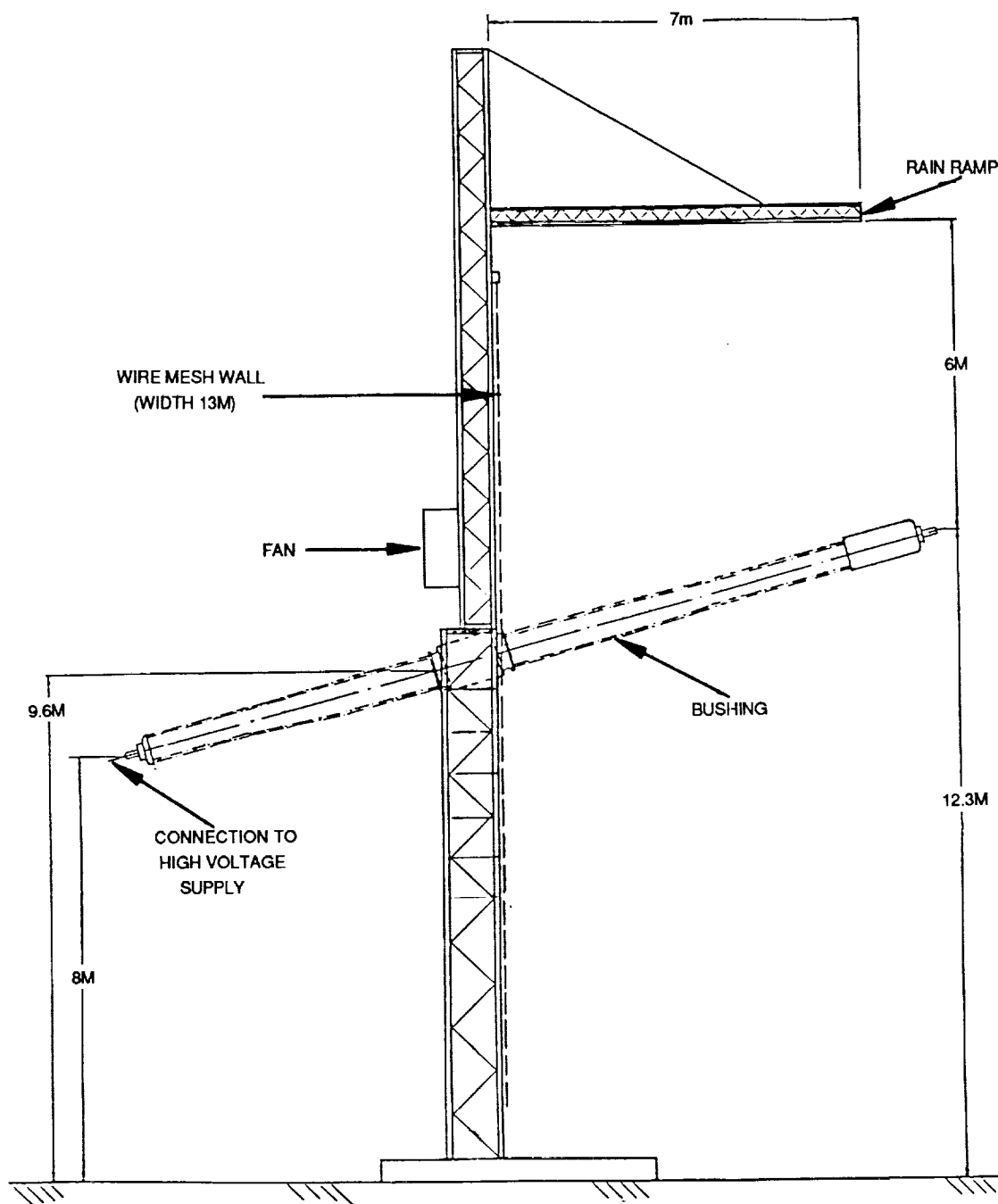


Figure 7. Bushing inside high voltage hall

The bushing was inserted through an artificial wire mesh wall, 13 m wide and 22 m high. The bushing was mounted in the lower part of this wall, at an angle of 15° to the horizontal such that the lowest part of the bushing was 8 m above the ground. The high voltage supply was attached to this low point by means of a small wire.

A rain making apparatus 7 m long was positioned 6 m above the highest part of the bushing. A large fan was arranged in the wall just above the bushing to

blow air away from the wall to simulate wind eddies around the corner of the roof of an ac/dc converter building.

The field meter probe was installed near the center of the bushing just outside the wall penetration. The probe was supported on an apparatus developed by ASEA to transport the probe along the axis of the bushing from a location close to the wall out to a distance of about 2 m. The probe was installed with its axis horizontal, parallel to the wall and normal to the axis of the bushing, 50 cm from the outside of the rainsheds on the bushing.

A series of tests was performed with the bushing completely dry and partially wetted, at voltages between 300 kV and 800 kV. During some of these tests the positioning apparatus failed, and on other occasions the part of the field meter system which is supposed to resolve the total field into two component directions failed. As a result, the data that were gathered do not form a complete set. Nevertheless, the composite of the results from wet and dry tests show that the field close to the wall is intensified by up to a factor of 5 when only the outer portion of the bushing is wetted. This is shown in Figure 8.

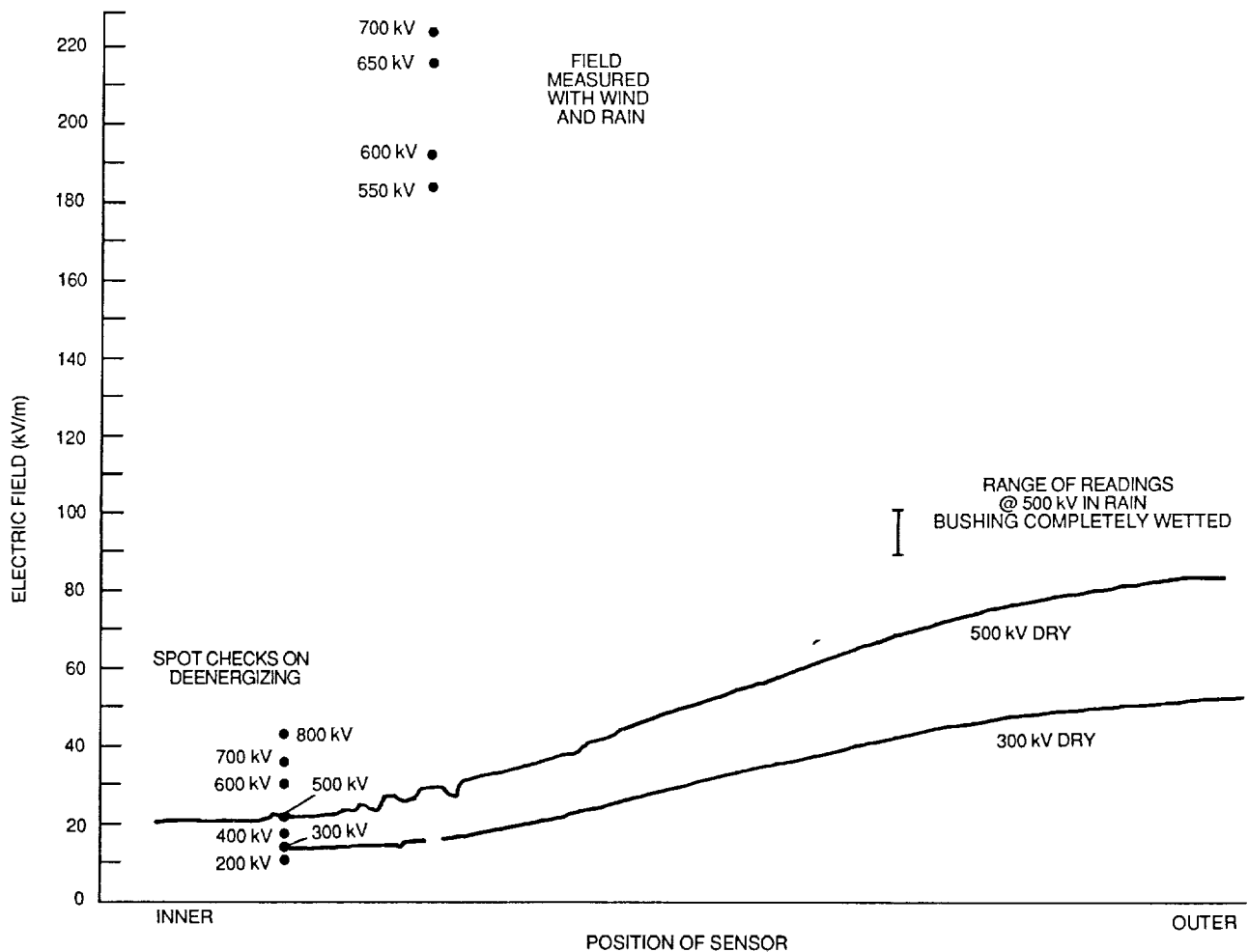


Figure 8. Composite of bushing test results

Although there were problems with the equipment, it is clear from Figure 8 that the data are self-consistent. The spot checks made when the positioner was broken, shown as round dots on the diagram, agree well with the scans made at 300 and 500 kV when it was functioning. Also, the integral of the observed axial field under dry conditions seems consistent with the voltage applied to the center conductor of the bushing.

The increase in field intensity in the vicinity of the wall is in broad agreement with a theoretical model proposed by ASEA for the anomalous flash-overs. While the data presented are not conclusive, they are certainly highly suggestive that the rain and wind in combination cause a voltage distribution along the surface of the insulator which is far different than that which would be obtained under completely dry or completely wet conditions.

#### Concluding Remarks

Early in 1988, the emphasis of the fiber optics work being done by the Communications and Control Project changed. The development of hardware to measure electric and magnetic fields in air came to an end, and work on distribution automation applications of fiber optics started. Apart from some loose ends that need tidying up, we shall not be addressing the problems that have so fascinated us for the last few years.

It has certainly been an interesting area of investigation. The instrument that started it all, the space-potential dc electric field meter, was intended to put the measurement of dc electric fields in air on an equal footing with ac electric fields. In the end, it seems that our prototypes have actually advanced the state of the art a little: the probe of our dc electric field meter is smaller and has a wider dynamic range than its ac counterparts. The last prototype meter has a probe length of 5 cm, and a diameter of only 2 cm. Measurements made with this meter have already led to an increased understanding of the problems of one kind of dc insulation system.

This device was adapted to the problem of making a measurement of ac electric fields. The resulting field meter retains the advantages of small size, and large dynamic range. In fact, since there is no need for the ac meter probe to rotate, it is smaller than the dc probe from which it was developed. The probe is spherical, only 2 cm (3/4 in) in diameter.

With the publication of the final report of the Scientific Advisory Panel of the New York State Power Lines Project, and the concomitant renewed interest in power line fields, the technology was extended to the measurement of magnetic fields. The probe of the DOE/JPL magnetic field meter is 2 cm in diameter, and is electrically isolated from the receiver. Because the field can be expected to contain harmonics, the meter cannot take advantage of synchronous detection. Instead, it uses filters to measure the fundamental and harmonic components of the field separately. Nevertheless, the dynamic range of the meter is only slightly less than that of its electric field counterparts.

Finally, the development of these meters has demonstrated that an electrically isolated probe, simple enough to be made as a hybrid IC on a very small substrate, and using so little power that it can be optically powered, can be used as the sending end of a moderately accurate fm data link.

PART TWO

MAGNETIC AND ELECTRIC FIELD METERS  
DEVELOPED FOR THE U.S. DEPARTMENT OF ENERGY

Page 1 of 1

## 1. INTRODUCTION: FROM ELECTRIC TO MAGNETIC FIELDS

### 1.1. The Measurement of Electric Fields in the Transmission Line Environment

For many years, the magnitude of the electric fields near power transmission lines has been of interest to researchers interested in biological effects. To gain insight into any possible interactions between power line electric fields and biological subjects, researchers want to map the electric field in air around the biological subject using probes that do not affect that field. The acquisition of data describing the way that the power line field is altered by the presence of the biological specimen, and a variety of other measurements, has led to the development of mathematical models of the specimen. Some of these models are quite refined, and it is possible, in some cases, to predict the currents induced in various parts of the body by exposure to a 60 cycle power line field (Deno, 1977; Kaune, 1986).

In the case of ac lines, the development of these models, and their verification by experimental measurements, is a very straightforward subject. Probes to measure ac electric fields in air are relatively straightforward—if somewhat large—devices, and their use is fairly widespread. However, until the development of the free-body dc field meter reported by this group in recent years, the measurement of dc fields away from the surface of the ground could not, in practical terms, be accomplished.<sup>1</sup>

This means that any model of the biological subject, as far as the dc electric field was concerned, was unverifiable until recently. Such models had to be based on a somewhat imperfect analogy with ac models.

The availability of a free body dc electric field meter, therefore, represents a milestone in the investigation of electric field effects. The use of this probe should lead to improved models of biological subjects exposed to dc electric fields.

There are some effects that make it abundantly clear to even a casual observer that dc and ac fields interact differently with biological specimens. For example, only under a dc line does one's hair stand on end. We shall see later in Appendix A that even an object as apparently simple as a ceramic insulator behaves in a fundamentally different manner under dc excitation than under ac excitation, and that the experimental measurement of the electric fields near such an insulator can furnish information of value to the designer of power system hardware. Theoretical models of such insulation systems derived from ac models simply do not work.

The technology developed for the dc electric field meter included a miniaturized hybrid electronic circuit, optical transmission of the data from the probe to a receiver across a rotating joint, and synchronous detection of the data at the receiver, in order to create a system with a large dynamic range and an

---

<sup>1</sup> All of the earlier instruments designed to measure dc electric fields were themselves grounded, and had to be used in the plane of the ground, or in such a way that the distortion they caused outside the ground plane could be compensated for. This was only possible in the case of a field that had previously been determined to be uniform, and which was not distorted by the presence of a biological subject.

electrically isolated probe. It seemed a natural extension of this work to create an improved ac electric field meter, and this was done in 1986.

The DOE/JPL ac electric field meter embodied no new principles to make the measurement, but its implementation resulted in a device with a very much smaller probe than any of its counterparts, and a much wider dynamic range than anything else that was available. An important factor in the small size of the probe of the ac field meter was the method of powering it: it was energized by laser light from a fiber. The photodiode array that converted the incoming infrared radiation into electrical form was much smaller than any battery. Synchronous detection was largely responsible for the large dynamic range, which in the case of the ac field meter approached 100 dB. Since this method of detection was common to both the ac and dc electric field meters, an attempt was made during the development of this metering system to combine as much of the circuitry as possible and produce a receiver capable of operating with either the ac or the dc field probe.

## 1.2. Design Approach, Magnetic Field Meter

The shape of most field meters used in power line measurements has been governed by the need to include the readout device in the probe (see, for example, Deno and Zaffanella, 1975). Accordingly, the side of the probe facing the operator was flat, and the probe overall was box-shaped. Since the DOE/JPL ac field meter had a readout at the remote end of a fiber optic cable, the shape of its probe could be chosen arbitrarily. A spherical shape has two advantages: its sensitivity can be calculated from theoretical considerations, and it results in minimum disturbance of the field. Therefore, this shape was chosen for the ac field meter probe. Details of this and other spherical probes are given by Kirkham, Johnston, Jackson and Sheu, (1987).

During 1987, a report on the biological effects of power line fields was published by the New York State Power Lines Project (Ahlbom, Albert, Fraser-Smith, Grodzinsky, Marron, Martin, Persinger, Shelanski and Wolpow, 1987). The report suggested the possibility of a link between the magnetic fields associated with the transmission, distribution or use of electric power and health effects, particularly an increased rate of certain kinds of cancer.

The linkage between the power line as cause and the increased cancer as effect was far from established and certainly not understood. Nevertheless, the report aroused considerable interest in the topic of magnetic field effects. Further investigations must be made into the possible relationship between power line magnetic fields and health effects, and certainly part of these investigations must be experimental. This provided the motivation for our involvement in the topic of magnetic field measurement.

There are several differences between the magnetic fields associated with power lines and the electric fields associated with them. First, the electric fields are relatively constant in time, because most power transmission and distribution systems are operated at a constant voltage. This contrasts with the situation of the magnetic field, which fluctuates on a moment-to-moment basis and with a daily cycle, because it is determined by the load on the power system. Similar observations apply to both transmission and distribution circuits.

The changing nature of the magnetic field means that the "exposure" of a biological subject cannot simply be determined by multiplying the exposure time by the value of the field established by a spot measurement. Some kind of integrating meter which could furnish, for example, an amplitude probability distribution (APD) of the exposure to the field would seem to be a reasonable way to bound the problem of knowing the exposure. However, an exposure meter such as this is simply a probe (of the kind already developed for the measurement of electric fields) connected to some kind of classifying data acquisition system.

Consequently, it was thought worthwhile to adapt the ac electric field probe and measuring system to the problem of measuring magnetic fields. This proposed modification would then result in the availability for experimental investigations of an electrically-isolated magnetic field probe.

A second important difference between electric and magnetic fields is in the dynamic range of the measurement. Electric fields greater than about 1 MV/m (10 kV/cm) cannot be measured because breakdown of the air around the probe itself will be a limit. At the other extreme, electric fields smaller than about 10 volts per meter are not of interest in an outdoor environment because typical fair weather ambients are in the range of 100 V/m. Therefore, equipment with a voltage dynamic range of 100 dB can be used to cover the entire span of interest for power line electric fields. The equipment developed by JPL for the U.S. Department of Energy has shown that it is possible to make measurements over this kind of dynamic range without making any changes in the probe itself. In our instrument, the necessary range switching is accomplished entirely within the receiver unit.

A similar dynamic range is required of the magnetic field meter for use in biological studies. The magnetic field near a household appliance, for example, can approach 1 mT (milliTesla: 1 milliTesla = 10 Gauss). The peak field under a high voltage transmission circuit could be in the order of 70  $\mu$ T and the ambient 60-Hz background (in the remote countryside?) is probably about 10 nT, superimposed on the 30  $\mu$ T steady-state Earth's field. To cover a useful range, a dynamic range of the same order as the electric field meter would seem to be indicated. It would seem that a single probe of the kind developed for the measurement of electric fields can furnish the required dynamic range. However, magnetic fields can cover a much wider range of values. Should fields higher than a few mT be present, for example, near machinery, it may be necessary to de-sensitize the probe.

A third distinction between electric and magnetic fields is in the spectral purity of the field. The ac electric field is predominantly 60 Hz (in the U.S.) and the distortion of that field is limited to a very few percent. Distortion of the voltage waveform corresponds to distortion of the 60 cycle source, which is normally very difficult because the power system generators are designed for constant voltage operation, and the power system has a rather low impedance. In some cases, the limit on voltage distortion is a statutory one, but in most cases, the power system is strong enough to prevent more than a few percent total harmonic distortion appearing on the voltage.

The same cannot be said for the magnetic field. Current is drawn by loads that contain iron, and the nonlinearity of the magnetization curve of the iron

causes the current waveform to be rich in harmonics, predominantly the third harmonic. Harmonics are also caused by switching devices, such as speed controllers for small electric motors, and light dimmers. These can cause second and higher order harmonics extending into the RF region. In terms of their energy content, the predominant distortion is the third harmonic caused by iron in transformers and motors. To be most useful, a magnetic field measuring system must be capable of furnishing some information about the spectrum of the magnetic field, or at least about its low-order harmonics.

The dc magnetic field of the earth typically has a magnitude of  $30 \mu\text{T}$ , a value comparable with that at the edge of the right-of-way of high voltage lines. Since this pre-existing field is so large, and since HVdc lines are so few in number and produce the same kind of field as the naturally occurring earth's field, there seemed little to be gained from our developing a dc version of the magnetic field meter. In any case, there are a number of magnetometers that can make measurements of fields of this size, available for use in a variety of applications.

### 1.3. Organization of Report

Section 2 of this report describes the development of a magnetic field meter system based on the work done earlier for the measurement of electric fields. As a result of this work, we have now demonstrated that an integrated field measuring system with one receiver can be made that can work with probes for the measurement of electric fields due to ac or dc power lines, and magnetic fields due to ac power lines.

Section 3 covers changes that were made recently in the electric field meters. The probe of the dc field meter was made smaller, and its design was considerably simplified in 1987. The electronics of the receiver were also modified, as were the electronics of the receiver for the ac electric field meter.

Section 4 summarizes the work done over the last several years on the development of field meters at JPL. Since this report is the last document in a series of publications on the topic, it was thought that a historical review of the work would be interesting.

At the end of 1987 some tests were made using the dc electric field meter with the new probe design in the proximity of a high voltage dc bushing. The results of these measurements are presented in Appendix A.

Appendix B gives the derivation of the equations of the Helmholtz arrangement of calibration coils for magnetic fields.

Appendix C describes the computer program used to present measured field data in the form of contour maps.

Appendix D contains the References for the complete document.

## 2. MAGNETIC FIELD METER SYSTEM

### 2.1. Design Approach

It was recognized early in the design of the magnetic field meter system that there would be advantages to retaining as much of the heritage of the ac electric field meter system as possible. The magnetic field probe would be electrically isolated from the receiver and display sections, capable of furnishing information about magnetic fields over a wide dynamic range (at least 100 nT to 1 mT) without the need to approach the probe. This system could then be used in applications where electrical isolation was important, or as a spot check device in ordinary magnetic field measurements; or the receiver system could be connected to a computer for exposure measurements.

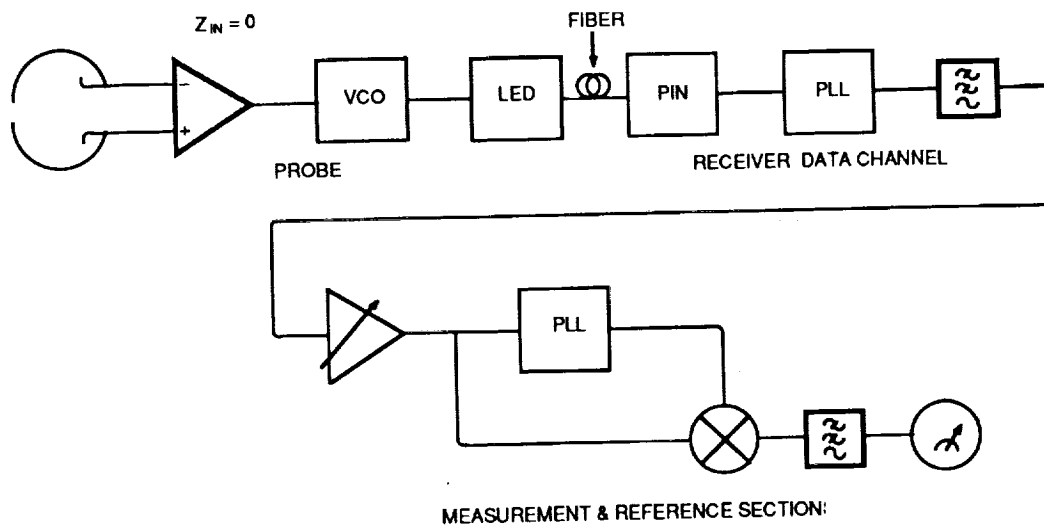
It was desired to retain two features in particular of the ac electric field meter; its small size, and its capability for calibration from first principles. If the magnetic field were measured by determining the open-circuit voltage induced by the fluctuating field in an accurately measured coil of wire, then calibration from first principles should again be possible. However, the first stage of the probe electronics of the electric field meter was configured as an electrometer amplifier, with zero input impedance. To measure the open circuit voltage in a coil of wire, an infinite input impedance would be required. This meant a redesign of the electronics in the probe.

Much of the electronics in the receiver could be retained without change, since the function of a good deal of this electronics was simply to reconstruct the waveform of the modulating signal in the probe. On the other hand, the presence of harmonics in the waveform meant that difficulty could be anticipated if synchronous detection were retained. Therefore, some experiments were conducted using the already-built ac electric field meter system to ascertain the viability of filtering rather than synchronous detection. Figure 2-1 compares the measurement system employed in the electric field meter and that developed for the magnetic field meter.

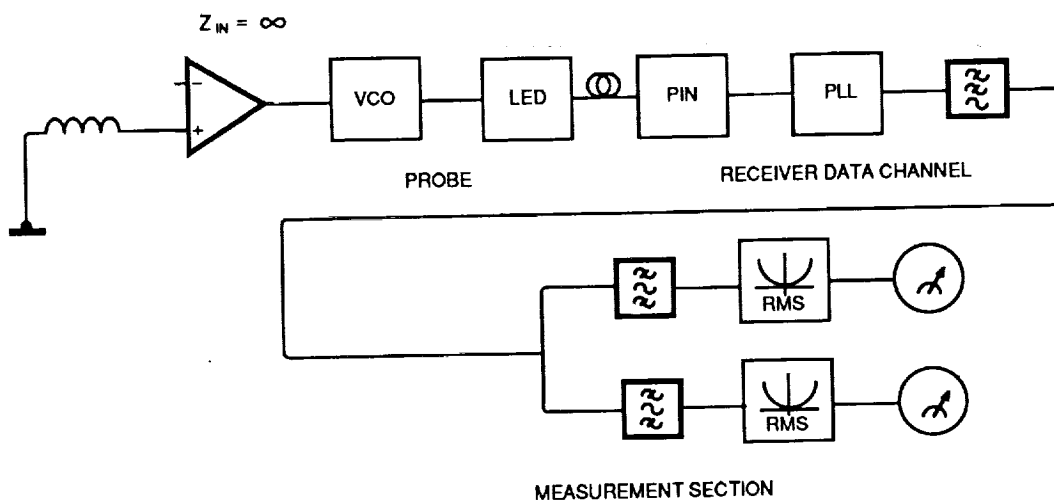
In the electric field meter, the induced charge modulates a VCO, and after transmission of the information by optical means to the receiver, the modulating waveform is reconstructed by a phase locked loop, in what has been termed the receiver data channel. The signal is then passed to the measurement section which, since synchronous detection is used, includes a second phase locked loop to reconstruct a reference signal for switching in the synchronous detector. The measurement section has gain adjustable over four orders of magnitude.

In the magnetic field meter, an input voltage modulates a VCO just as the input charge did in the electric field version. The receiver data channel reconstructs this modulating waveform.

However, since synchronous detection cannot conveniently be used to give the harmonic content of a highly distorted waveform, a different scheme is used and separate rms detectors indicate the amplitude of the fundamental, the second and third harmonic (which is often the predominant distorting frequency) and the broadband energy separately. Our goal was to measure the field including harmonic distortion up to 1 kHz.



(a) Electric field meter system



(b) Magnetic field meter system

Figure 2-1. Comparison of electric and magnetic field meter systems

Both the electric and magnetic versions of the system have probes which are powered from the receiver by optical means.

In view of the similarity of the two metering systems, it was decided to make separate circuit board modules to carry out the various functions. Clearly, each probe could also be considered a module. By designing separate receiver data channels and measurement sections for the electric and magnetic meters, a series of circuit boards were built which, when plugged into the appropriate card cage in the receiver, could configure it to measure ac electric or magnetic fields, or dc electric fields.

The next section describes in detail the design of these modules for the magnetic field meter.

## 2.2. Design Details

The modularization of the field meter system involved redesign of the circuit boards for the electric field meters (both ac and dc) as well as the design of a new system for ac magnetic fields. In addition, of course, a new probe had to be designed for the magnetic field meter. We will begin our description with the probe for the magnetic meter and continue with the description of the various other modules.

### 2.2.1. Probe

The hybrid integrated circuit for the magnetic field meter measurement probe differs from its predecessors in two ways. First, the electric field meter system required an electrometer amplifier as a first stage, with zero input impedance, whereas the magnetic field meter required an infinite input impedance if calibration from first principles was to be possible. Second, since this meter was not part of a rotating system, mechanical balance was not an important consideration in the layout of the components on the hybrid substrate. Figure 2-2 shows the circuit diagram of the hybrid.

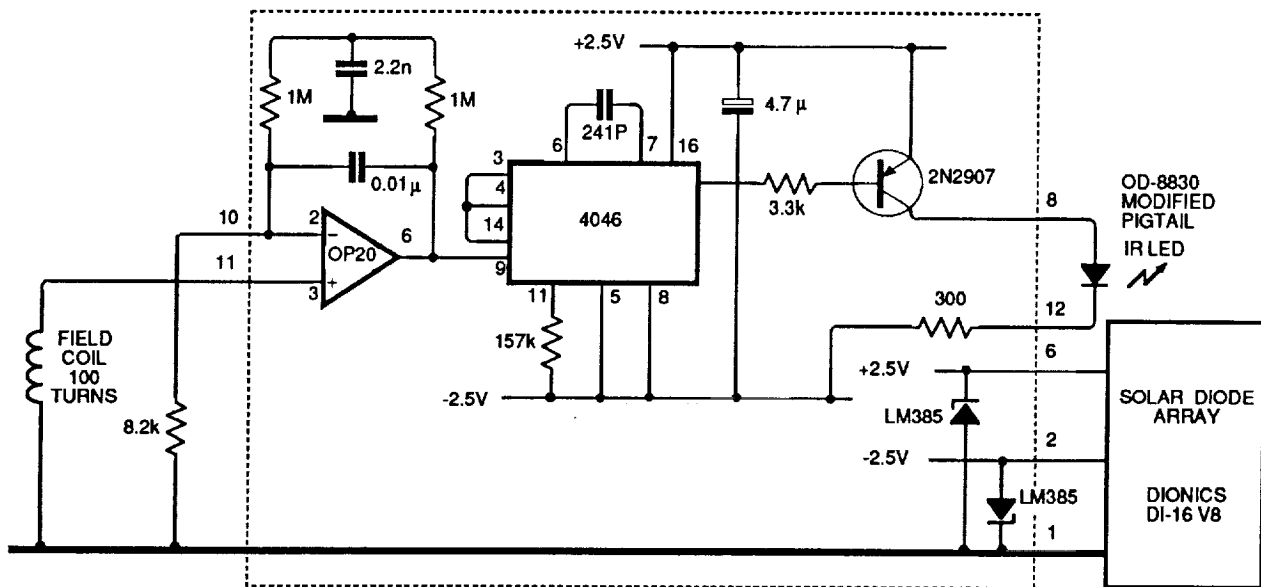


Figure 2-2. Circuit of hybrid IC in magnetic probe

The pickup coil is connected to the noninverting input of the first stage operation amplifier. This ensures that the source will not be loaded: the input impedance of an amplifier in this configuration is very high. The amplifier is arranged to have an integrating characteristic to compensate for the fact that the induced voltage is proportional to the rate of change of the

magnetic field. Consequently, the output of the first amplifier is a voltage replica of the field to which the coil is exposed.<sup>2</sup>

There is no range switch on the probe. Although simple switches were tried during the development of the probe<sup>3</sup>, the non-inverting integrator design did not lend itself to gain changes of much above 10:1, a scarcely worthwhile increase in dynamic range. The number of turns in the pickup coil, in combination with the gain of the first stage, sets the sensitivity of the instrument.

The first stage signal then modulates the voltage controlled oscillator (VCO) in a way exactly analogous with our earlier electric field meters. Short pulses are generated in the phase-locked loop chip, amplified by the light emitting diode driver stage, and coupled from the LED (which is not part of the hybrid circuit) into the optical fiber for communication to the receiver. The center frequency of the VCO is approximately the same as the VCO in the ac electric field meter, namely 10 kHz.

One improvement in the design of this hybrid was the inclusion on the hybrid substrate of the voltage regulator diodes. These serve to stabilize the power supply voltage for the circuitry on the hybrid at  $\pm 2.5$  volts. Note that no dropper resistors are included for these diodes. The photodiode arrays driving these circuits have sufficient internal resistance, and the current handling capability of the regulator diodes is not exceeded<sup>4</sup>.

Figure 2-3 shows the layout of the components on the magnetic field sensor probe. One difference between the layout of this hybrid and those used in the electric field meter probes is that the more massive components are no longer located near the center of the hybrid for the purposes of mechanical balance.

---

<sup>2</sup> It would have been very easy to arrange for the first stage to have a flat frequency response, so that the output of the first stage would represent the voltage induced by the field to which the coil was exposed. Indeed, it seems that there is at least one magnetic field meter available on the market that has this characteristic (Leeper, 1987). However, such a characteristic would provide the overall meter with essentially a rising output with frequency, and would unjustifiably emphasize the harmonics in the field. We could see little point in choosing to emphasize these harmonics, and it was our opinion that the rising characteristic which came about because of the derivative nature of the induced voltage was an accident of physics and not to be regarded in any way as a desirable feature of an instrument which purported to measure magnetic field. Consequently, the output of the first stage is a replica of the field to which the coil is exposed, and contains fundamental and harmonics in the same proportion as the magnetic field.

<sup>3</sup> One such switch was a very simple mechanical device. A screw was inserted through the shell of the probe and grounded the resistor which controls the gain of the first stage. This causes the gain of the stage to increase. However, when this approach was used to change the gain of the stage by 100:1, the frequency response of the integrator was far from ideal at the low gain setting. A revised probe design, using an FET follower input stage and an inverting-mode integrator, could be combined with such a range switch to provide an additional 40- or even 60-dB dynamic range. This switch design is shown in Figure 2-10.

<sup>4</sup> During 1987, we discovered a range of commercially available diode arrays. These were made in silicon, with dielectric isolation. Continued problems with producing our own photodiode arrays made use of these components the obvious choice. Because their design has been optimized, the efficiency is comparable to our earlier gallium arsenide arrays. The manufacturer is DIONICS Inc, of Westbury NY.

ORIGINAL PAGE IS  
OF POOR QUALITY

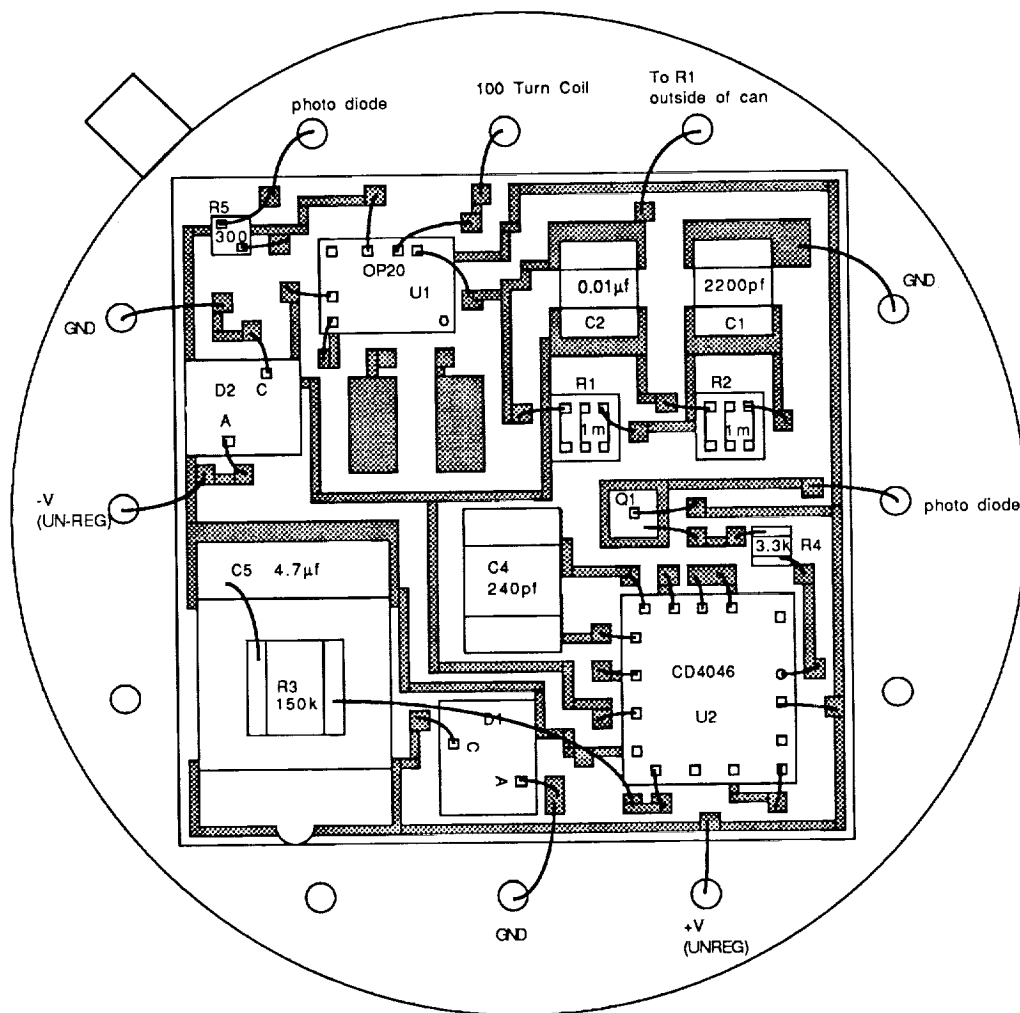


Figure 2-3. Parts layout, magnetic field hybrid

An additional feature of this hybrid is that the header to which the ceramic substrate is attached is not made of the conventional material. That material is magnetic: usually the header is made of steel and the pinouts are Kovar, another magnetic material. Since the presence of material with a high permeability would certainly distort the field that we were trying to measure, special nonmagnetic headers (made of fiberglass) and pinouts were fabricated for this application. Figure 2-4 is a photograph of the completed hybrid IC.

#### 2.2.2. Laser Power Supply

The laser power supply serves to generate the optical energy which is used to power the probe. The opportunity to improve the efficiency of this process was presented by the need to redesign the circuit board as a separate module.

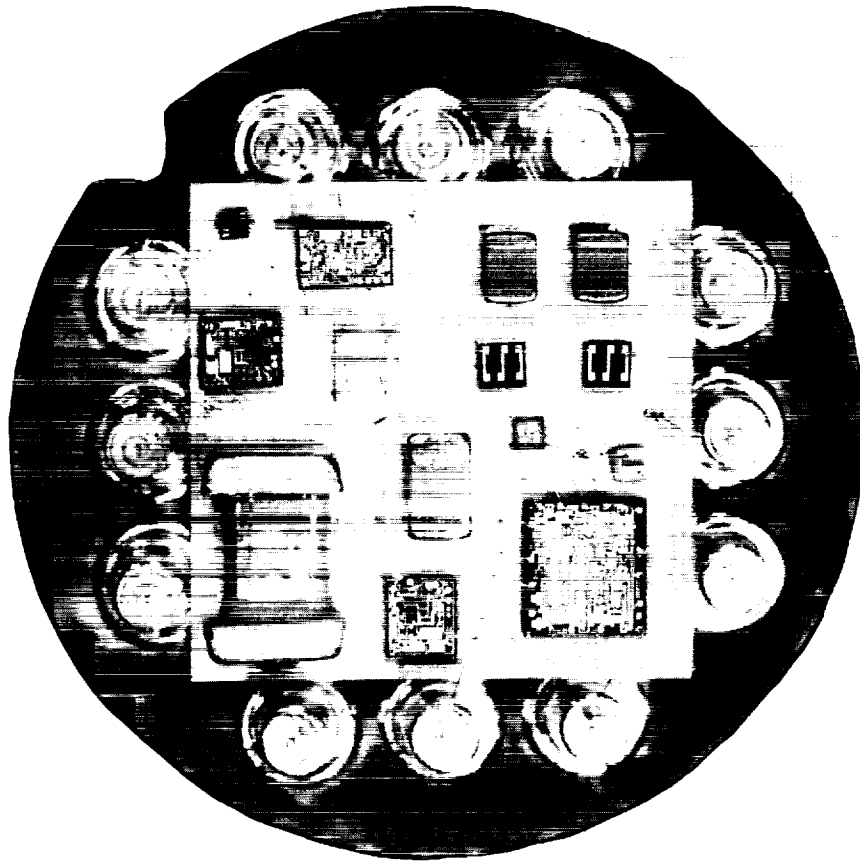


Figure 2-4. Photograph of hybrid IC for magnetic field probe

By abandoning the simplicity of the three-terminal regulator and returning to the more complex approach of an LM723 integrated circuit, we have been able to decrease the forward voltage drop in the regulator circuit considerably. The new power supply design, which uses an external pass transistor attached to the IC regulator, can operate stably on batteries (or power supplies) as low as about 8 volts, and has the additional safety feature of being regulated both in voltage and current modes.

Because the multistriple lasers which we use to energize the probe are known to be sensitive to transients in their supply current, we did retain the slow-start concept as a "last resort" regulator prior to the lasers themselves. In an attempt to make the circuit operate most efficiently, and with least forward voltage drop, a germanium slow-start transistor has been used in the new design.

Figure 2-5 shows the schematic of the new laser power supply.

[illegible]

2-7

### 2.2.3. Data Board

The optical pulses from the probe are reconverted back to electrical form by a PIN diode receiver. A phase-locked loop circuit reconstructs the modulating waveform. The circuit which accomplishes this, and possibly a moderate degree of filtering of that signal, is designated the data channel. It has now been constructed as a separate module. The module used in the prototype can be switched between the electric and magnetic field probes. Its circuit diagram is shown in Figure 2-6.

In the earlier electric field version, the reconstructed signal was filtered by a state variable filter with a two-pole low pass characteristic and a cut-off frequency of 500 Hz, before being passed to a pair of gain-adjusting potentiometers. This filter is replaced in the magnetic meter by the multi-pole filter used to measure wideband (up to 1 kHz) energy. The gain adjusting potentiometers allow the subsequent amplifier to have the appropriate gains for both electric and magnetic field probes over its four switch positions, each of which represents an order of magnitude difference in gain.

The data board is equipped with its own regulating power supplies and also contains the tracking power supplies (see Kirkham *et al.*, 1987) which can be adjusted to make the receiver VCO track the probe VCO properly.

### 2.2.4. Measurement Board

It was mentioned earlier that the synchronous detection which had been used to provide the wide dynamic range for the electric field measurements would probably be unsatisfactory in the case of the magnetic measurements, which were expected to be highly distorted. The phase-locked loop system used in the synchronous detector would be able to lock onto the distorted waveforms. However, the phase relationship between the fundamental and the harmonics could not be specified in advance, and hence the average indicated by the output of the synchronous detector would not, under most circumstances, adequately reflect the magnitude of the fundamental of the field being measured, let alone its harmonics.

Instead, a filter arrangement was designed to permit separation of the fundamental, second and third harmonics, and their separate measurement. The broadband energy is also measured. A block diagram of the circuit board which accomplished this is shown in Figure 2-7.

The bandpass filters shown in Figure 2-7 are centered at 60, 120 and 180 Hz. Each is constructed as a six pole Butterworth-characteristic filter. Each pair of poles in the filter is realized by means of a state-variable implementation, as shown in Figure 2-8.

The broadband filter, designed to be flat between about 10 Hz and 1 kHz, is realized using a slightly different configuration. The low frequency cut-off of the filter is accomplished by a capacitor-coupled amplifier, providing a single-pole response. This is followed by three state-variable filters, configured in the low-pass mode. The high frequency roll-off created by the six poles of the filter is thus quite sharp. This helps to minimize the noise contribution of the optical fm carrier.

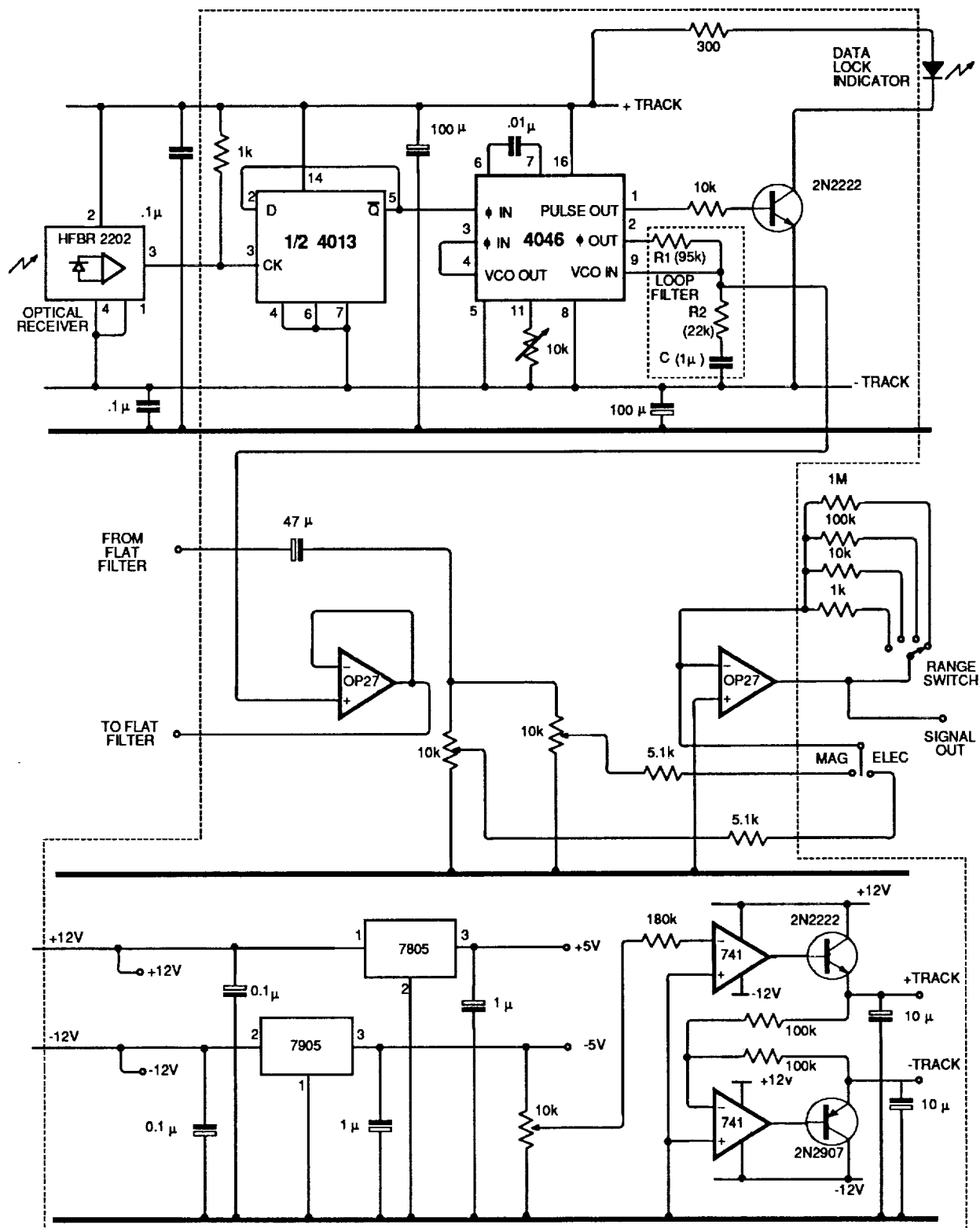


Figure 2-6. Magnetic field meter data board

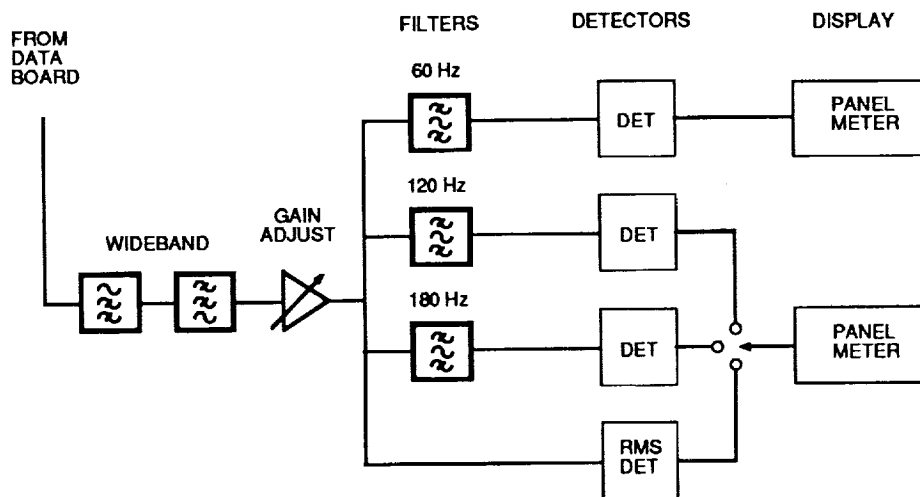


Figure 2-7. Block diagram of measurement board

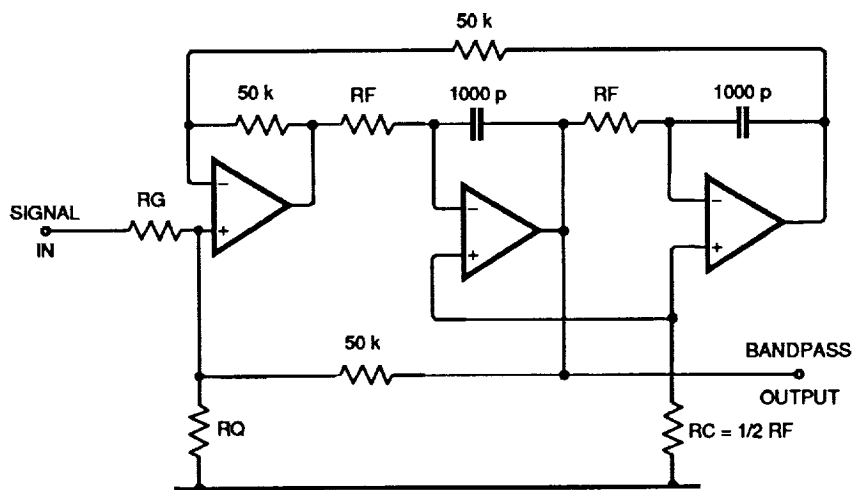


Figure 2-8. State variable filter circuit

The broadband filter is placed ahead of the gain-adjusting stage in order that the dynamic range of the amplifier is not exceeded by the noise spikes in the signal. This would lead to nonlinear operation, and the device would be impossible to calibrate. As is good practice to prevent ringing in high Q stages, the three state variable filter sections which are cascaded to construct the six-pole Butterworth filters each begin with the lowest-Q pair of poles. Table 2-1 shows the component value calculated for the filters. In the prototype, these values were realized by a combination of fixed and variable resistors. The filters were "tuned" to the desired response.

Table 2-1. Filter component values

Bandpass Center Frequency	Filter Section Number	RF (Ohms)	RG (Ohms)	RQ (Ohms)
60 Hz	1	11.99 k	38.4 k	252
	2	11.36 k	38.4 k	126
	3	11.16 k	38.4 k	126
120 Hz	1	5.300 k	38.4 k	252
	2	5.330 k	38.4 k	126
	3	5.277 k	38.4 k	126
180 Hz	1	3.533 k	38.4 k	252
	2	3.548 k	38.4 k	126
	3	3.518 k	38.4 k	126
Broadband (Low-pass configuration)	1	31.8 k	50 k	90.5 k
	2	31.8 k	50 k	35.6 k
	3	31.8 k	50 k	8.7 k

Figure 2-9 shows how the rms detector is arranged to measure the broadband energy of the field. It may be noted that the rms detector circuit has been equipped with an offset adjustment. In practice, it is by no means clear that this is essential. In the future it may be possible to simplify the circuit somewhat by removing it. We have observed no particular problems with offset, which has typically been in the order of 1 millivolt. With our panel meters requiring 200 millivolts full scale, a 1 millivolt offset represents typically the kind of error that could be tolerated.

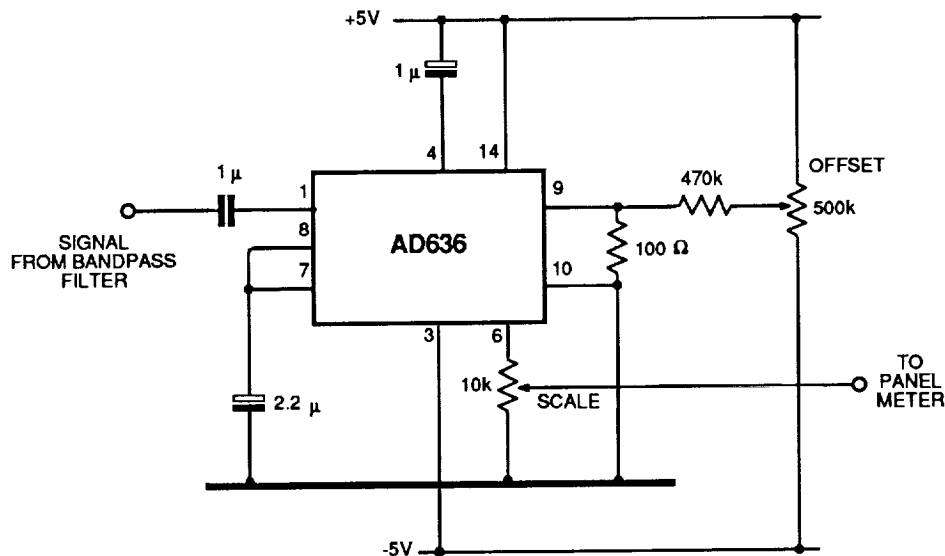


Figure 2-9. RMS detector circuit

This board is also equipped with its own regulated power supply, a schematic of which will not be shown since it is simply an application of the conventional three terminal regulator.

#### 2.2.5. Mechanical Construction

The construction of the magnetic meter probe is based on the design of the electric field meter built earlier. The probe is spherical, with the hybrid IC about at the center of the sphere. Two phenolic formers are used to hold the IC in place. To them are attached the "paddle" that holds the probe assembly on the end of the support pole, and the two hemispherical electrodes. In the magnetic meter, the electrodes are not part of the sensing system, they merely control the electric field intensification. The sensing element is a coil of fine wire wound in a groove in one of the phenolic formers.

A photodiode array, made by Dionics Inc., is mounted on the paddle, at the rear of the hybrid IC, and the fiber feeding energy to it is fixed a few mm away. The paddle arrangement is rather simpler than in the case of the earlier electric field probe because there is only one photodiode array, furnishing power to both the positive and negative supplies. The LED which sends the output data to the receiver is mounted on the opposite side of the paddle.

Figure 2-10 is a cross-section showing the construction of the probe. The photodiode array, mounted on a ceramic substrate, is shown in Figure 2-11. Figure 2-12 is a photograph of the completed probe, with one of the outer hemispheres removed to show the internal details of the device. The photodiode array and the range resistors used during prototype development can be seen.

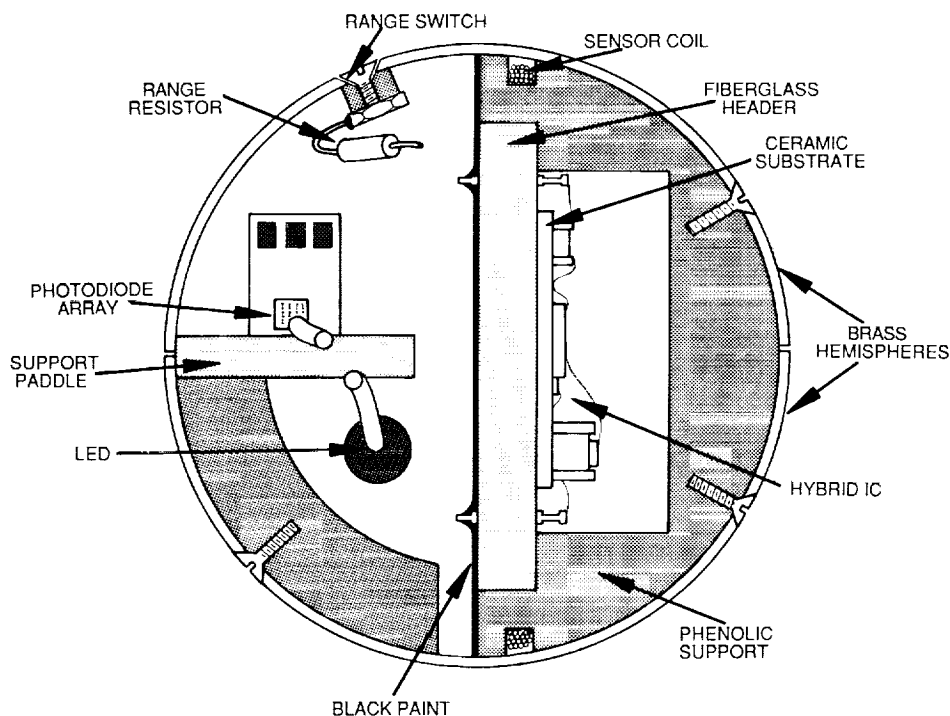


Figure 2-10. Cross-section through magnetic field meter probe



Figure 2-11. Photodiode array, mounted on ceramic substrate

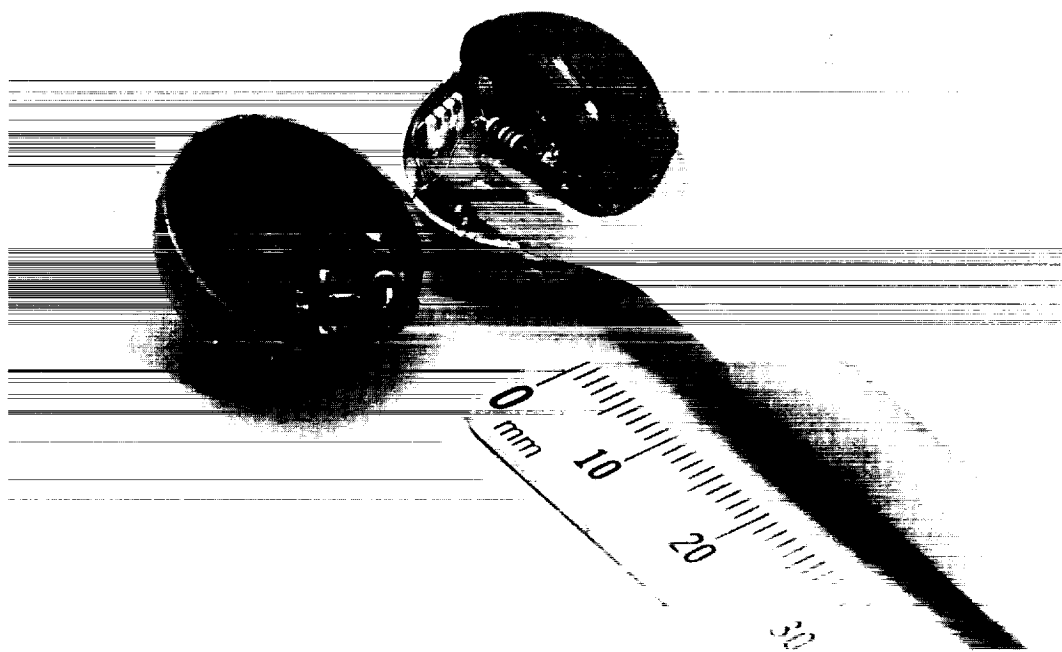


Figure 2-12. Magnetic field meter probe

## 2.3. Calibration

### 2.3.1. Calibration from First Principles

Since the input impedance of the first stage of the probe is extremely high compared to the source impedance of the coil, the calibration from first principles can be done quite accurately. One need only know the area (or radius) of the coil of wire, the number of turns  $N$ , and the frequency (which for calibration purposes can be taken as 60 Hz) and then apply the relationship:

$$e = - N \frac{d\phi}{dt} \quad (2-1)$$

where  $e$  is the voltage induced by a changing flux  $\phi$ . The flux may be assumed to be sinusoidal with time for calibration purposes, and the total flux  $\phi$  is given by the flux density  $B$ , for which the instrument is being calibrated, and the area of the coil. If the rms value of the flux density is used, Equation 2-1 will yield the rms value of the induced voltage. Thus, with 60-Hz excitation,

$$e = 1184.35 B r^2 \quad (2-2)$$

for each turn of the coil. Here  $e$  is in volts if  $B$  is in Tesla (or Webers/m<sup>2</sup>) and  $r$  is in meters. A known voltage  $e$  is applied to the probe and the gain of the receiver is adjusted until the meter reads the appropriate value  $B$  of flux density.

In our design, we have  $r = 8.5$  mm, and a coil of 100 turns, so that

$$e = 8.557 \quad (2-3)$$

for a field of 1 Tesla. Since we are typically dealing with fields smaller than this by a factor of  $10^6$ , the input voltage to the hybrid IC is typically in the order of  $\mu$ V.

The calibration procedure is as follows. To represent a field of 1 mT, which is close to the largest field that the meter can read, a voltage of 8.56 mV, at 60 Hz, is applied to the input of the probe, in place of the pickup coil. The gain switch is set to the least sensitive position. The overall-gain adjusting potentiometer is set so that the outputs of the 60-Hz display and the rms detector indicate 1 mT. The frequency is then adjusted to 120 and 180 Hz in turn, and the corresponding gains adjusted so that the readings are one-half and one-third of the 60-Hz value respectively.

Internal gains are designed so that the readings on the displays are as large as possible, to maximize the usefulness of the display. The range switch has four positions, each one order of magnitude more sensitive than the last. In the least sensitive (highest field) position, a full scale reading corresponds to 1.999 mT. In the most sensitive (smallest field) position, a full scale reading corresponds to 1.999  $\mu$ T. It is possible to measure fields in the order of 0.1  $\mu$ T.

### 2.3.2. Experimental Calibration

As in the case of the electric measurement, it is good practice to verify the calibration experimentally. Just as a uniform electric field can easily be generated by applying a known potential to two parallel plates, the Helmholtz coil arrangement (see Appendix B for details) can be used to generate a magnetic field which is known and uniform over a small region, although the region of uniformity in the magnetic case is not as large as in an electric field cage of comparable volume. Our Helmholtz apparatus is about 0.3 meters in radius and length. Consequently, the field at the center of the apparatus is uniform over a region about 5 cm in extent, which is certainly large enough to permit calibration of the small probe used in our field meter system.

### 2.3.3. Uncertainties in Calibration

It can be seen from Equations 2-1 and 2-2 that uncertainties in the area, frequency, and number of turns of the probe coil are simply additive in their effect on the calibration accuracy. With care, the number of turns can, of course, be accurately determined. The frequency is known to be 60 Hz with great precision, so that the predominant source of uncertainty becomes the accuracy with which the area of the coil can be known. Since very fine wires (50 AWG) are used in its construction, the coil has only a small, although not infinitely small, extent in the radial direction. The wire used has a diameter of 0.0254 mm (0.001 in.), so that if the entire coil is constructed in a neatly wound arrangement of, say, two layers, the coil extends for about 1% of the radius. Since the coil thickness is such a large fraction of the radius, the combined uncertainty of measurement of the radius and assuming that the coil is located entirely at its center can be appreciable, say 1%.

Uncertainty in the calibrating voltage must be added to the total uncertainty, and may be on the order of 0.5%. If we consider all the sources of uncertainty in the calibration, it is unlikely that a first-principles calibration uncertainty better than 2% is possible.

In the case of the Helmholtz coil calibration setup, we obtain the following expression for the field at the center of the coil pair:

$$B = 4\mu_0 \pi r^2 N i \left[ \frac{1}{(r^2 + (r^2/4))^{3/2}} \right] \quad (2-4)$$

$$= \frac{32\mu_0 \pi N i}{(5)^{3/2} r} \quad (2-5)$$

where  $\mu_0$  is the permeability of air, and  $N$  the number of turns in each coil of the Helmholtz apparatus. Hence the uncertainty of the field at the center depends upon the number of turns, on the current, and on the radius, a parameter which was obtained only with moderate precision in our apparatus. (The method of construction that was used was such that the coils are only approximately circular.) Thus, while it is possible to know the number of turns precisely, the current can probably not be measured with an uncertainty less than one-half a percent in our laboratory, and somewhat larger errors are certainly accumulated in the dimensions of the device.

It may be concluded, then, that the Helmholtz arrangement provides a convenient way to check the accuracy of the first principles probe calibration, but the sources of uncertainty in the Helmholtz coil calibration are of similar magnitude to those in the first-principles calibration of the probe.

## 2.4. Experimental Results

### 2.4.1. Frequency Response

Unlike our electric field meters, which were single frequency devices, the magnetic field meter is designed to operate over a range of frequencies. The ac electric field meter operated essentially at 60 Hz, and the dc electric field meter operated in the vicinity of 500 Hz, but in neither case was the precise frequency response of the measurement system critical. In the case of magnetic fields, since we expect there to be some energy in the field at 120 and 180 Hz as well as at 60 Hz, it is important that the frequency response of the entire system be relatively flat. We will examine the design by following the signal from the probe to the display.

#### 2.4.1.1. Probe Frequency Response

The response of the probe itself must be that of an integrator, and decrease at 6 dB/octave, beginning with the lowest frequency to be expected in the field, 60 Hz. Figure 2-13 shows the measured frequency response of the probe. Since the integrator used in the probe employs the amplifier in the non-inverting mode, the roll-off with frequency does not continue indefinitely. When the feedback network reaches the point that there is essentially no impedance between the output terminal and the inverting input terminal, the non-inverting amplifier does not go to zero gain. Consequently, the output amplitude at high frequency is not zero. However, the dc gain of the stage in our application is sufficiently high that this departure from ideal is almost out of the range of interest for our present purposes. Thus, the integrator response appears to be sufficiently accurate for our measurement purposes up to the 1-kHz chosen for the upper limit of the frequency response.

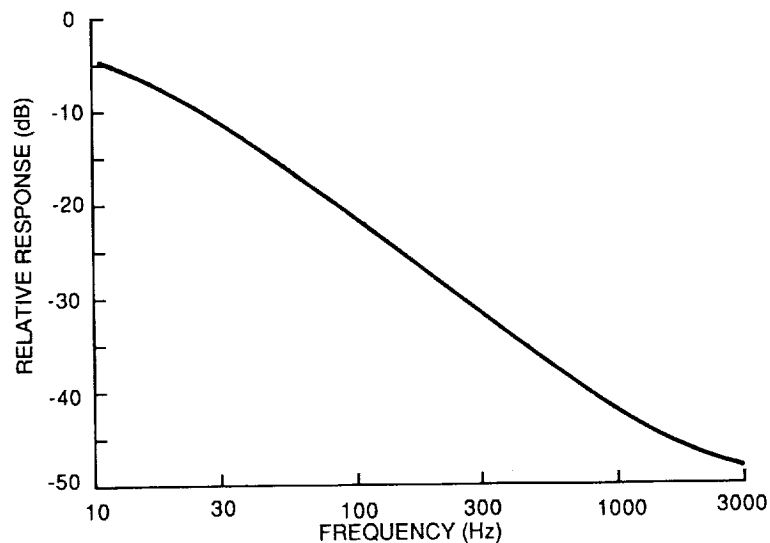


Figure 2-13. Probe frequency response

The deviation from ideal integrator performance can be shown directly, as in Figure 2-14. In the Figure, the deviation from the ideal integrator response is shown as a fraction of the response at 100 Hz, rather than being compressed logarithmically. This exaggerates small errors, compared to the normal method of using a dB-scale. Figure 2-14 shows that the probe response is relatively accurate between 60 and 180 Hz, the frequencies at which filtered measurements will be made. There is a falling response at low frequency, caused by the fact that the integrator has finite gain at dc. There is a slight valley in the output near 700 Hz (about 5% low compared to the peak at 100 Hz), and at higher frequencies the response rises sharply. This increase in output at high frequency is due to the use of the non-inverting integrator. The location of this rise was chosen to compensate for a slight decrease in the link response at high frequency.

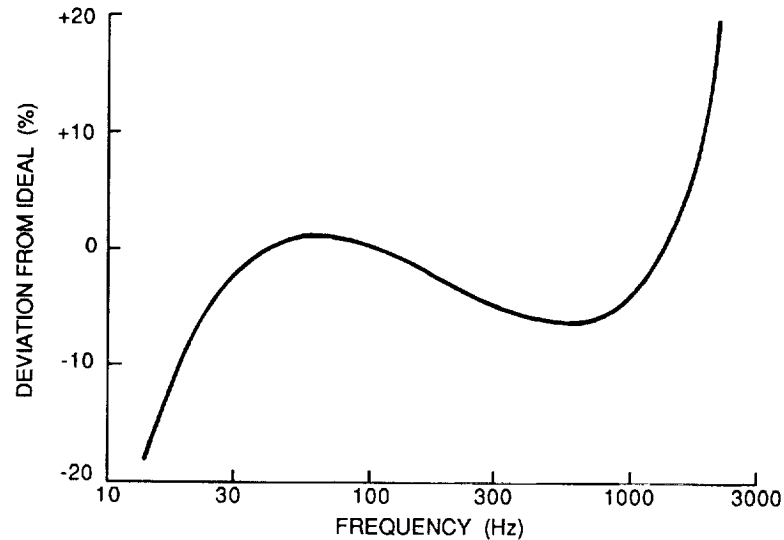


Figure 2-14. Probe deviation from ideal integrator

#### 2.4.1.2. Link Frequency Response

In the case of our previous meters, the frequency response of the data link had been relatively unimportant because of their operation at fixed frequency. In the present case, we require an overall response from the system which is flat up to 1 kHz, and the data link is an important part of that frequency response. Consequently, attention was paid to the phase locked loop in the receiver so as to tailor the overall response. Gardner (1966) shows how the loop filter affects the overall loop response. The natural frequency and the damping factor for a loop with a passive lag-lead filter are given by

$$\omega_n = \left( \frac{K_0 K_d}{\tau_1 + \tau_2} \right)^{1/2} \quad (2-7)$$

and

$$\zeta = \frac{1}{2} \left( \frac{K_0 K_d}{\tau_1 + \tau_2} \right)^{1/2} \left( \tau_2 + \frac{1}{K_0 K_d} \right) \quad (2-8)$$

where  $\omega_n$  is the natural frequency of the loop and  $\zeta$  is the damping factor.  $K_0$

is the VCO constant in radians per second per volt, and  $K_d$  is the phase detector gain constant with dimensions of volts per radian. This kind of filter has two independent time constants,  $\tau_1$  and  $\tau_2$ , the time constants of the lag (pole) and lead (zero) terms in the filter characteristic. The values are established by two resistors (identified as  $R_1$  and  $R_2$  in Figure 2-6) in combination with the filter capacitor. Because the values can be chosen independently, the values of  $\omega_n$  and  $\zeta$  can be specified separately.

The overshoot in the response of the resulting second order loop can be controlled by means of the damping factor  $\zeta$ . For  $\zeta \geq 5$ , there is practically no overshoot. Gardner shows that for such a loop, the response is relatively flat until several times the natural frequency of the loop.

For our purposes, we require a frequency response essentially flat out to 1 kHz. This leads to the choice of a natural frequency for the loop of 100 Hz, and a damping factor of 7. With a phase detector constant  $K_d$  of  $5/\pi$  V/rad (see below), and a measured VCO gain constant  $K_0$  of  $29 \times 10^3$  (rad/s)/V, the filter parameters became  $\tau_1 = 0.095$  s and  $\tau_2 = 0.0022$  s, leading to the component values shown in the circuit diagram, Figure 2-6.

The measured link frequency response is shown in Figure 2-15.

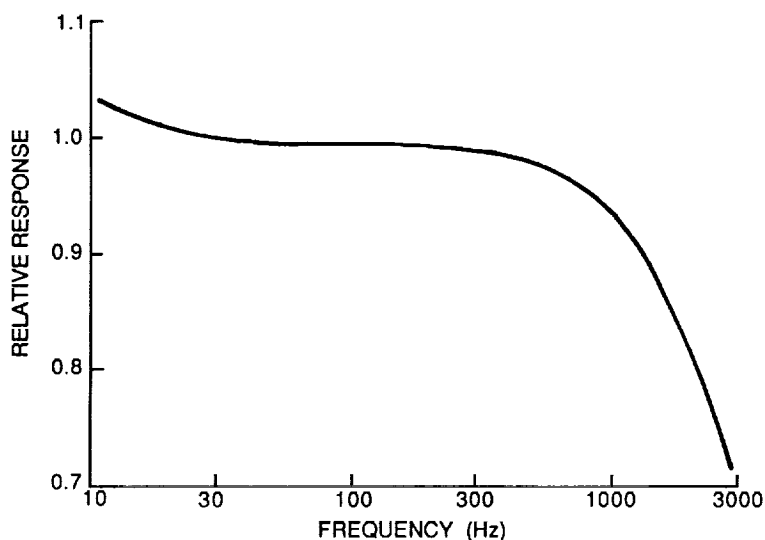


Figure 2-15. Link frequency response

Once again, the results are not compressed logarithmically. The link response is flat (within 1%) from about 25 Hz to 500 Hz. Above this, the response is attenuated. Nevertheless, the output is only 5% down at 1 kHz, compared to the response at 100 Hz.

#### 2.4.1.3. Choice of Phase Detector

The low-power phase-locked loop circuit 4046 has a choice of two phase detectors. One is a conventional multiplying-type phase detector using an

exclusive-OR network. The other is an edge-controlled digital memory network consisting of a multiplicity of flip-flops and control gates, and having a three-state output. While our earlier phase-locked loop detectors employed the edge-triggered phase detector for the loop, it was found during the development of this probe that the use of this detector for such a wide range of modulation frequencies was unsatisfactory.

It is a characteristic of this detector that it operates with almost zero phase angle between the VCO signal and the reference. While it has the convenient characteristic that it is a frequency detector as well as a phase detector, it has the disadvantage that when the loop is locked and the frequencies are matched the output is essentially a tri-state open circuit, except during the process of edge detection. At these times, the signal may be either a positive pulse or a negative pulse. The pulse duration is very short, and corresponds approximately to the phase difference between the two signals.

This phase difference was found to be extremely small, and the duration of the pulses so short that their shape was no longer rectangular, but rather trapezoidal. On occasions, because of the modulation, the pulses were so narrow that even the trapezoidal shape degenerated to a triangle, and the full amplitude of the output pulse was never achieved. This corresponds to a kind of nonlinear behavior in the loop, and resulted in significant errors at high modulation levels and high frequencies.

In order to achieve operation with modulation frequencies as high as one quarter of the carrier frequency, and the high modulation levels that we required, it was found necessary to use the other phase detector. This phase detector operates analogously to an overdriven mixer. To maximize the lock range, the signal and VCO signals must have 50% duty cycle. If the free-running frequency of the VCO is equal to the carrier frequency, a loop operating with this kind of phase detector will normally have a  $90^\circ$  phase relationship between the two signals. The phase detector output is then a square wave at twice the VCO frequency. As the reference frequency departs from the free-running frequency of the VCO, a phase error appears, and the mark/space ratio of the phase detector output changes. In the limit, the phase error approaches  $90^\circ$ , and the phase detector produces either a high or a low output, depending on the direction of the phase error. The phase detector constant,  $K_d$ , is thus dependent on the power supply voltage. In our design, the supply voltage is 2.5 V. Since this output would correspond to a phase error of  $\pi/2$  radians, the value of  $K_d$  is simply  $5/\pi$ .

Phase error can be kept small in a high-gain loop, but it does increase with frequency and depth of modulation. However, even with significant modulation depth, it is unlikely that the phase angle would ever depart sufficiently from the nominal value of  $90^\circ$  to cause the kind of nonlinearity problem observed with the edge-type phase detector. In practice this was found to be the case.

The incoming carrier frequency from the optical link was converted to a square wave by means of a simple flip-flop, and the phase-locked loop was modified to operate at 5 kHz. This means that the phase detector noise is at 10 kHz. It is then relatively straightforward to filter this noise from the desired signal for the purposes of measuring the energy in the modulation at frequencies up to 1 kHz.

#### 2.4.1.4. Broadband Filter Frequency Response

Because the loop filter contains a zero at a frequency not greatly above that of its dominant pole, the output of the phase-locked loop contains a considerable amount of energy at twice the reference frequency. Indeed, the output of the loop filter is an almost rectangular wave whose mark/space ratio varies as a function of the modulation in the loop.

In order to recover the modulating signal from this, it is necessary to apply further filtering. Consequently, the signal is applied first to the broadband filter, as shown in Figure 2-7. The filtering must be done first (before any linear amplification) in order to suppress any remnants of the phase detector square-wave output.

The response of this filter is shown in Figure 2-16, again not using dBs.

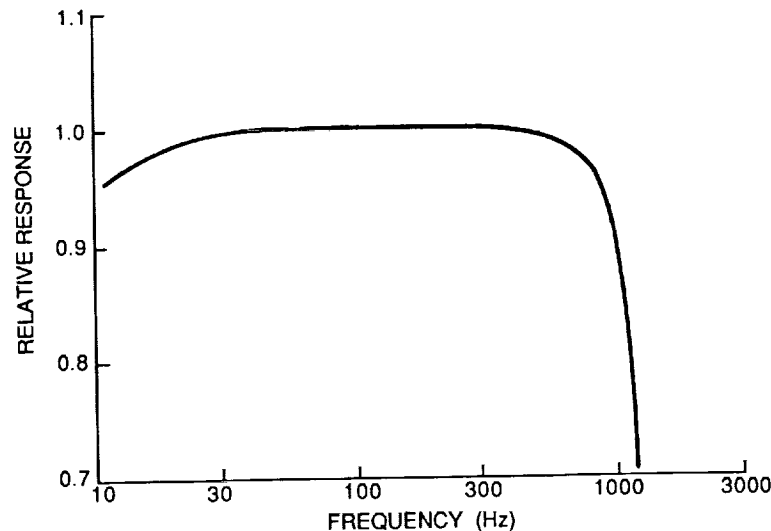


Figure 2-16. Broadband filter characteristic

The filter is very flat (because it was designed as a Butterworth filter), with a high-frequency rolloff that is just perceptible at about 500 Hz. The filter output is 10% down at 1 kHz.

#### 2.4.1.5. Overall Frequency Response

The frequency response of the complete system, consisting of the probe, the fm data link, and the flat filter is shown in Figure 2-17. Once again, this curve is not logarithmically compressed. It can be seen that the system is essentially independent of frequency from 60 Hz to 800 Hz. At 1 kHz, the system is only about 5% low. Overall, the response is so flat that there should be no need to correct the individual-frequency stages for gain errors. The slightly low response at the very edge of the passband is thought to be of no consequence. Expressed in dB, the system response is flat ( $\pm 1$ dB) from 15 Hz to 1200 Hz, or (since the response is not peaky)  $+0 -1$  dB from 25 Hz to over 1000 Hz.

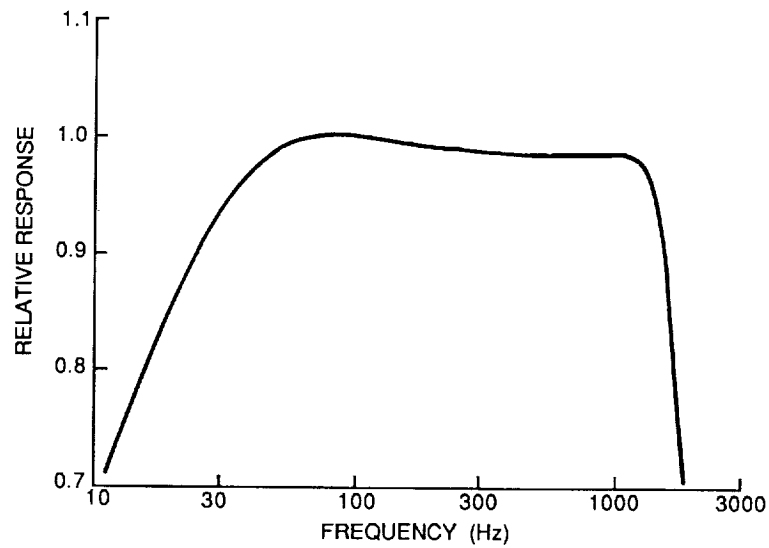


Figure 2-17. Overall system response

#### 2.4.1.6. Single-Frequency Bandpass Filters

Following a 20-dB preamplifier and the gain adjustment stage, which has four orders of magnitude of adjustable gain, the signal is passed to measurement circuits for the narrow-band measurements at 60, 120 and 180 Hz. These components of the signal are separated by means of the active filters discussed above. The measured frequency response of these filters is shown below in Figures 2-18 through 2-20.

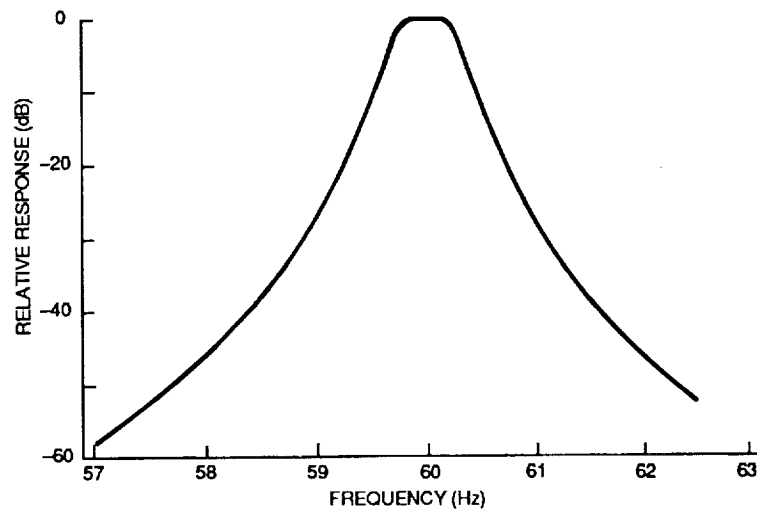


Figure 2-18. Filter characteristic, 60-Hz filter

It will be seen that these filters, each based on the 6-pole Butterworth design described earlier, are rather narrow. It is ultimately the quality of these filters that determines the dynamic range of the instrument. Whereas in our earlier electric field meters we were able to use synchronous detection to achieve a high degree of noise rejection, that must now be achieved by means of filtering. It will be seen later that the filters whose characteristics are shown here furnish the receiver with a dynamic range roughly comparable with that achieved using our synchronous detectors.

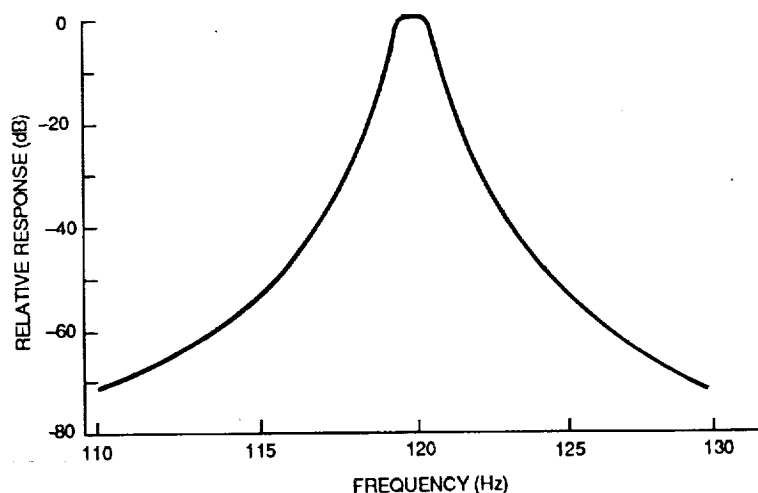


Figure 2-19. Filter characteristic, 120-Hz filter

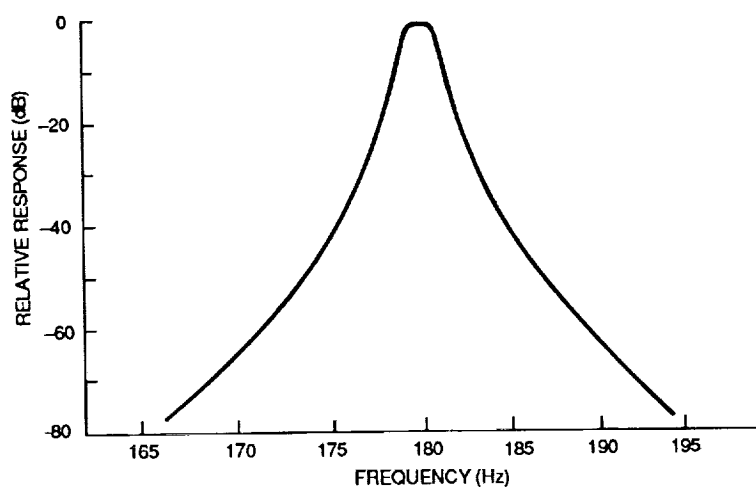


Figure 2-20. Filter characteristic, 180-Hz filter

#### 2.4.2. Photodiode Array

The Dionics DI-16 V8 array was tested using a controllable load, and its I-V curve was obtained. This is shown below in Figure 2-21. The data shown in Figure 2-21 were obtained by illuminating the array by means of a fat fiber located approximately 5 mm from the array, and energized by means of a 50-mW laser.

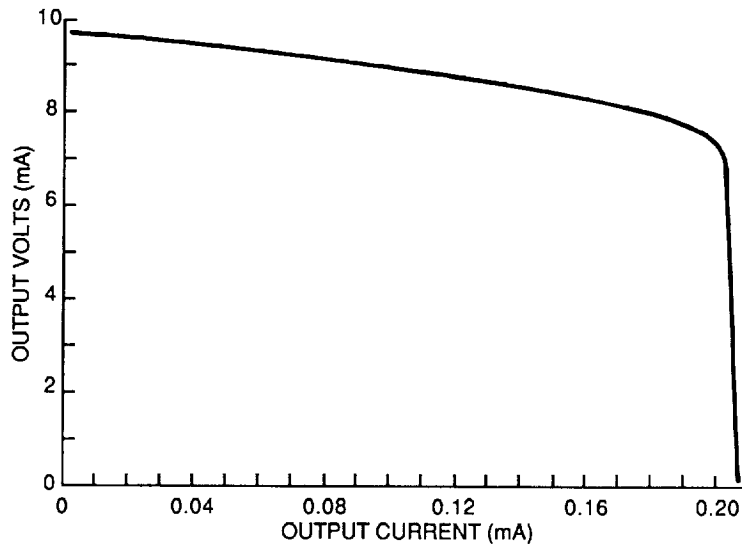


Figure 2-21. Diode array characteristic

Open circuit, the array furnishes over 9 V, and short circuit the current is somewhat over 200  $\mu$ A. Peak power is  $\sim 1.5$  mW. In our application, we require about 130  $\mu$ A at  $\pm 2.5$  V, or  $\sim 0.7$  mW. This seemed like a readily obtainable goal from this array. An advantage of this device over our earlier arrays was that the entire probe could be energized from just one fiber, instead of using one for the positive and one for the negative supply.

The laser that we used to energize the probe furnished a nominal 50 mW (optical) with a laser current of 300 mA. The margin of power can be estimated from a curve of load voltage against laser current, as shown in Figure 2-22.

It will be seen that sufficient energy is available for the probe with a laser current of a little less than 300 mA. There is a small margin in the performance. A greater margin has been observed in other samples of the same laser.

#### 2.4.3. Light Sensitivity of Hybrid

An unexpected result was obtained when the first nonmagnetic hybrid IC was energized by means of the laser. Compared to the power consumption of the IC, a considerable amount of optical energy is inserted into the probe. While some of it is absorbed by the diode array, some of it is reflected and illuminates the interior of the hemispheres. It was discovered that the hybrid integrated circuit, now mounted on a fiberglass header, was light-sensitive.

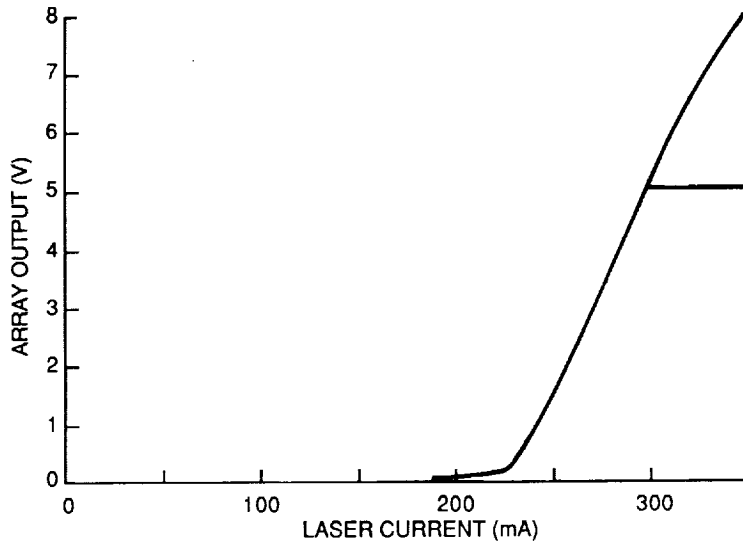


Figure 2-22. Performance of laser/array combination

Apparently enough of the infrared energy from the laser was penetrating the fiberglass to appear on the circuit side of the substrate. The resulting photons acted as input current in the sensitive input stages of the integrating operational amplifier. Under some conditions, it was found that enough energy was available to cause the integrator stage to saturate. At this point of course, the entire probe ceased to function. The solution was to paint the exterior of the fiberglass header with an opaque paint.

#### 2.4.4. Dynamic Range

In contrast with our earlier electric field meters, the magnetic field meter has a wide frequency response and does not make use of synchronous detection. These two features make the question of providing the instrument with a wide dynamic range particularly challenging. A wider bandwidth can ordinarily be expected to provide a greater amount of noise in a system, and the use of synchronous detection enables the recovery of signals from under a large noise. In the present design, the dynamic range can be expected to be smaller than that of the electric field meters, particularly as far as the wideband measurement of the signal from the magnetic field probe is concerned.

##### 2.4.4.1. Probe Saturation

The maximum field that can be measured is limited by saturation in the system. The system was designed so that the probe saturated before the receiver, so that for ordinary conditions the amount of modulation on the optical link was maximized. This maximizes the dynamic range, if noise is introduced in the link.

The design goal for our field measuring system was a maximum field of 2 mT. (Actually, the displays would go blank for a reading greater than 1.999 mT.) To ensure linearity up to this point, the probe was designed to saturate at about 2.3 mT. Because the first stage of the probe is operated as an integrator, its output is larger at lower frequencies. Therefore a 60-Hz signal

will cause saturation first. The trade-off here is between the number of turns in the coil, and the gain of the first stage amplifier.

The use of a noninverting integrator led to a situation in which the response departed from that of an ideal integrator at high frequencies, see Figure 2-14. The frequency at which this departure occurred was deliberately chosen to compensate for a corresponding high-frequency roll-off in the optical link. This decision fixed the gain of the integrator, with the result that the only free parameter to establish the proper saturation field was the number of turns in the coil. In our particular case, a 100-turn coil producing about 17 mV at 2 mT was used. A signal of about 20 mV at 60 Hz was sufficient to cause clipping in the integrator output.

#### 2.4.4.2. Noise Floor

At the other extreme, the noise level in the system sets the lowest signal that can be measured. A wideband signal ordinarily contains more noise than a narrowband signal. Because of this, the wideband measurement of the magnetic field can be expected to reach its noise floor ahead of the single-frequency measurements at 60, 120 and 180 Hz. In fact, if the noise is Gaussian, the difference in dynamic range between the various measurements can be obtained simply by examining the difference in bandwidths. For example, two filters whose bandwidths are  $B_1$  and  $B_2$  can be expected to have dynamic ranges differing by a factor of  $B_1/B_2$ , assuming that all of the noise is entering at the input to both filters.

The 60-Hz filter is about 1 Hz wide. The wideband and narrowband filters thus have bandwidths in the ratio of approximately 1000 to 1. It was expected that the narrowband measurements would have a dynamic range two orders of magnitude (40 dB) greater than the wideband measurement. In fact, the noise floor of the narrowband measurements is better than that of the wideband, but by a rather smaller amount than expected.

In our field meter, the noise floors of the various filters differed by a factor that seemed closer to  $\sqrt{B_1/B_2}$  than it did to  $B_1/B_2$ . Therefore, to maximize the improvement in dynamic range due to the narrowness of the single-frequency filters, they must be as narrow as possible, within the limitations of realizable audio filters. The use of even higher-Q filters is indicated, but these may be difficult to implement.

#### 2.4.4.3. Experimental Results

The dynamic ranges of the wideband measurement and the 60-Hz measurement are shown in Figure 2-23, which compares the experimentally determined error in each measurement as a function of applied field. By using an external voltmeter, it was possible to show the instrument output above the 2-mT at which the panel meters indicate over-range.

The graph shows an apparently constant error of less than 1% for fields between  $2 \times 10^{-6}$  T and  $2 \times 10^{-3}$  T. This approach was used to represent the uncertainties caused by the range resistors and the resolution of the display. There is not a constant error, rather the line indicates that 1% is reasonable accuracy to expect from the measurement. Above 2 mT, the error increases very rapidly.

This is the effect of clipping in the probe. The error is such that the meter reads consistently low. Below  $10^{-6}$  T for the 60-Hz measurement, or  $10^{-5}$  T for the broadband measurement, the error increases gradually, as noise makes an increasingly large contribution to the reading. The meter reads high.

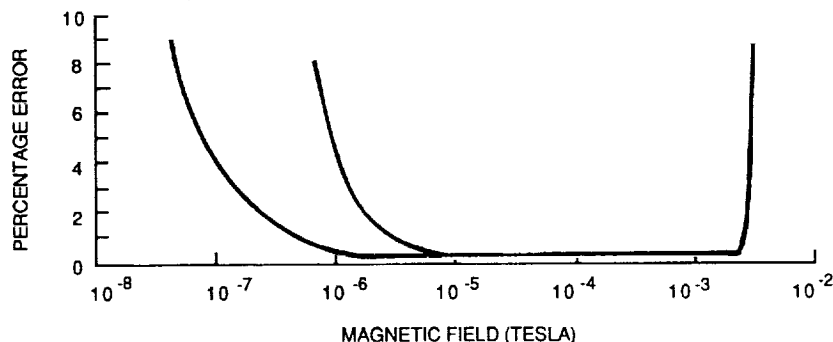


Figure 2-23. Dynamic range of field meter

The dynamic range of the wideband measurement is about 3 orders of magnitude (actually 66 dB), from 1  $\mu$ T to 2 mT (or 10 mG to 20 G). The dynamic range of the 60-Hz measurement is somewhat over 4 orders of magnitude (about 88 dB), from about 80 nT to 2 mT (or 0.8 mG to 20 G). These results show that, despite the narrowness of the 60-Hz filter, the measurement is only a little over 20 dB more sensitive than the wideband 1-kHz measurement. If a more sensitive instrument is needed, the 100-turn coil could be replaced by one with more turns. The scaling is simply linear in the number of turns.

The source of the noise in the measurements was investigated experimentally. A high-quality signal source was substituted in turn for the digital signals at various points in the system, with no modulation. It was found that the system noise was essentially unchanged when the probe signal was replaced, or when the PLL demodulator was driven directly by the signal generator. The probe and the link were therefore eliminated as noise sources. When the PLL output was replaced by a square wave pulse train, the system noise was considerably reduced. It was concluded that the predominant source of noise in the system was, as may be expected, phase jitter in the PLL demodulator. There was very little that could be done to reduce this effect. The next largest source of noise seemed to be shot noise in the amplifiers of the flat filter. Since all subsequent stages see this noise, it is important that it be minimized. High quality amplifiers were used in our prototype.

Finally, it seems that the noise is not Gaussian. Its spectral density seems to correspond more to pink noise than white; equal energy is contained in any two octaves of the spectrum, rather than in any two regions of equal bandwidth. The issue was not pursued further: a complete investigation of the noise properties of the PLL was beyond the scope of the present study.

#### 2.4.5. Calibration Accuracy

The dynamic range tests shown above were performed "synthetically." As in the calibration procedure, a signal generator was used to inject a voltage into the

probe. This was the only practical way to obtain readings near the low end of the dynamic range, since the magnetic field noise floor of our laboratory was higher than the electronic noise floor of the equipment. Further, the output was monitored on a separate voltmeter, so that readings above the clipping point of the probe (and the blanking point of the displays) could be obtained. To provide verification of the accuracy of the calibration, the probe was inserted into the Helmholtz calibration apparatus.

Fields in the order of  $10^{-4}$  T were used as spot checks on the calibration. Such fields were at least two orders of magnitude greater than the magnetic field noise floor of our laboratory. No difference greater than 1% was found between the calculated field and the measured field. It was concluded that the synthetic calibration we used was at least as accurate as an experimental one would have been, and had a much wider dynamic range.

#### 2.4.6. Example of Field Measurement

For demonstration purposes measurements were made, using this system, of the magnetic field near a small 1500-W hair dryer. In the past we have presented field measurements of this kind in the form of lines representing the vectors of the field. On this occasion it was thought to be more useful to show the field as contours of equal magnitude. In order to develop such a contour map from the measured data a computer program was written. Outputs of this program, showing the contours of the magnetic field at the fundamental frequency, the second and third harmonics and the wideband energy are shown in Figures 2-24, 2-25 and 2-26. The program is described in Appendix C.

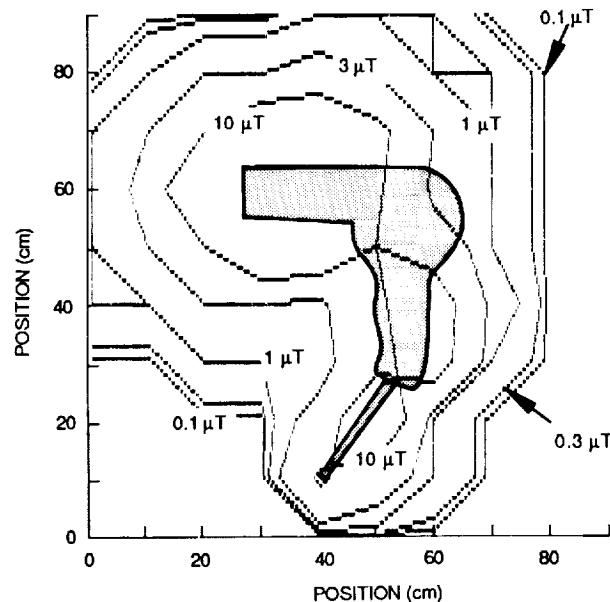


Figure 2-24. 60-Hz magnetic field around hair dryer

The fundamental field, shown in Figure 2-24, has the same general shape as the hair dryer. There seem to be contributions to the field from both the motor and the heater coils, as may be expected. The flexible wire by which the hair

dryer is energized has only a relatively small external field, presumably because the two conductors are close together.

The data shown in the Figure were measured in the plane of the device. The contour that appears to cross the hair dryer results from the plotting program's interpolation across that region.

The outer field contour, corresponding to  $0.1 \mu\text{T}$ , is shown very close to the contour for  $0.3 \mu\text{T}$ . In fact, while it is a small field, this contour is above the noise floor of the field meter, and evidently represents the effect of the ambient magnetic field in our laboratory.

It may be estimated from the figure that the peak field at 60 Hz was in the order of  $20 \mu\text{T}$  (200 mGauss). In fact, values of this order were measured, but do not appear in Figure 2-24 because of our choice of contours.

The magnetic field at 120 Hz is shown in Figure 2-25.

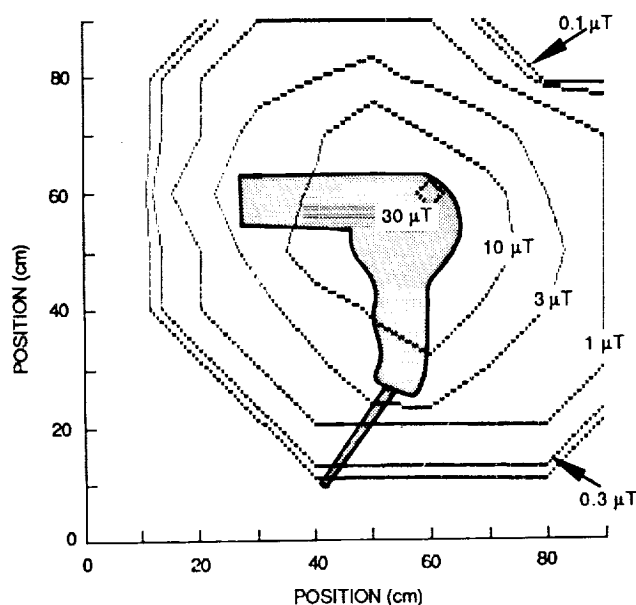


Figure 2-25. 120-Hz magnetic field around hair dryer

The 120-Hz field is evidently quite different from the fundamental field. This field is almost circular in appearance, and is probably centered on the motor of the hair dryer. Fields as high as  $30 \mu\text{T}$  (300 mGauss) are seen.

There was a small 180-Hz component to the field. This is shown in Figure 2-26.

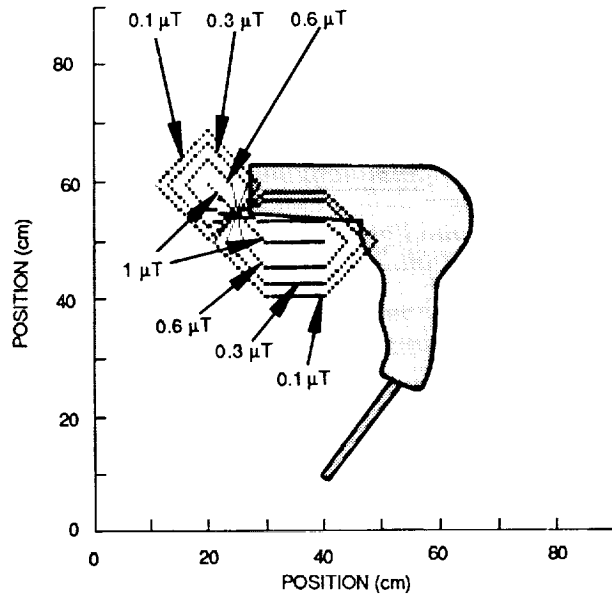


Figure 2-26. 180-Hz magnetic field around hair dryer

The contours of the field measured by the rms detector with the wideband response are shown in Figure 2-27.

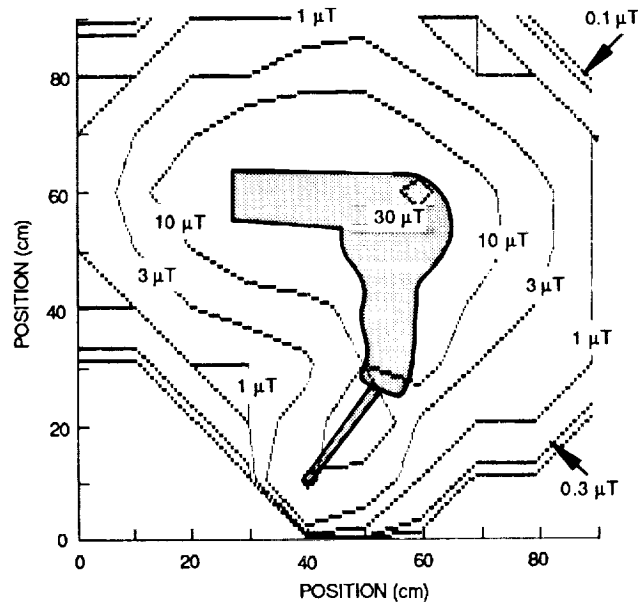


Figure 2-27. Wideband magnetic field around hair dryer

It was thought that it might be interesting to measure the magnetic field in an office. Most convenient was the office of the first author of this report. This office contains a personal computer and a laser printer, on which the original of this document was prepared. A 60-Hz field of about  $0.1 \mu\text{T}$  (1 mG)

was measured in the area in front of the terminal. However, investigation showed that this field was originating in the printer, located nearby. A 60-Hz field of about 1  $\mu$ T was measured near the printer, and values as high as 7  $\mu$ T were observed at the surface of the printer itself. No measurable fields at 120 or 180 Hz were observed.

Perhaps it should be stressed that we attach no particular significance to the results presented here. These experimental data are given merely to indicate the type of measurement that can be made with the prototype field meter. While none of the measurements actually required the use of an electrically isolated probe, the results do show that fields that are quite small in magnitude and that are not spatially uniform can be measured with the device.

It is concluded that the small optically-powered probe and its filtered measurement receiver provides a system for the measurement of magnetic fields over a practical range of values, with the advantage of electrical isolation.

### 3. MODIFICATIONS TO ELECTRIC FIELD METERS

While most of our efforts during 1987 were on the development of a magnetic field meter, we did spend some time improving both the ac electric field meter and the dc electric field meter that were developed earlier. The improvements to the ac meter were in the design of the receiver; the probe of the dc field meter was improved by making it even smaller. These changes are described in this section.

#### 3.1. AC Field Meter

The probe of the ac electric field meter was as small as it could conveniently be made (2 cm diameter). However, improvements were made to the receiver system as it was being modularized to accommodate the magnetic field probe.

##### 3.1.1. Synchronous Detector

During the 1986 and 1987 development of the electric field meter system, the synchronous detector was improved by the use of a circuit known as the conditional inverter. This circuit enabled us to simplify considerably the design of the ac electric field meter as it evolved from the dc field meter, and eliminated the need for offset adjustments in the stages following the synchronous detector. (In the end, this circuit was found to be so good it was retrofitted to the dc field meter.)

The ac synchronous detector differed from its dc counterpart in another, more fundamental respect. Whereas the dc synchronous detector was synchronized to a strong pulse coming from the reflective spot on the edge of the rotating shell of the field meter, the ac detector had to synchronize itself by phase locking to the signal that it was measuring. While both synchronous detectors employed phase-locked loops to achieve their synchronism, the ac version was required to lock onto a signal whose amplitude could vary over several orders of magnitude. This proved to be rather difficult to achieve. The result of slight frequency drift in the VCO of the phase-locked loop was an uncontrolled phase error between the switching signals and the signal being measured. The effect of this phase error was a measurement error, which became increasingly large as the signal became smaller.

The opportunity to redesign the VCO was therefore taken when the requirement to modularize this board arose. Figure 3-1 shows the new ac synchronous detector, and includes the new design for the VCO.

It will be noticed that the VCO in this case is running at a much higher frequency than the 60 cycles to which it is being locked. In fact, the center frequency of the VCO is 245.76 kHz, and a ripple counter is used to divide down to 120 Hz ( $245760 \div 2^{11}$ ) and 60 Hz ( $245760 \div 2^{12}$ ). Because of the kind of frequency division employed, the phase relationship between the 60-Hz and 120-Hz signal is fixed and can be used in a simple clocking circuit, as shown in the figure, to generate the required 90° phase shift between the two 60-Hz pulse trains driving the switches of the conditional inverters.



The remainder of the circuit is the same as its predecessor. The magnitude of the incoming signal is given directly by the output of one of the conditional inverters, which is filtered using a passive filter. The signal from the other conditional inverter is amplified and used as the error voltage to hold the VCO in lock.

Experiments have shown that this system is very much more stable than its previous implementation. The phase error over the temperature range likely to be encountered in normal use (0 to 40°C) is negligibly small.

### 3.2. DC Field Meter

During 1987, changes were made to both the receiver of the dc field meter and the probe. These changes are described next.

#### 3.2.1. Data Channel

The general configuration of the data channel for the dc field meter is identical to that for the ac. There are, however, two differences. First, the free-running frequency of the VCO is higher in the case of the dc field meter and, second, since the rotation frequency of the probe is almost an order of magnitude higher than the 60 Hz expected from the ac equipment, the cutoff frequency of the low-pass filter which follows the phase-locked loop is set somewhat higher.

These changes result in the employment of slightly different values on the dc implementation of the data channel board. The resulting values are shown in Figure 3-2.

#### 3.2.2. Synchronous Detector

As we modularized the measurement systems for the ac and dc electric and magnetic meters, we were given the opportunity to redesign all of the electronics. However, since our 1987 objective was the development of a magnetic field meter, not the improvement of earlier electric field meters, only minor modifications were made to the existing designs.

In the case of the dc electric field meter, the most significant improvement to the synchronous detector circuitry was the addition of a system of colored lights to indicate whether the speed of the probe was within normal operating limits. Most of the circuit shown in Figure 3-3 is identical to its predecessor. However, in addition to providing a tachometer signal for a front panel meter (in this case, switched in the receiver to one of the meters ordinarily used to indicate one of the components of the electric field), the tachometer signal is also furnished to an arrangement of operational amplifiers used to indicate high and low speeds.

These operation amplifiers are contained within U3, as shown in the figure. The first stage is used to generate a nominal zero voltage when the probe is running at the proper speed. This is done in a very straightforward inverting configuration with an offset adjustment potentiometer. The two remaining stages operate open-loop, and compare the actual voltage on the output of the first stage with the voltage on an offset control.

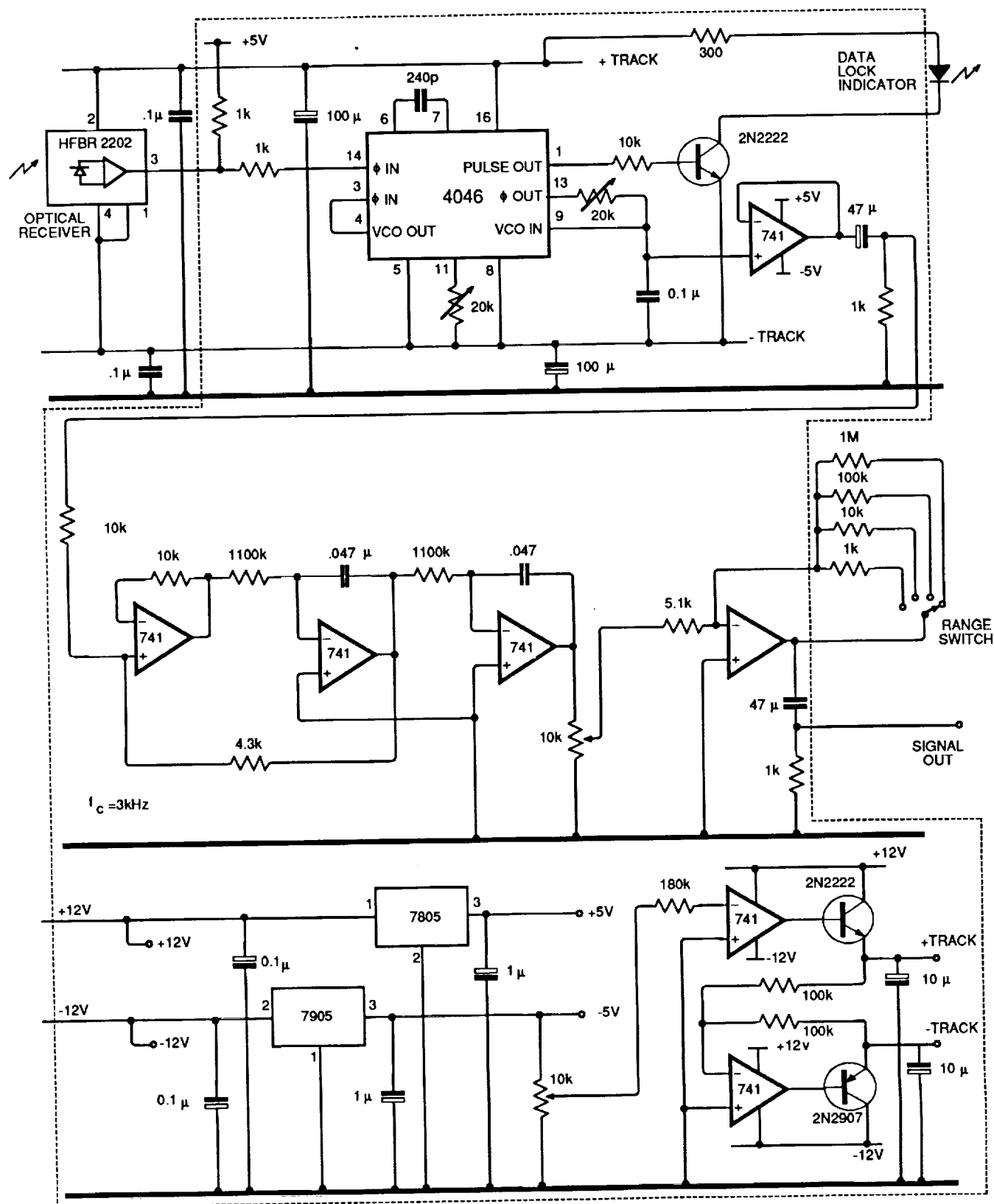


Figure 3-2. DC field meter, data channel

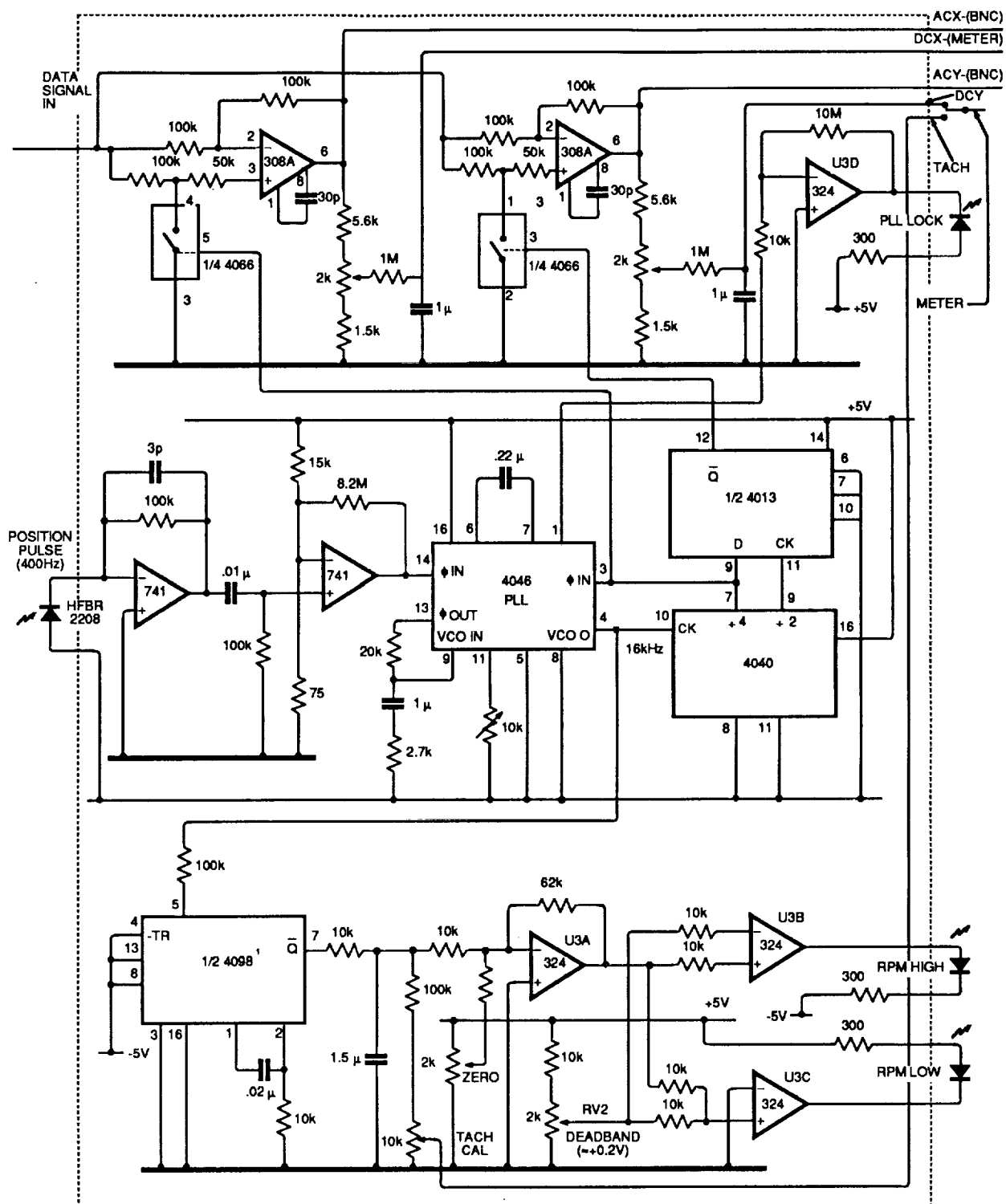


Figure 3-3. DC synchronous detector board

Operation is as follows: During normal operation, the tachometer circuit provides a negative voltage which increases as the speed of the probe increases. The first amplifier in the speed-indicating circuitry inverts this, and provides nominally a zero voltage at the correct speed, positive voltage if the speed is high and a negative voltage if the speed is low. The comparator stages are arranged so that both the high and low limits are set by one potentiometer. Deadband control potentiometer RV2 provides a positive voltage on the order of 0.2 volts. The "low" indicator stage, U3C, examines a voltage midway between the offset tachometer voltage and the deadband voltage.

Since the deadband voltage is positive and the tachometer voltage is normally zero, the mid-point voltage is slightly positive. This voltage is applied to the non-inverting input of an open-loop amplifier so that the output of the amplifier will be high, and the LED attached to that stage will not light. However, if the tachometer voltage becomes slightly more negative than the deadband voltage is positive, the mid-point voltage will be negative, the output of the open loop amplifier will be negative, and the LED will be applied between the plus and minus supplies. Therefore it will light, and can be used as an indication of low speed.

The other speed indicator light is connected to another open loop amplifier, U3B, that measures the difference between the deadband voltage and the tachometer voltage. If the tachometer voltage is zero and the deadband voltage is slightly positive, this difference is equivalent to a positive voltage at the inverting input of the stage; in other words, a negative voltage will appear at the output. There will be no output from the LED. However, if the tachometer voltage becomes more positive, since it is applied to the non-inverting terminal of the amplifier, the output of the amplifier becomes positive and the LED will light. This occurs when the tachometer voltage is more positive than the deadband voltage, so that the indication on the two LEDs is symmetrical about the values set by the offset potentiometer.

In operation we have found this light indication method to be a very convenient way of monitoring the speed, without the necessity to read a tachometer.

### 3.3. Considerations of Probe Shape

If a conducting sphere is inserted into a uniform electric field, the field at the surface of the sphere is intensified to a value three times the undistorted value at the two polar points on the sphere. This is true whether the field is ac or dc, provided there is no charge accumulated on the sphere. If an infinitely long cylinder is inserted instead, the field intensification has a factor of two, provided that the axis of the cylinder is at a right angle to the direction of the field.

Our early work on the measurement of dc electric fields in air showed that the effect of the image of accumulated charge would be reduced if the diameter of the conducting cylinder were reduced. Consequently, the designs of the dc field meter produced by this group over the last couple of years have evolved towards thinner and longer geometries.

It became clear during the development of the ac electric field meter that some allowance should be made for the possibility that the electric field has a

component along the axis of the measuring instrument. While the general shape of the field may be known approximately beforehand, it is impossible to state *a priori* that there is no component of the field in the axial direction. In the case of cylindrical geometry, the field enhancement in the axial direction greatly exceeds two or three, and can only be reduced by improving the aspect ratio of the cross section of the probe, that is to say, making it wider and shorter, rather than thinner and longer. The ultimate evolution in this direction is, of course, the sphere.

It was decided in 1987 that some improvement in the overall performance of the dc field meter system could be made by shortening the probe. This change would be mechanical in nature only. The entire optical and electrical system was to remain unaltered.

The probe electronics were housed in a cylinder of 2 cm diameter and 4 cm length. In the prototype probes, the fixed part of the housing extended the total length of the probe to approximately 10 cm. In other words, more than half of the probe length consisted of mechanical support and was not part of the measurement system.

It was decided to redesign this nonrotating portion to shorten the probe as much as possible. Figures 3-4 through 3-6 show the old and new probes, exploded and assembled. It can be seen that the new probe system is only 5 cm long, approximately half the length of its predecessor. This has been accomplished with no loss in performance; indeed the hardware is simplified so that manufacturing costs are reduced considerably.

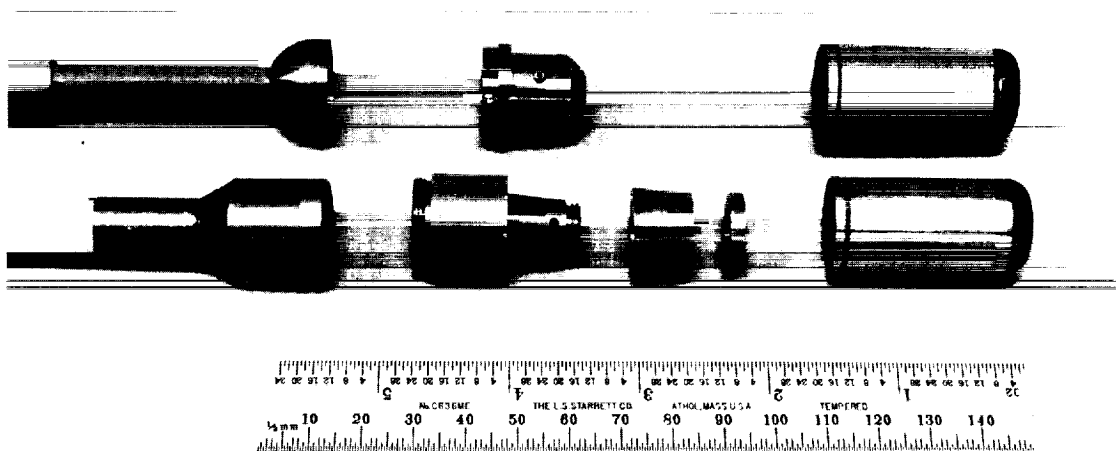


Figure 3-4. Exploded view of probes

This simplification in construction is evident in Figure 3-4. Whereas the nonrotating portion of the dc field meter previously contained four machined brass components, it now contains only two, both of which are somewhat simpler. In Figure 3-4 the inlet and exhaust passages for the turbine are machined into a tapered component (on the inside, so that they cannot be seen in this figure) which is slipped over another tapered component and held in place with a locking ring. It is essential that these tapered components fit together accurately, since they contain the high-pressure and low-pressure sides of the

turbine air. The machining of these grooves and tapers proves to be an unnecessary complication in the single piece design above.

High pressure air is admitted into the brass housing by way of a simple drilled hole. This hole is parallel to the axis of the device, and is a blind hole. A radial hole is drilled through the blind hole into the center of the housing to admit high pressure air to the HP side of the turbine. The point at which the radial hole cuts through the outside of the housing is plugged with a set-screw. (This screw can be seen in the figure.) The low-pressure exhaust from the turbine is effected simply by a number of holes drilled radially through the housing at the position of the low-pressure exhaust. The exhaust air flow then provides a cushion of air and slight pressure between the brass housing and the rotating shell. One of the exhaust holes (there are three in the prototype) can be seen in the figure.

Further savings in complexity and length are effected by a redesign of the fiber-optic ferrules and drive air supply which, in the modified design, are all housed in a hemispherical end of diameter 2 cm. Figure 3-5 shows a cross section through the original housing and the modified one, and shows how the ferrules for the fiber optics and the air supply have been modified to allow for this much shorter length.

Figure 3-6 shows the assembled probes. In the figure, the dark material at the right end of each probe is a conducting paint used to reduce the field intensification at that end of the probe.

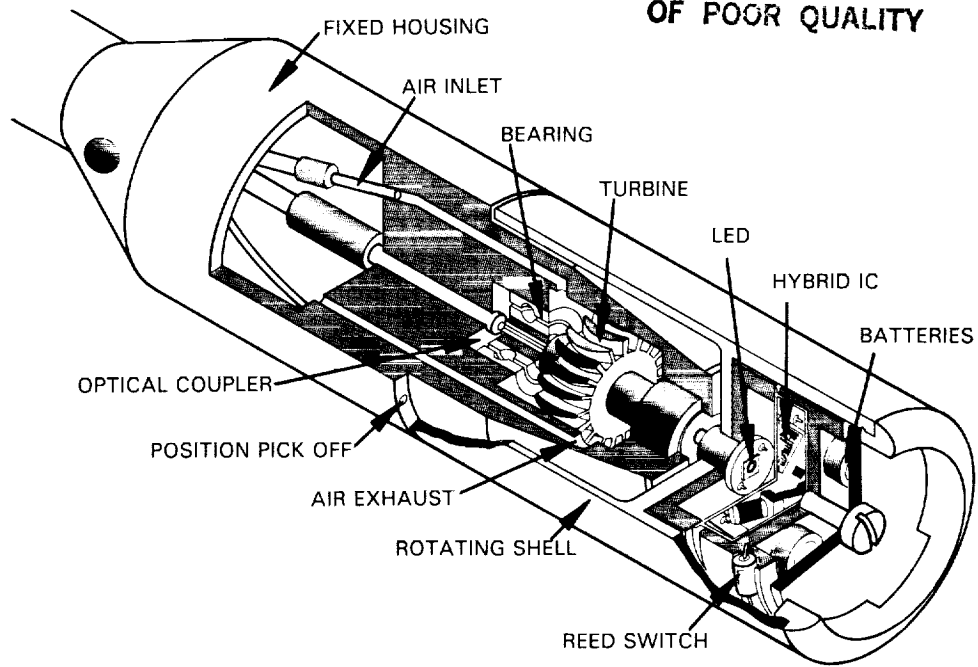
#### 3.4. Suggestions for Future Work

The new dc probe and meter system were taken to a high voltage laboratory operated by ASEA in Sweden to participate in tests that were being conducted on a high voltage dc bushing. Details of these tests are contained in Appendix A. While these tests were being performed, a number of possible improvements were discussed.

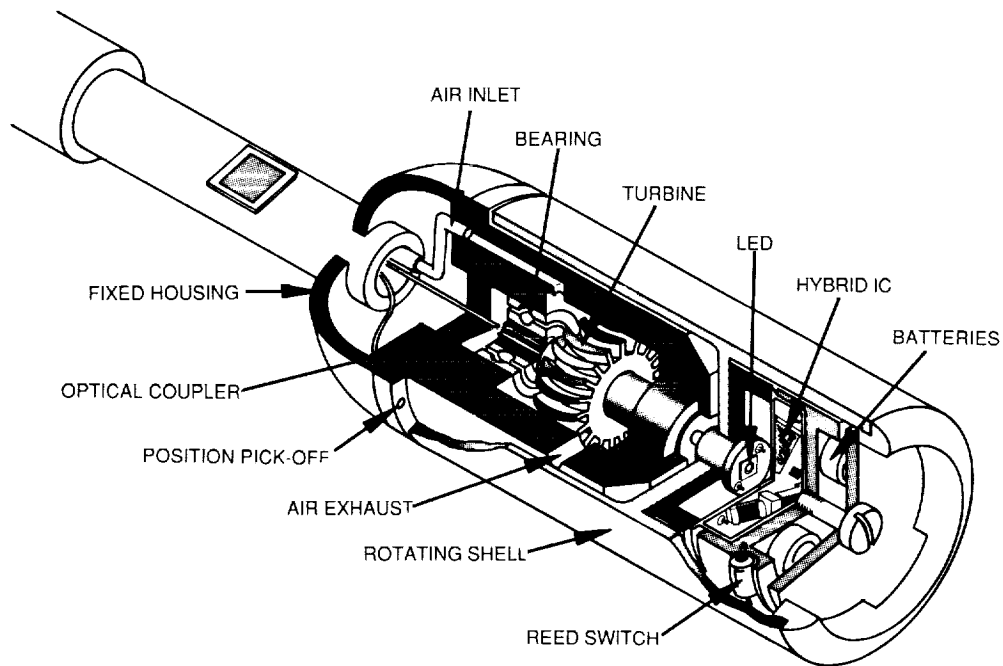
In the present implementation of the dc field meter system, the speed of the rotating probe is controlled by means of the air pressure in the turbine supply. In one of our prototypes, this pressure can be adjusted in response to the reading on a tachometer which is permanently available. In another prototype, colored lights are used to indicate when the speed is going out of range, either fast or slow. It would considerably simplify the application of this field meter if the speed control were automated, which would not be difficult to do. Suitable servo valves for air systems operating at the 2-atmosphere level are readily available.

A further improvement (which was suggested by Dr. Sven Hörnfeldt of ASEA) is to put an ac generator on the probe in place of its present battery supply. Since the probe rotates rapidly (24 000 rpm), it is thought that only a relatively few turns will be needed in a permanent magnet type generator to produce sufficient voltage to drive the electronics of the probe. A rather simple configuration of permanent magnets and pickup coils is envisioned, possibly using a three-phase arrangement with germanium or silicon diode rectifiers mounted in the rotating probe. The external magnetic field would be relatively well contained by a proper design of the generator stator.

ORIGINAL PAGE IS  
OF POOR QUALITY



(a) Original design



(b) After shortening the housing

Figure 3-5. Cutaway isometric views of probe

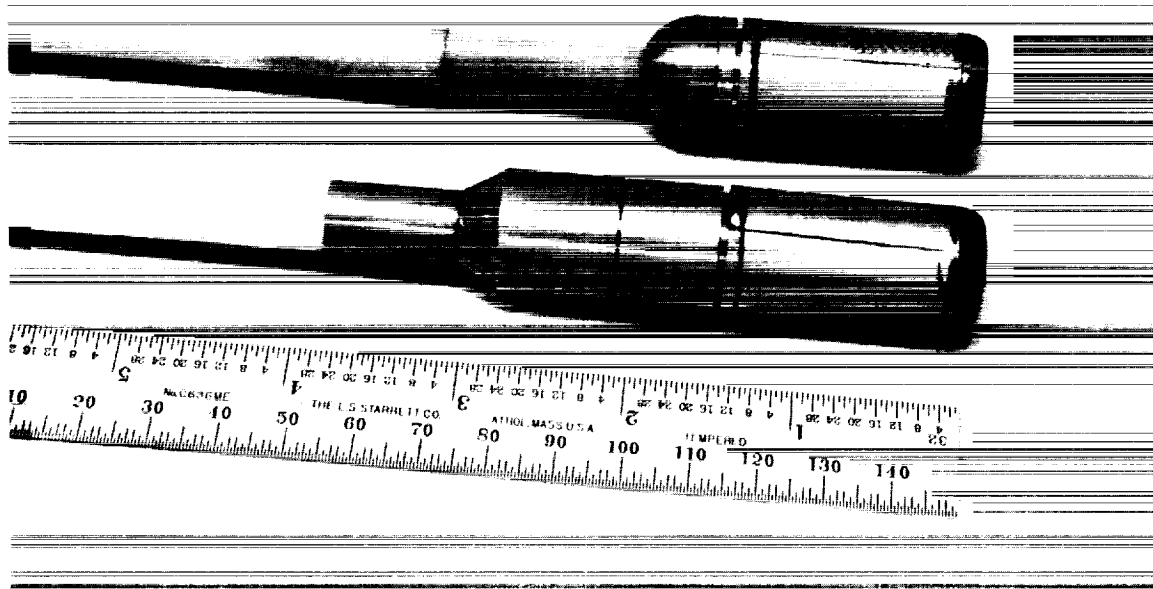


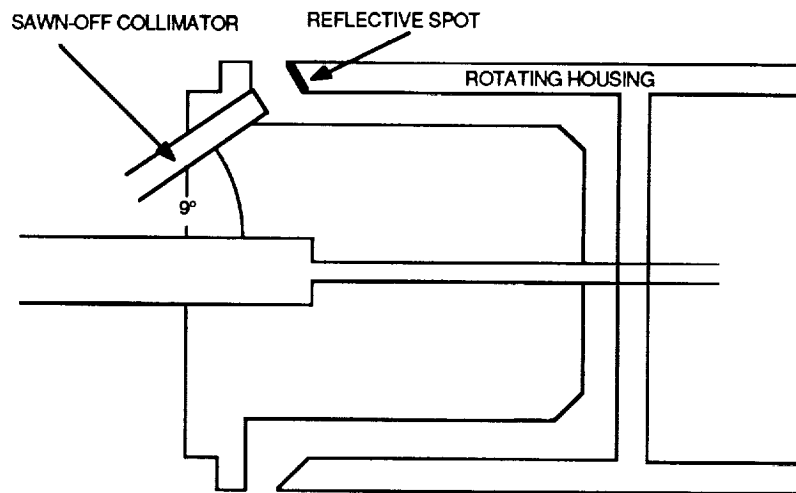
Figure 3-6. Photograph of assembled probes

During the tests in Sweden reported in Appendix A, some problems were experienced with the phase-locked loop associated with the position pulse. Since at the time the probe was in an environment of high wind and considerable rain, it may reasonably be supposed that this failure was due to water being deposited on the collimator lens of the position-sensing fiber. This supposition is supported by the fact that the position pulse system spontaneously recovered from its problem after approximately half an hour.

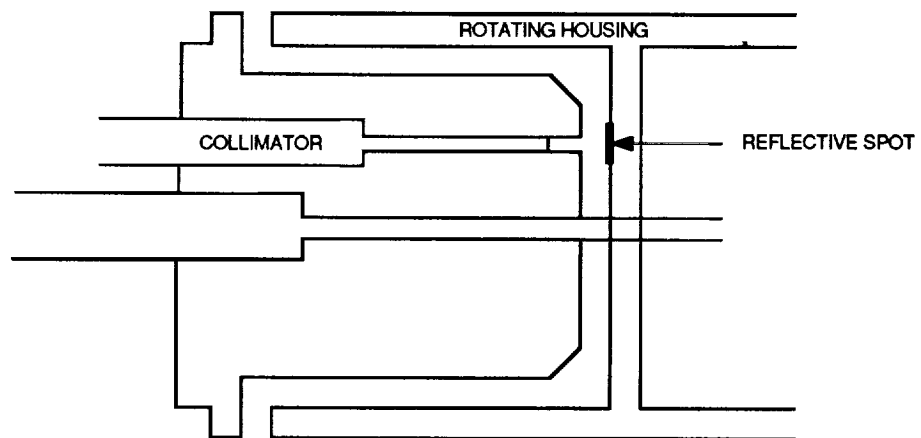
A further redesign of this portion of the probe has therefore been undertaken. The idea for the modified position pulse system is shown in Figure 3-7.

Since in the modified design there is no straightforward way to adjust the angle of the collimated beam coming from the fiber, alignment of the beam with the reflecting spot would be difficult. It will be necessary to design the reflection system to ensure that a sufficient fraction of the light impinging on the reflective spot returns to the collimator without careful adjustment. This would be practically impossible to do with an ordinary mirror.

To solve this problem, it will be necessary to test a number of different reflective surfaces to see which has the most promise as a reflective spot in our position indicating system. This work will be reported later.



(a) Original design



(b) Proposed improvement

Figure 3-7. Modified position pulse system

PAGE \_\_\_\_\_ INTENTIONALLY BLANK

#### 4. CONCLUSIONS

In January 1988, the emphasis of the fiber optics work being done by the Communications and Control Project changed. The development of hardware to measure electric and magnetic fields in air came to an end, and work on distribution automation applications of fiber optics started. Apart from some loose ends that need tidying up, we shall not be addressing the problems that have so fascinated us for the last few years. Therefore, in addition to describing the work done in the last year, it was considered useful to include an overall summary, or history, of the project's work in the area of field measurements.

##### 4.1. DC Field Meter

The dc electric field meter was the first power line field meter we developed. The rotating field mill meter evolved principally in 1984, 1985 and 1986. Until the DOE/JPL meter was developed, measurement could not be made of dc electric fields in air outside of the surface of the ground. The availability of the meter was thus a milestone in the experimental investigation of dc electric fields.

In 1984 and 1986, we took our various dc electric field meters to the General Electric High Voltage Transmission Research Facility (HVTRF) in Lenox, MA, for tests in a realistic power line environment. In 1984, the meter was the one we called the Beer Can, 20 cm long and 8 cm in diameter. In 1986, it was the miniaturized turbine-driven probe, 10 cm long and 2 cm in diameter. On both occasions, our equipment had generally correlated well with the fixed instrumentation of HVTRF, but had given lower values for the field.

An experiment that might have helped us understand the difference between the readings of the JPL meter and the fixed instrumentation of the HVTRF was performed near Sylmar in February 1987. Sylmar is the southern terminus of the Pacific Intertie, a combined system of two ac lines and one dc line running between the Pacific northwest and the Los Angeles area. It is the closest dc line to Pasadena. Unfortunately, highly variable winds and a light rain at the time of the test caused the electric field under the line to vary considerably. It was impossible to sort out the effect we were looking for from the random field fluctuations.

A much steadier field was measured later in February, at the Grizzly test site of Bonneville Power Administration. This site is near the northern end of the Pacific Intertie. On this occasion, our field meter gave readings that were a little higher than the fixed instrumentation.

We do not understand all of these differences. Since the discrepancies between our readings and the "accepted values" were in the order of 10%, no one was inclined to be particularly concerned as the tests were being performed. However, unexplained differences demand at least some attention. Since some of the higher readings could have been caused by the simple fact of leakage down the pole supporting the probe of our meter, we did investigate this problem during 1987. With splices of PTFE (trade mark Teflon) between segments of G-10 fiberglass, the pole can be made almost leakage free. We also redesigned the probe housing late in the year, and produced a new version only 5 cm long.

Dr. Jan Martinsson, Director of Research and a Vice-President of ASEA, the Swedish electrical manufacturer, visited our laboratory in October 1987. His purpose was to see our dc field meter in action. The measurement of the field near high voltage insulation systems was needed to provide data that could help understand some anomalous flashovers that have been occurring on dc bushings. There is presently no other device that can make this measurement.

We were invited to participate in tests at the ASEA high voltage laboratory in Sweden in November. This was a unique opportunity for a JPL-developed measurement system to contribute to one-of-a-kind tests. The JPL field meter was installed near the central part of a 600-kV bushing, and field measurements made with the bushing energized at various voltages, both wet and dry. The results indicated that (1) the flashover problem is almost certainly due to non-uniform wetting of the insulator and (2) a device like our field meter can furnish useful data. Fields as high as 220 kV/m were measured by the JPL probe, with enough water in the vicinity to cause visible corona. A report on this work is included as Appendix A.

#### 4.1.1. Significance of the DC Field Meter

An important result of this work is the confirmation that dc and ac behave very differently. For some while, it has been known that insulation systems stressed with dc perform differently than those with ac applied. The results obtained in Sweden confirm that difference.

A simple insulator can be visualized as a column of nonconducting material between two conducting plates. If this system is stressed with ac, the voltage between the plates divides uniformly in the air next to the insulating column, and uniformly in the material of the insulator. Suppose the insulator is 2 m long, and has 200 kV applied. If one could measure the voltage along the insulator or in the air next to it, one would find that for every cm moved, one gained 1 kV. If the insulator were made of several pieces in series, the voltage division would be dominated by the capacitance of the segments. While the capacitance of a high voltage insulator is very small, its resistance is so high that, even at power frequencies, capacitance becomes the determining factor in voltage distribution.

When the same insulator is stressed with dc, the voltage distribution is determined by the dc resistance of the material, and by any charge trapped on its surface. The bulk resistivity of most insulators is so high that, for all practical purposes, surface conditions determine voltage distribution. The capacitance of series segments becomes unimportant, but cleanliness of surface can be crucial.

To some extent, it is impossible to build a high voltage insulator that will work for dc. Surface conditions may dominate the performance of an outdoor insulator, but cannot be predicted at the time it is made. Some companies have tried to control the surface conditions of their insulators by deliberately making them slightly leaky.

Insulators stressed with dc and ac behave differently. It can be said that, in this application, dc is not well understood. An understanding of what is happening to an insulating object cannot be obtained by making measurements at

the ground. To begin with, no information about the direction of the field can be obtained with most grounded instruments, because the field is always simply perpendicular to the instrument. Nor can the object be modelled by comparing it with ac results. Only experimental results, showing field magnitude and direction away from the ground, obtained with dc stress, will improve our understanding of how systems work with dc applied.

Insulators are not the only application area for the instrument: it might also be useful in animal studies. Since most of the animals that are used to model humans in the power line field-effects studies are mammals, they are covered in hair or fur. These materials are extremely good insulators. (It may be remembered how rubbing a cat's fur with amber is used to demonstrate static electricity.) Real dc lines produce free ions in air. Therefore, trapped charge on the surface of the animal is inevitable. The question of how this charge modifies the field, and vice versa, cannot be answered without free-body measurements.

Because of its small size and wide dynamic range, the DOE/JPL field meter can provide answers to questions in many areas. A photograph of the latest version of the dc field probe is shown in Figure 4-1. It can be seen that the probe is much shorter than earlier versions, leading to less field enhancement in the axial direction. The square object on the pole is the polonium ion source, used to couple the probe to the air potential.

#### 4.2. AC Field Meter

The first prototype of our ac electric field meter was finished in 1987. This meter is based on the dc field meter, and uses much of the same technology. The meter probe is much smaller than any available until now, and has a dynamic range approaching that of the dc meter — about 100 dB.

The pacing item on this task was the power supply. The probe is powered by light, converted from infrared radiation by gallium arsenide photodiodes. The original intention was to use an array of diodes fabricated at JPL as an integrated circuit. This proved to be a lengthy development. Eventually, it was decided not to wait any longer for the integrated circuit array, but to power the probe by a hybrid array fabricated from discrete diodes. While this approach is less efficient, it did get us a working ac field meter.

One of the advantages of powering the probe by optical means is that the diode array is a very small power source. This enabled us to produce one of the smallest field meters ever made. In terms of probes with active components inside them, ours is probably the smallest one ever built. This means that it can measure close to objects in the field, and can provide better spatial resolution than most earlier instrumentation.

A problem with the optical powering of the probe of the ac meter was that the voltage generated by the photodiodes was very sensitive to vibrations in the fibers energizing them. The fluctuations in the voltage resulted in noise in the signal coming from the probe. This noise had a de-stabilizing effect on the phase-locked loop that generated the 60-Hz switching signals for the synchronous detector. The problem was particularly acute when only a small signal was available.

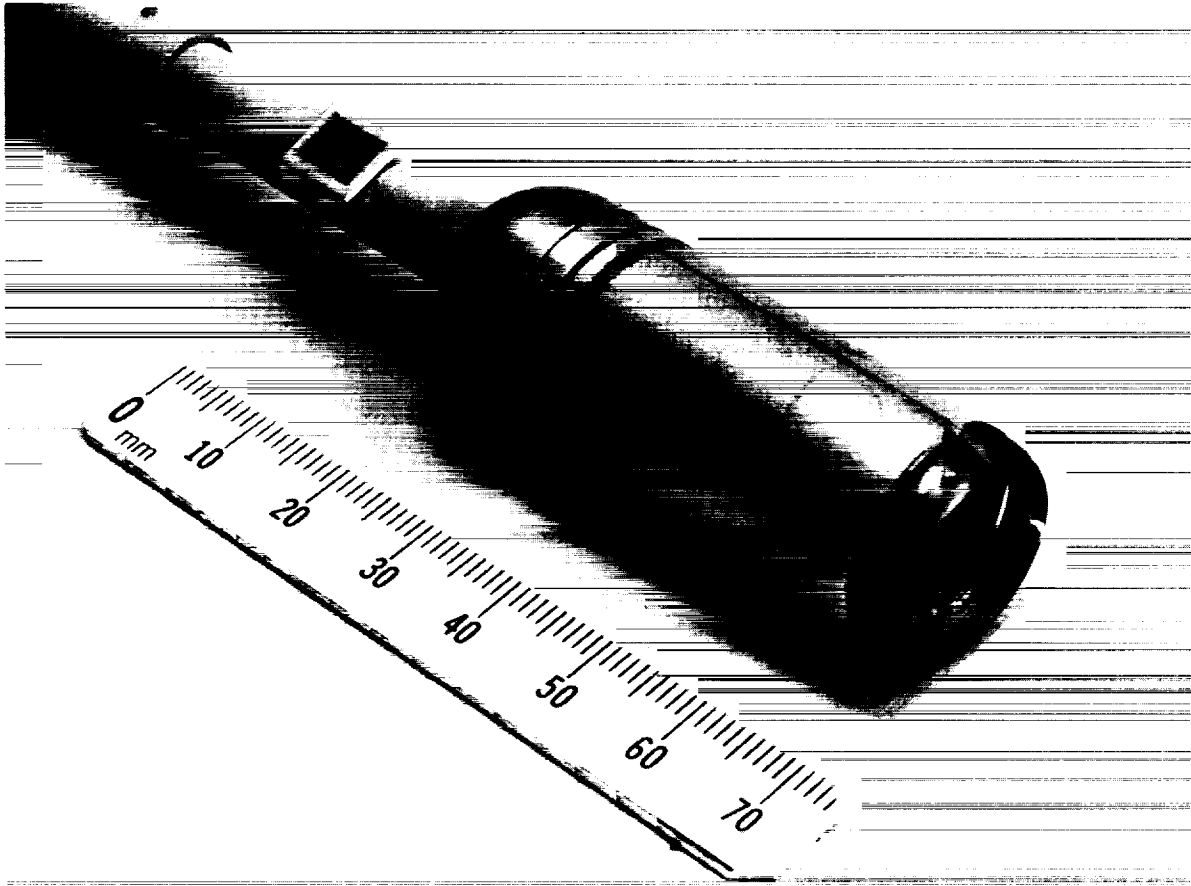


Figure 4-1. DC electric field meter probe

The solution was to regulate the supply. This was not easy to do, since zener diodes at the low voltages in use are not particularly "sharp". However, an "active zener" (actually a band-gap voltage reference) was found, with suitable characteristics. The use of this system of regulation has solved the problem.

A further performance improvement was obtained later in the year when we developed the multi-purpose receiver for field measurements. This unit was capable of accommodating the signals from the dc electric field meter, the ac electric field meter and a new ac magnetic field meter. Some drift problems in the receiver were fixed, and the range of the ac electric meter was extended down below 5 V/m.

Because the ac field meter probe is spherical, it is possible to calibrate it from first principles, rather than by inserting it into a test cage with known parameters. Following calibration, the meter was taken to the National Bureau of Standards, in April 1987. Dr. Martin Misakian of NBS set up a calibration test for the meter, and the accuracy of the calibration was checked.

It was thought that the field to which the meter was exposed was known with an uncertainty less than 0.5%. Our meter was within this tolerance on the range for which it had been calibrated. The difference in readings was a little

higher on the other range tested; to simplify calibration, the meter has only one scale adjustment.

The meter was taken to AEP's Ultra High Voltage Test Station in Indiana in May 1987. Tests were done to examine the field near ceramic insulators, and in a biological test chamber used by AEP. Only a small meter like ours could have made these measurements.

The meter showed that small fluctuations with spatial variations of only a few centimeters could be detected in the test chamber. No such fluctuations were observed alongside the insulator string, at least at a distance of a few cm outside the skirts of the insulators.

A photograph of the probe, with half of the electrode structure removed, is shown in Figure 4-2. The photodiode arrays can be seen, as well as the three fibers used (two to bring power in and one to take data out of the probe).



Figure 4-2. AC electric field meter probe

#### 4.3. Magnetic Field Meter

During 1987, a report on the biological effects of power line fields was published by the New York State Power Lines Project. The report suggested the possibility of a link between the magnetic fields associated with the transmission, distribution or use of electric power and some health effects, particularly an increased rate of certain types of cancer.

The linkage between the power line as cause and the increased cancer as effect was far from established and certainly not understood. Nevertheless, the report aroused considerable interest in the topic of magnetic field effects. Further investigations must be made into the possible relationship between power line magnetic fields and health effects, and certainly part of these investigations must be experimental. This provided the motivation for our involvement in the area of magnetic field measurement.

It was thought worthwhile to adapt the ac electric field probe and measuring system to the problem of measuring magnetic fields. This proposed modification would then result in the availability for experimental investigations of an electrically isolated ac magnetic field probe<sup>5</sup>.

One of the several distinctions that can be drawn between electric and magnetic fields is the spectral purity of the field. The ac electric field is predominantly 60 Hz (in the U.S.) and the distortion of that field is limited to a very few percent. Distortion of the voltage waveform corresponds to distortion of the 60 cycle source, which is normally very difficult because the power system generators are designed for constant voltage operation, and the power system has a rather low impedance. In some cases, the limit on voltage distortion is a statutory one, but in most cases, the power system is strong enough to prevent more than a few percent total harmonic distortion appearing on the voltage.

The same cannot be said for the magnetic field. Current is drawn by loads that contain iron, and the nonlinearity of the magnetization curve of the iron causes the current waveform to be rich in harmonics, predominantly the third harmonic. Harmonics are also caused by switching devices, such as speed controllers for small electric motors and light dimmers. These can cause harmonics extending into the RF region. In terms of their energy content, the predominant distortion is the third harmonic caused by iron in transformers and motors. It would seem that to be most useful, a magnetic field measuring system must be capable of furnishing some information about the spectrum of the magnetic field, or at the very least about its third harmonic.

The modification of the probe circuit that we developed for the electric field meters (as a hybrid IC) was completed in 1987. The circuit differs from the electric field version in the first stage. For the measurement of E-field, current is measured in an amplifier with short-circuit input impedance. For B-field, we measure the open-circuit voltage induced in a coil. There is another important difference between the electric and magnetic versions of the probe: new headers for the hybrid ICs for the magnetic version of our field probe had to be made from a non-magnetic material.

The pacing item on the testing of the prototype magnetic field probe was the optical power diode array, as it was on the electric field version. In the end, we found a source of integrated circuit photodiodes suitable for the purpose, and were able to power the hybrid using a commercially available silicon array. It may be expected that more applications of this technique will be reported; considerable interest has been shown in the use of optical power at meetings at which this topic has been discussed.

The probe is shown in Figure 4-3.

---

<sup>5</sup> The almost-stationary magnetic field of the earth typically has a magnitude of several tens of micro-Tesla, a value comparable with that at the edge of the right-of-way of high voltage lines. Since this pre-existing field is so large, and since HVdc lines are so few in number, and produce the same kind of field as the naturally-occurring earth's field, there seemed little to be gained from our developing a dc version of the magnetic field meter. In any case, there are a number of magnetometers available to make measurements of fields of this size, available for use in a variety of applications.

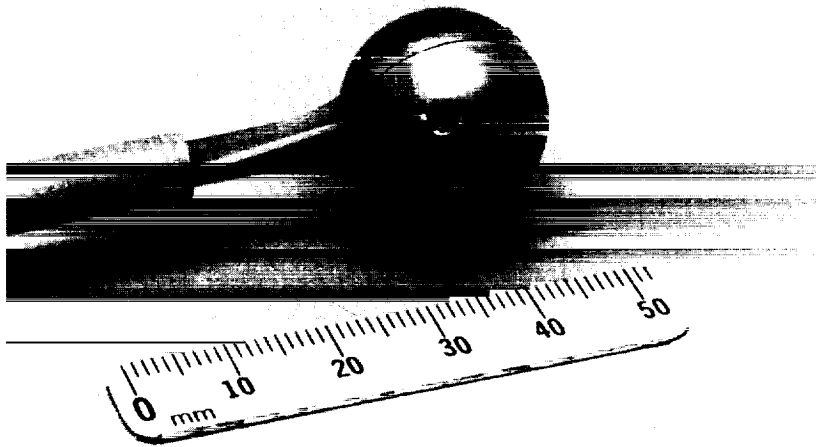


Figure 4-3. AC magnetic field meter probe

#### 4.4. Field Meter Receiver

The electric and magnetic field probes are used in conjunction with a re-designed receiver. The receiver design is different from the earlier electric field meters. Our tests of the magnetic field near domestic appliances (a typical application for a device like ours) show the presence of a large amount of harmonics in the field. Therefore, the measurement system for the magnetic meter was redesigned to facilitate the measurement of fields with a complex waveform. The electric field meters use synchronous detection to increase the dynamic range, and to provide information about the magnitude of the field in two orthogonal directions. This method does not lend itself to harmonic measurements, however. For the magnetic field meter, filters were used to separate the components of the field.

These considerations led us to design a receiver system that could work with any of the field probes we have developed. By swapping a few circuit boards, one receiver can be configured to measure the two directional components of a dc electric field, the fundamental, the second and third harmonics and the wideband energy content of an ac magnetic field, or the magnitude of an ac electric field.

A photograph of the multi-purpose receiver is shown in Figure 4-4.

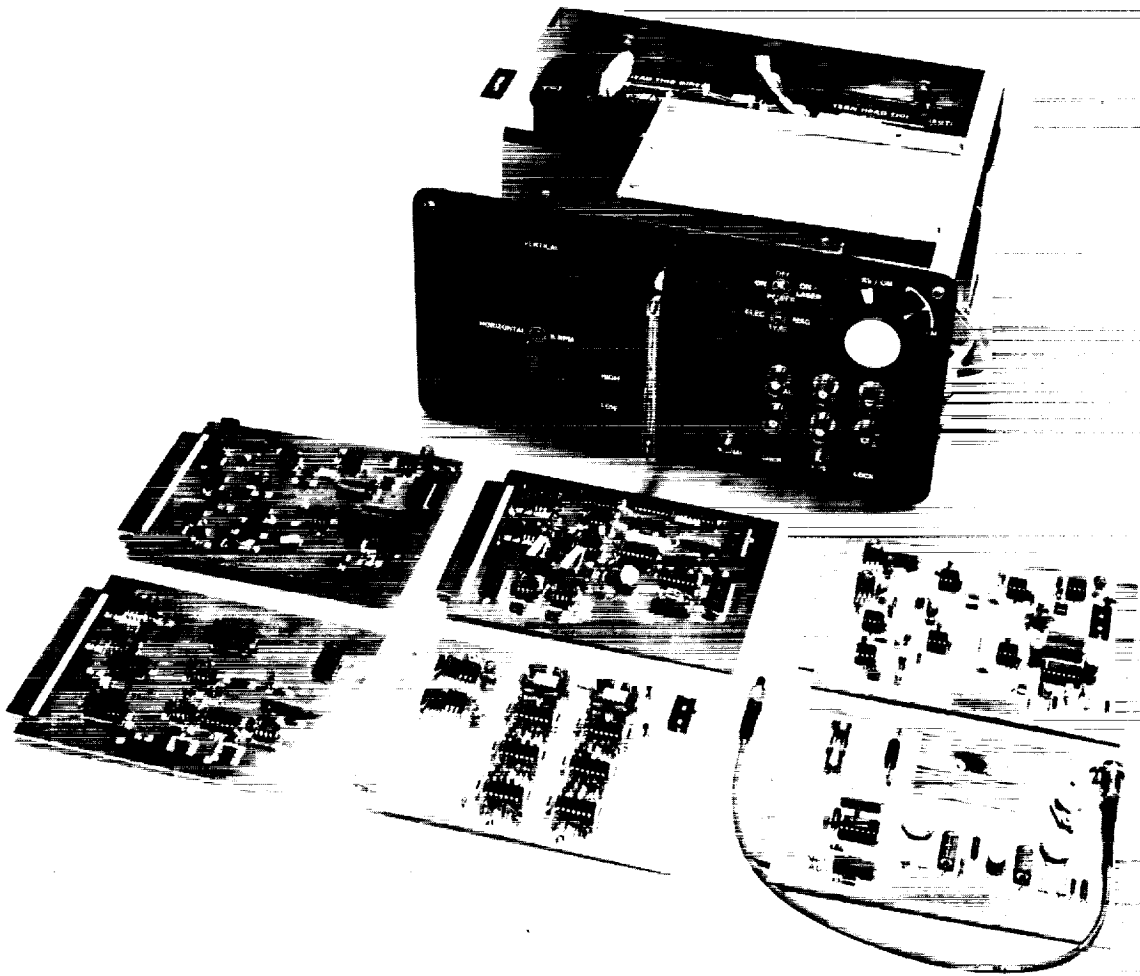


Figure 4-4. Multi-purpose field meter receiver  
From the rear left, going clockwise,  
the boards are Data, Synchronous  
Detector, Data, Laser Power Supply,  
Measurement, Synchronous Detector.

#### 4.5. Summary of Field Meter Results

It was experimentally determined that the dynamic range of the wideband measurement was a little over 3 orders of magnitude (actually 66 dB), from  $1 \mu\text{T}$  to 2 mT (or 10 mG to 20 G). Because of the much narrower filtering used, the dynamic range of the 60-Hz measurement is somewhat over 4 orders of magnitude (about 88 dB), from about 80 nT to 2 mT (or 0.8 mG to 20 G).

It is thought that this is a most useful range for the measurement of low-value fields. If a more sensitive instrument is needed, the 100-turn coil used in our prototype could be replaced with one with more turns. The scaling is simply linear in the number of turns. In our laboratory, increased sensitivity

would not increase the usefulness of the device, since the ambient magnetic field is already higher than the limit of measurements with the prototype meter. It would also be possible to redesign the probe electronics slightly, to allow the use of a 40-dB gain change switch.

#### 4.6. Concluding Remarks

The development of the DOE/JPL field meters has certainly been interesting. The work has taken us into many areas of technology: electronics, optics, physics, aerodynamics, and numerical methods. We have rubbed shoulders with investigators of field effects, and insulation systems.

The instrument that started it all, the space-potential dc electric field meter, was originally intended to put the measurement of dc electric fields in air on an equal footing with ac electric fields. In the end, it seems that our prototypes have actually advanced the state of the art a little: the probe of our dc electric field meter is smaller and has a wider dynamic range than its ac counterparts. The last prototype of the dc electric meter has a probe length of 5 cm, and a diameter of only 2 cm. Measurements made with this meter have already led to an increased understanding of the problems of one kind of dc insulation system.

This device was first adapted to the problem of making a measurement of ac electric fields, and later (following the publication of the final report of the Scientific Advisory Panel of the New York State Power Lines Project) to the measurement of magnetic fields. Because of its origins, the probe of the DOE/JPL magnetic field meter is electrically isolated from the receiver.

Finally, the development of these meters has demonstrated that an electrically isolated probe, simple enough to be fabricated as a hybrid IC on a very small substrate, and using so little power that it can be optically powered, can be used as the sending end of a moderately accurate fm data link. The system uses readily available parts, and could be assembled by any competent micro-electronics facility. There are indications that there are many other power system applications of such a data link.

~~CONFIDENTIAL~~

**APPENDIX A**

**REPORT ON VISIT TO ASEA, SWEDEN  
November 10-17, 1987**

1705 \_\_\_\_\_ 10/10/10 10/10/10

## APPENDIX A

### REPORT ON VISIT TO ASEA, SWEDEN November 10-17, 1987

From time to time, anomalous flashovers have been observed on high voltage dc insulators and bushings. These flashovers are termed anomalous because, in spite of the fact that dc insulators are bigger than ac insulators, they do sometimes flash over under normal service conditions (see, for example, Lampe, Eriksson and Peixoto, 1984). These flashovers are external to the insulator, and usually cause no permanent damage, but they do result in at least a temporary shutdown of the dc system of which they are a part. No satisfactory explanation for these flashovers has been devised, and they have not been reproducible under laboratory conditions.

In an attempt to understand the mechanism behind HVdc bushing flashovers, ASEA, in Sweden, scheduled a series of tests of a high-voltage dc bushing under dry and artificial rain conditions in their high-voltage hall in Ludvika. Because of the work done by the Communications & Control project on the measurement of dc electric fields in air, Task Manager Kirkham was invited to participate in these tests, and to make measurements of the electric field in the vicinity of the bushing.

This Appendix describes the experimental arrangement and the results obtained.

#### A.1. Background Information

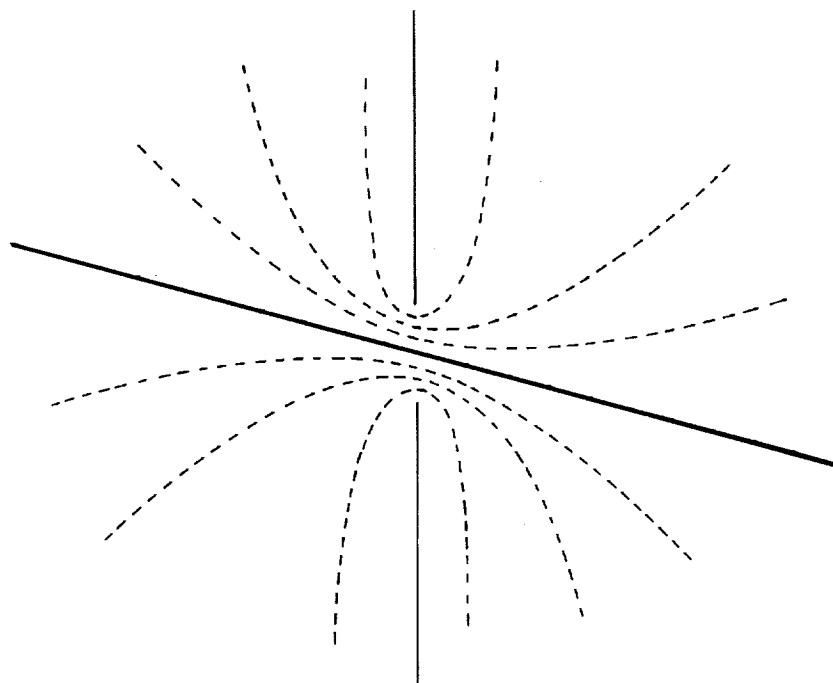
The term "bushing" is applied to the insulating system required to pass a high voltage conductor through a grounded object. This grounded object might be the wall of a building or the tank of a transformer. There are two general principles in the design of bushings. First, the solid insulation inside the bushing (usually oil-impregnated paper) can withstand a higher electric stress than air. Second, the likely weak point in the insulation system is the surface of the insulator (usually glazed ceramic) on the side of the bushing which is exposed to the weather. Because of these design constraints, bushings tend to be long thin objects like the insulator on an automotive spark plug and, similarly, they tend to be asymmetrical, the longer insulation being on the outdoor side.

In the case of a transformer penetration, the asymmetry is most pronounced, since the interior of the bushing is immersed in insulating oil, and the outside is exposed to the weather. The asymmetry is less pronounced in a bushing for access through the wall of the converter station in an HVdc system.

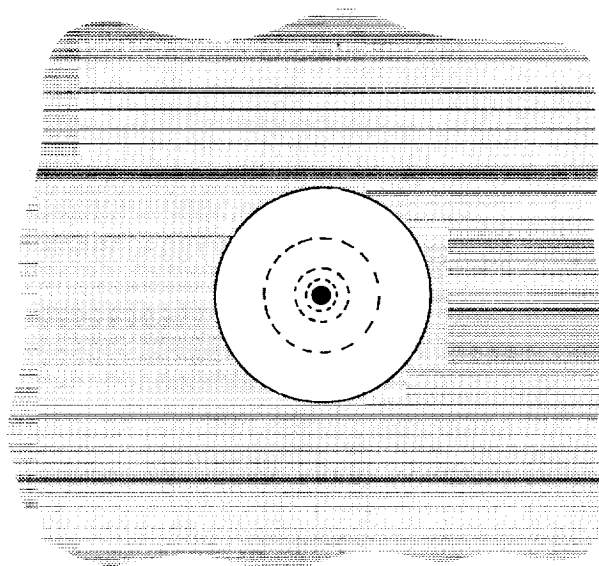
The tests performed at ASEA were of a bushing similar to the ones used on  $\pm 600$  kV systems. Altogether, this device is 15 m long, approximately 9 meters of which are on the outside of the converter station. (The overall configuration of the bushing is shown in Figure A-9).

If we take a cross section through such a bushing, and simplify for the time being by neglecting the presence of the solid insulating material, we obtain an

idea of the potential distribution, as shown in Figure A-1. Because of the presence of the wall, the field is concentrated at the point where the conductor passes through the wall, and unless measures are taken to reduce it, the electric stress at this point may be damaging.



(a) in plane of bushing



(b) in plane of wall

Figure A-1. Cross sections through wall penetration

If we take a cross section through the bushing across the axis of the conductor, at the point where it passes through the wall, we find that the stress is distributed non-uniformly. The highest intensity is found close to the surface of the conductor, and there is a decrease going something like  $1/r$  as one moves away from the inner conductor, as shown in Figure A-1b.

In order to control the stress, and to provide a measure of insurance against material inhomogeneities, conducting cylinders are inserted into the solid insulation in the vicinity of the wall, in such a way that the radial stress is more uniform, and the axial stress is reduced near the wall. Figure A-2 shows the physical arrangement.

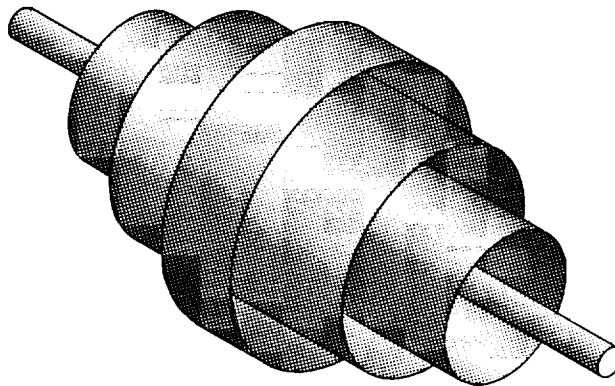


Figure A-2. Grading cylinders inside bushing

In a radial sense, these conducting cylinders have the effect of making the voltage distribution more uniform. If we visualize the system as being energized with ac, it is straightforward to see that the distribution of voltage across these cylinders is governed by the capacitance between them. The cylinders are arranged so that the product of length and radius is constant. This means that capacitance between them is constant, and so the voltage drop across them is uniform. Although Figure A-2 shows only three cylinders, in practice the number of cylinders is about 30 or 40, to give finer control of the electric stresses in the bushing.

If the bushing is energized with dc, it is supposed that the distribution of voltage goes in accordance with the very large, but finite, bulk resistance of the solid insulation material, and follows approximately the same law as that given by a capacitive distribution.

In an axial direction, these cylinders have a much greater effect. Instead of concentrating near the wall itself, the electric field stress is now spread out more uniformly down the length of the insulator. This can be seen from the equipotential lines in Figure A-3, which is derived from a field solution calculated by an insulator manufacturer (Naito, Matsuoka, Ito and Morikawa, 1988).

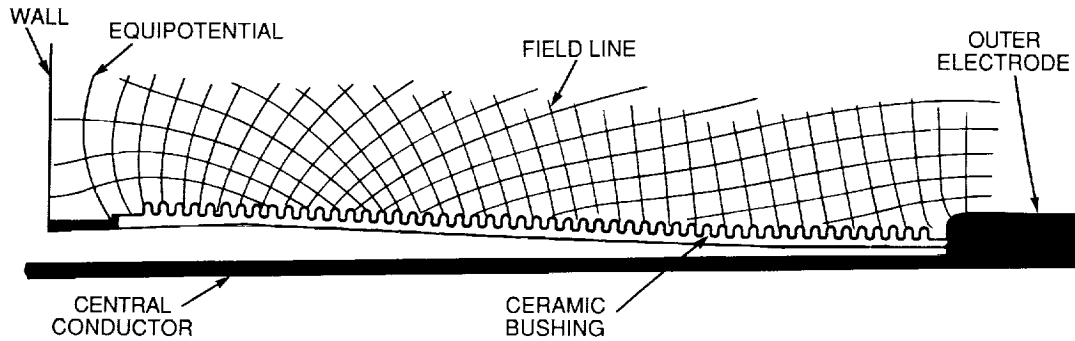


Figure A-3. Equipotential lines of electric field along graded bushing

With this background, we may now proceed to a discussion of the tests performed in Sweden. These tests can be considered in three parts. First, tests were performed at the high-voltage laboratory in Västerås, using two DOE/JPL field meters and a field meter devised by Dr. Sven Hörnfeldt of ASEA. These tests were conducted with the purpose of characterizing the various instruments. Second, tests were made of the high-voltage bushing itself, in the high-voltage hall in Ludvika. It was hoped that these tests would increase our understanding of the anomalous flashover problem. Third, tests were again performed in the Västerås laboratory, in order to calibrate-out non-linearities on the DOE/JPL field meter system that were observed during the experiments at Ludvika.

#### A.2. Initial Tests in Västerås

Tests were performed in the high-voltage hall at Västerås to characterize the DOE/JPL meter in terms of its performance at measuring the high-intensity electric field in the vicinity of a toroidal high-voltage electrode.

A positioning mechanism had been built by ASEA to carry the probe (either the DOE/JPL probe or one under development by ASEA) over a linear distance of approximately a meter in the vicinity of the high-voltage output of the dc supply. The procedure used was to locate the probe a few centimeters from the surface of the electrode, and to record the field readings as the probe was moved away, about 1 m. The data were recorded on an X-Y plotter.

The ASEA field meter system consisted of an electro-optic crystal (manufactured by Sumitomo of Japan) housed inside a rotating, conducting sphere. The sphere comprised two hemispherical electrodes, 4 cm in diameter, which were connected to the voltage terminals of the electro-optic crystal with slip rings. Rotation was effected by means of a dielectric turbine external to the electrode arrangement. The nominal speed was 3000 rpm, and speed was controlled by means of air pressure.

Our tests showed that there were problems with the slip rings. It was concluded after these tests that the performance of the ASEA field meter would not be adequate for the purposes of the subsequent tests in Ludvika. The instrument had been under development for only a short time, and was not completely perfected.

Tests were next performed on the DOE/JPL field meter system. Figures A-4 and A-5 show curves of the electric field as a function of time. Since the positioner moved the probe at a constant speed, the curve can be interpreted (approximately) as field against position.

In Figure A-4, the small high-frequency fluctuations in the field were traced to vibrations of the transport mechanism occasioned by its somewhat abrupt start. In Figure A-5, the motor driving the transport mechanism was inadvertently started in the wrong direction, and the field was measured from a distance of about 4 cm from the electrode up to the surface of the electrode. (The probe was actually striking the electrode surface before the condition was recognized and the motor reversed.) Neither the probe nor the transport mechanism suffered any damage. The electrode was energized at 58 kV at the time.

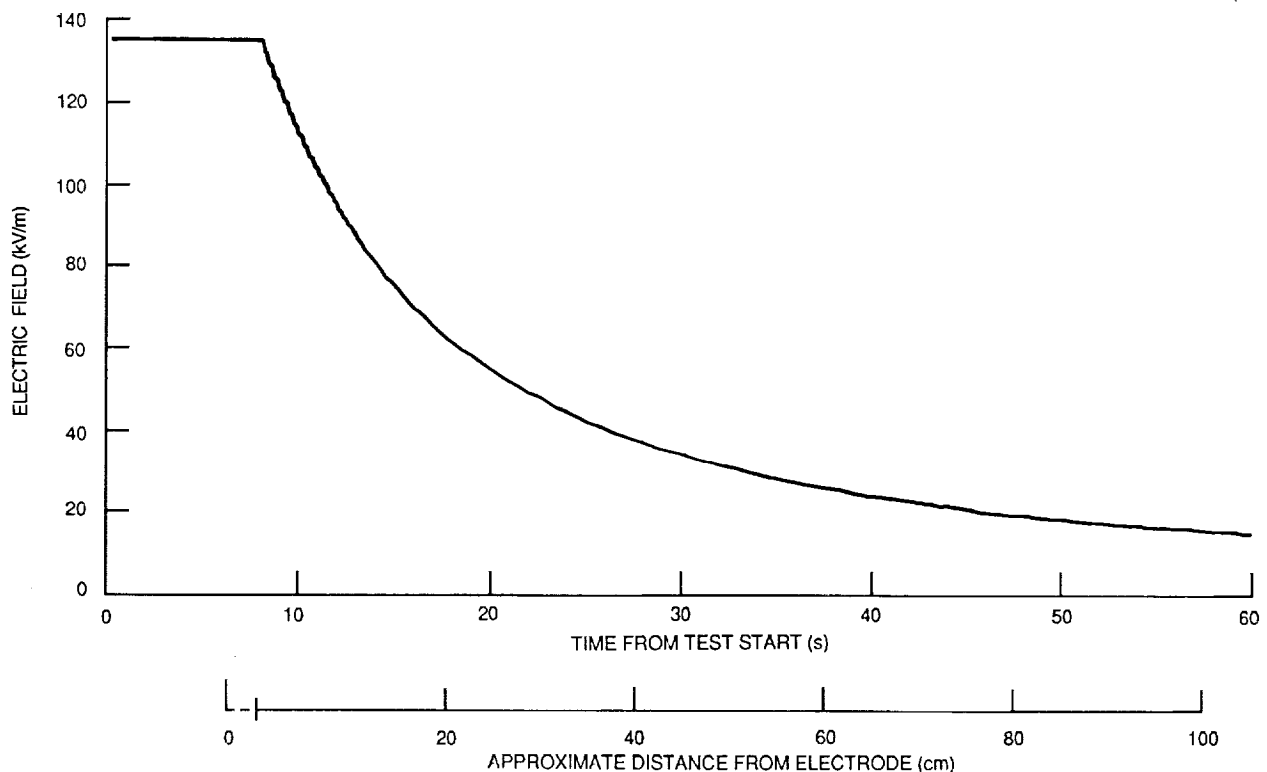


Figure A-4. Results obtained with DOE/JPL meter

The data obtained in these tests in Västerås will be compared with theoretical calculations of the field near the toroidal electrode obtained using ASEA's field-mapping program ACE. An example of the output of this program is shown in Figure A-6.

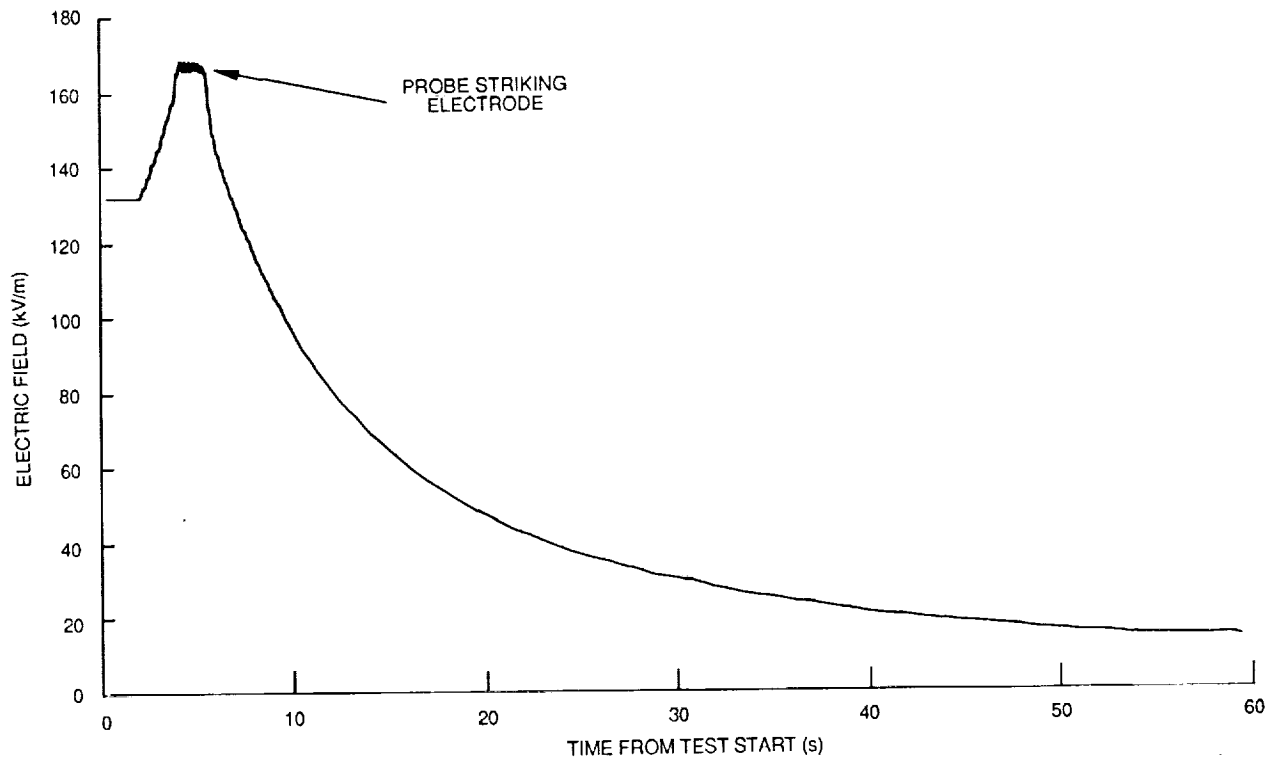


Figure A-5. Results obtained with DOE/JPL meter

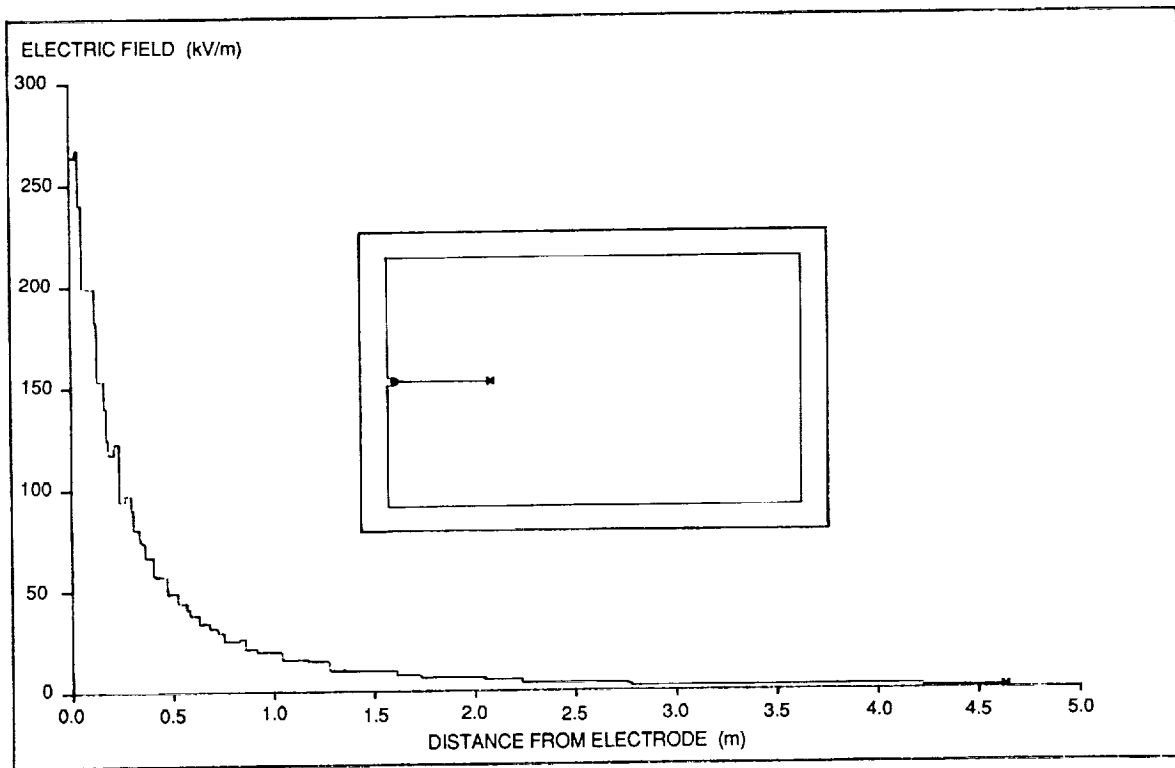


Figure A-6. Calculated field near toroidal electrode (ACE output)

One further series of tests broadly examined the linearity of the probe system at voltages up to 400 kV dc, the limit of the high-voltage supply in Västerås. For these tests, the probe was located 1 m from the electrode and the voltage was varied from 80 kV to 400 kV. These results are shown in Figure A-7.

It may be noted in Figure A-7 that the extrapolated data do not pass through the origin. While it is possible that the field meter is giving wrong readings, this seems unlikely. The field meter output is a 3½ digit display, and the observed offset has not been greater than one digit. It seems more probable that the analog voltmeter on the high voltage supply was inaccurate. However, the offset in the curve was not noticed at the time, so further investigation was not carried out.

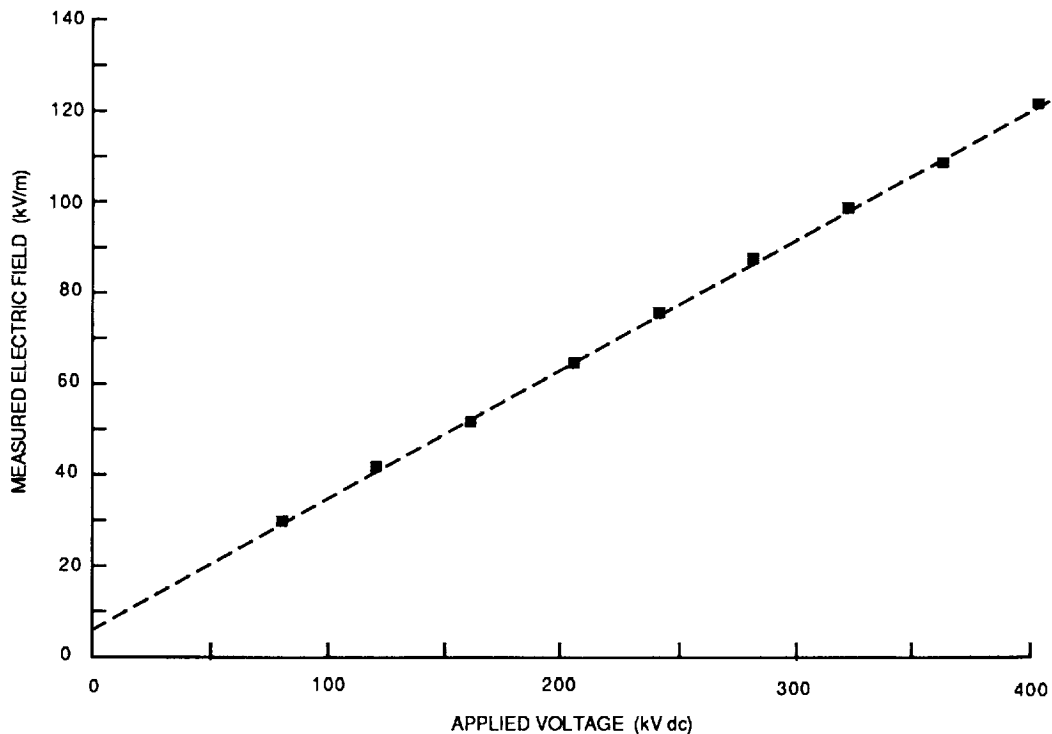


Figure A-7. Linearity tests of DOE/JPL meter

### A.3. Tests at Ludvika

Figure A-8 shows the town of Ludvika and the area occupied by ASEA. In the foreground of the picture is a large rectangular building, which is the high voltage hall. The narrowest dimension of this building is 45 m. Inside, a 55 m long, 35 m high section housed the bushing under test.



Photo courtesy ABB, Ludvika, Sweden

Figure A-8. Ludvika, and the high voltage test facility of the ASEA company

Figure A-9 shows the test arrangement inside the high voltage hall. The bushing itself, some 15 m long, was inserted through an artificial metal wall 13 m wide and 22 m high. The bushing was mounted in the lower part of this wall at an angle of  $15^\circ$  to the horizontal, such that the lowest part of the bushing was 8 m above the ground. The high voltage supply was attached to this low point by means of a rather small wire, estimated to be  $<1$  mm in diameter.

A rain-making apparatus 7 m in length was positioned 6 m above the highest part of the bushing, and a large fan was arranged just above the bushing to blow air away from the wall, to simulate the wind eddies around the corner of the roof of an HVdc converter building.

The field meter probe, mounted on the transport apparatus tested earlier in Västerås, was installed near the center of the bushing just outside where it penetrates the wall. The transport apparatus was able to transport the probe along the axis of the bushing from close to the wall out to a distance of about 2 m. The probe was installed with its axis parallel to the wall, and normal to the axis of the bushing, 50 cm from the outside of the rain sheds on the bushing. The fiber and the air hose were about 2 m radially from the bushing. The fiber connections and the air hose then were passed through the wire mesh wall to the receiver, which was mounted at a height of about 9 m from the floor of the high voltage hall. The outputs of the receiver were connected to the recording instrumentation in the control room by way of coaxial extension cables. This indirect arrangement was used because a set of fiber optic extension cables and connectors, prepared at the last minute before leaving JPL, were excessively lossy and did not work.

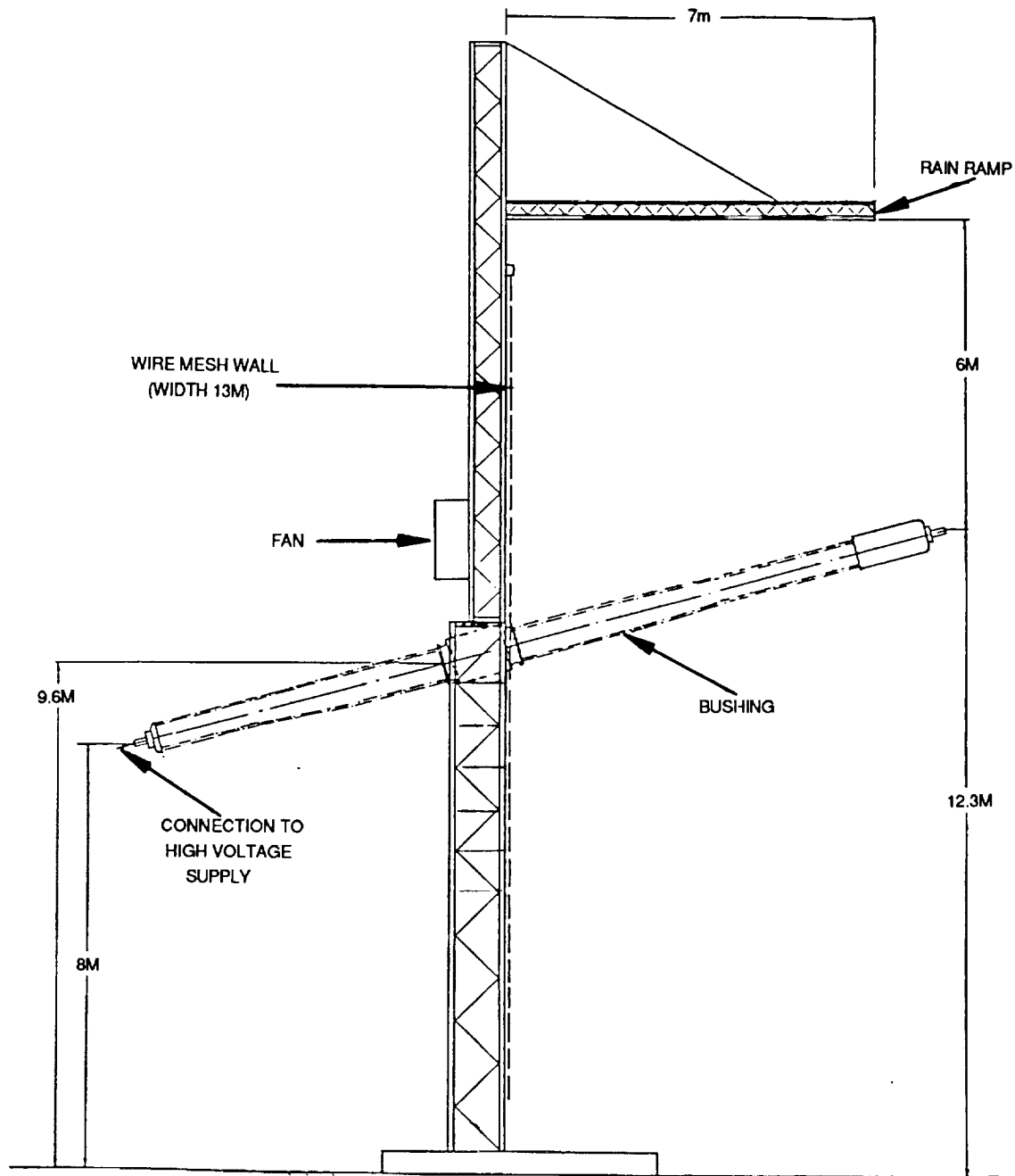


Figure A-9. Test arrangement inside high voltage hall

The test series, which was scheduled to last approximately a week, consisted of energizing the bushing at a number of different voltages up to 800 kV, under both wet and dry conditions. First, tests were conducted with the bushing dry. There was an opportunity to scan the electric field over the 2-m area near the wall at both 300 and 500 kV. These results are presented in Figure A-10. The origin of the position scale (i.e., the position of the wall) has been estimated.

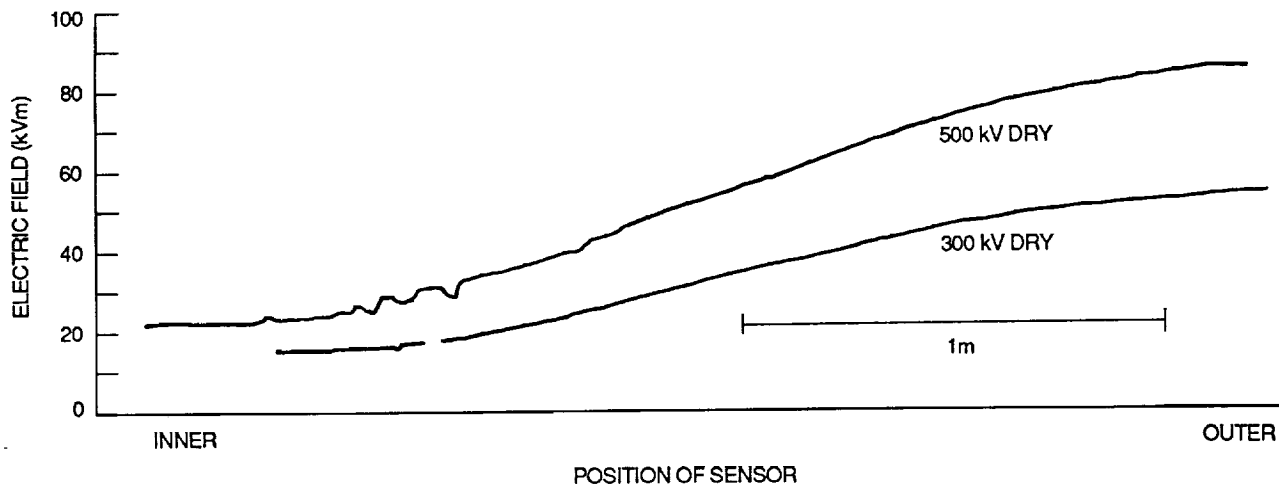


Figure A-10. Electric field scan, dry bushing

The small "wiggles" at the left end of the 500 kV trace have not been explained.

The probe transport system was failing at this point, so further data were recorded with the probe only at the inner position, approximately 3/4 m from the wall. The bushing was energized to 800 kV and then de-energized from 800 kV down to zero in steps of 100 kV, and the field readings were noted. These results will be discussed later. For a short while following this, the probe transport mechanism was again working, and a scan of the field in the vicinity of the wall was made with the bushing de-energized. These results are shown in Figure A-12.

It may be noticed that the field at the outer end was recorded as positive and at the inner end negative. The convention in use was that the recorded data represented the axial (for the bushing) component of the field. Results where the field passes through zero like this indicate a change in the direction of the axial component. Unfortunately, the radial component was not measured because of the orientation of the probe, so the exact significance of this change in direction was to remain somewhat a question. It should be noted, however, that the conductor through the bushing was grounded at the time, as well as the wall through which it passed. Thus, any charge on the material inside the bushing must rearrange itself so that the total voltage (the integral of the field) is zero.

The entire scan shown in this figure occupied approximately 2 minutes, during which the charge on the bushing could be expected to remain very constant. Later tests showed that the time constant for charge trapped on the bushing to leak off was in the order of an hour. There are also processes occurring in the dielectric that have time constants in the order of days.

During the next series of tests, the positioner system again failed, and it was not used at all following this.

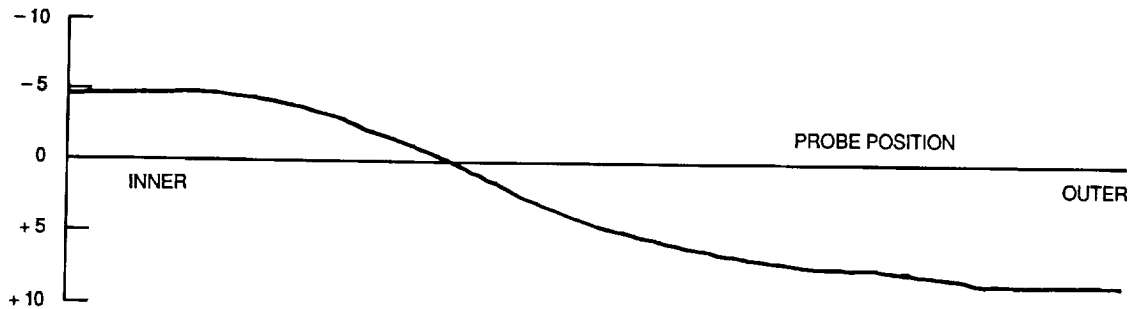


Figure A-11. Scan of de-energized bushing

The rain and fan systems were turned on for the next test series. During this series, there was a failure of the JPL field meter detector, probably caused by a drop of water over the collimator on the position-sensing fiber. The effect of this failure was that data were received representing the magnitude of the field, but it was not possible to determine its direction. The meter failure can be observed in Figure A-12, which shows data recorded at 500 kV under rain conditions. The field was approximately 100 kV/m prior to the detector failure.

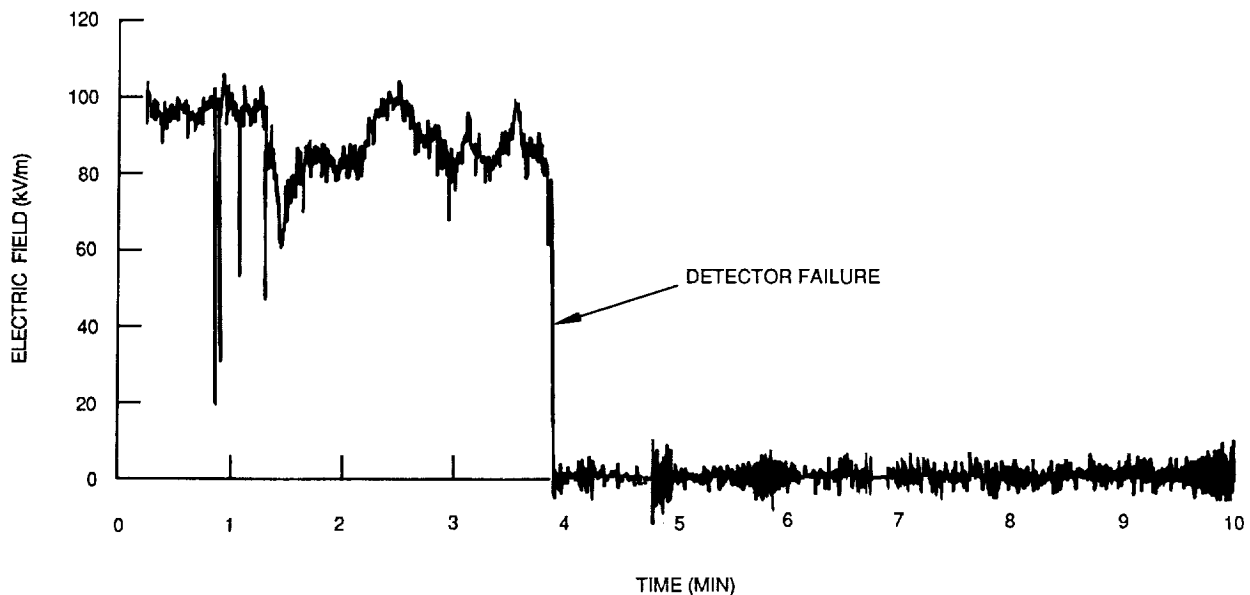


Figure A-12. Data at 500 kV, showing field meter failure

The large brief downward excursions of the reading during the first minute or so of the results shown in Figure A-12 are almost certainly due to momentary failures of the field meter system, which failed more completely at 4 minutes in the figure. On the other hand, the slower fluctuations of smaller amplitude are almost certainly genuine field variations caused by the rain and wind. The environmental variables can evidently cause the field at the location of the probe to vary from about 100 kV/m down to about 60 kV/m.

The test series consisted of incrementing the applied voltage in 50-kV steps, each lasting 10 minutes. Since the field meter was still providing amplitude

data to the control room, these data were recorded by hand, by means of an ac voltmeter applied to the 400-Hz signal coming from the field meter. These results will be presented later.

Later during this test series, at a potential above 700 kV, problems were experienced with the high voltage apparatus which caused the entire test series to be terminated. All subsequent results obtained in Ludvika were of a de-energized bushing discharging under open-circuit conditions. These results are shown in Figure A-13. The irregularities seen in Figure A-13 are due to the proximity of a group of people on a grounded bucket-truck arrangement. Note that they have no permanent effect on the redistribution of charge inside the bushing.

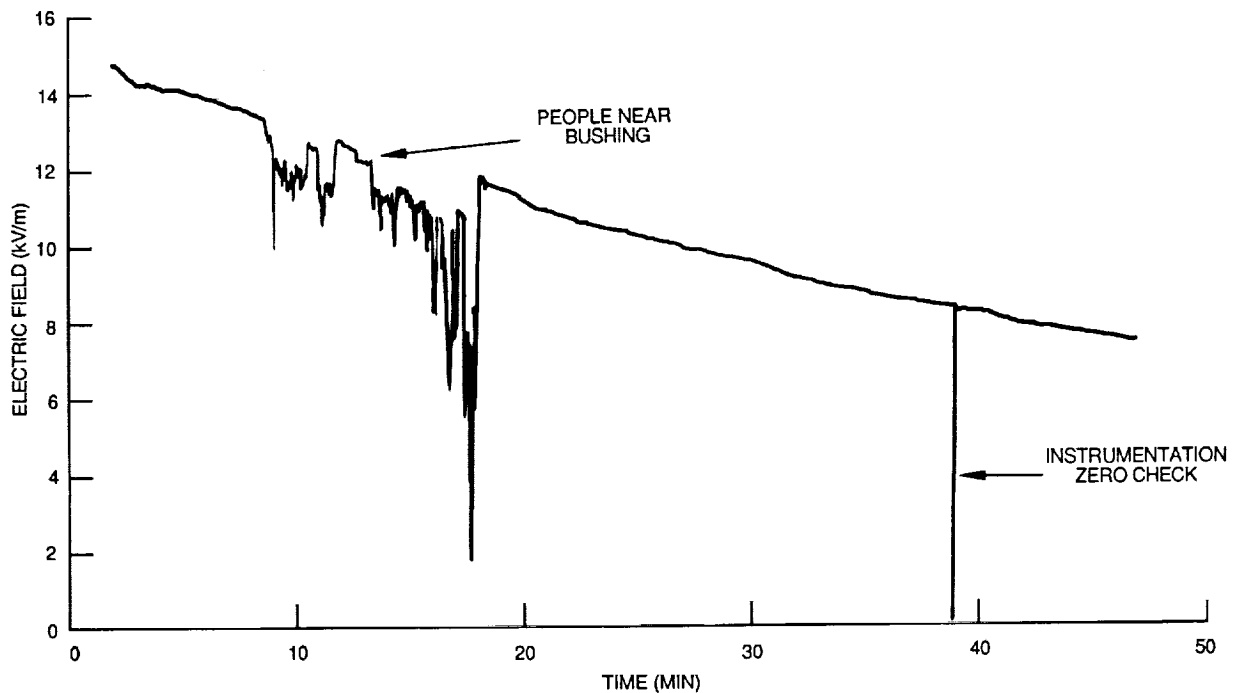


Figure A-13. Discharge of de-energized bushing

#### A.4. The Effect of Incomplete Wetting of the Bushing

The ASEA engineers had theorized that, under some conditions of wind and weather, part of the bushing could be dry and part of it wet, and that this uneven distribution of wetting could lead to an enhanced electric field at the surface of the insulator, as compared to the field when the insulator was completely dry or completely wetted. Consequently, the tests with the rain and the fan on at the same time were designed to simulate conditions which would wet the insulator near the high voltage end, and would leave it dry near the wall.

Since, as we know from our tests on the fiberglass pole used to hold the probe, even a very slight leakage can look like a short circuit as far as dc fields are concerned, we would expect an enhanced field in the dry region of the bushing under these circumstances. Since the integral of this field over distance gives the voltage, the field must decrease over the wetted region of

the insulator. The original intention of the tests in Ludvika was to scan the field in the intensified area.

Because of the failures of the positioning apparatus and the water drop induced problems with the position-sensing fiber on our probe during these tests, it cannot be said unequivocally that we have demonstrated that this theoretical understanding is correct. However, we are able to present evidence strongly suggestive of the correctness of this interpretation of what is happening on the surface of the bushing. For example, Figure A-12 showed apparently genuine field fluctuations with quite large magnitude.

Further confirmation of ASEA's model is obtained by comparing the wet and dry results. Figure A-14 shows the data obtained from the dry tests with the positioner working, the dry tests with the positioner stuck with the probe near the wall, and the wet tests when the positioner was stuck part-way out from the wall.

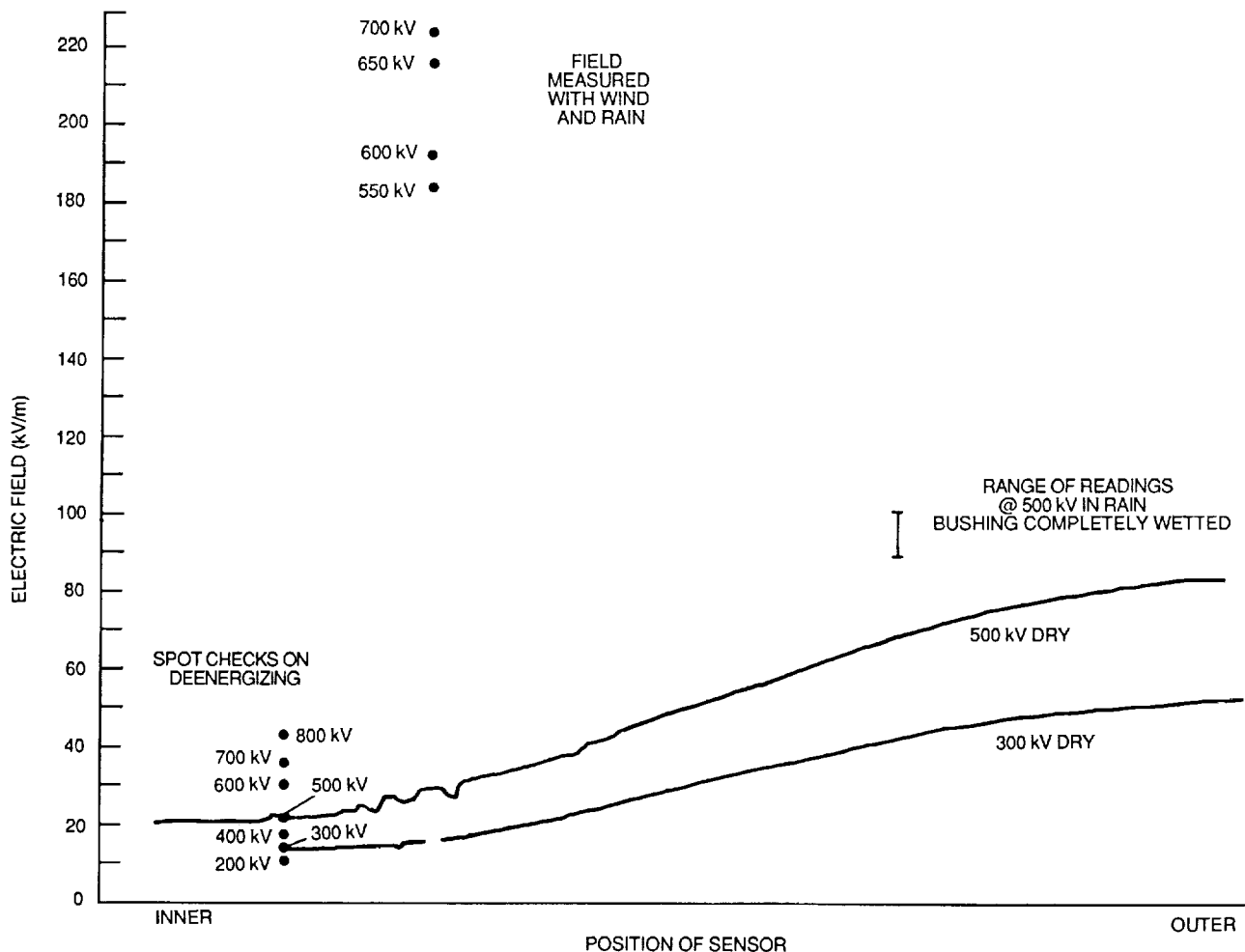


Figure A-14. Composite of results from wet and dry tests

It is immediately obvious in Figure A-14 that the field close to the wall is very much higher with rain and wind applied than under dry conditions. The

data for the wet conditions represent the magnitude of the dc field in the plane perpendicular to the axis of the probe, whereas the curves for dry conditions represent the magnitude of the component in the axial direction. It is assumed that the component in the radial direction is not detected, and also that there is no circumferential or azimuthal component of the field. These assumptions appear to be justified by considerations of symmetry, but they remain to be experimentally verified.

The data are self-consistent. The spot checks made when the positioner was broken (the round dots in Figure A-14) agree very well with the dry scans at 300 kV and 500 kV made when the positioner was functioning. Also, the integral of the observed axial field under dry conditions is consistent with the voltage applied to the center conductor. The increase in field intensity in the vicinity of the wall is in broad agreement with the model proposed by ASEA for the anomalous flashovers. The increase in field in this vicinity is a factor of five when the rain and wind are applied. Unless the axial component is by far the smallest component of the field, this can only be explained by a radical redistribution of the voltage down the bushing.

Therefore, while the data presented in Figure A-14 are not conclusive, they are certainly highly suggestive that the rain and wind combined cause a distribution of the voltage along the surface of the insulator which is far different than that which would be obtained under dry conditions.

#### A.5. Further Tests in Västerås

The DOE/JPL field meter consists of two parts, the probe and the receiver. These are connected by a pair of fiber optic cables, one for the position pulse and one for the data. The power margin (the amount by which the optical power in the fiber can be reduced without impacting the performance of the system) was thought to be high — about 13 dB in the case of the data fiber. In anticipation of operating the meters with a large separation between the probes and the receivers, 50-m extension fibers were fabricated. Unfortunately, there was insufficient time to test either meter with its extension cables prior to the trip to Sweden. When the extensions were tested (in Ludvika) it was found that the power margins were insufficient to allow for operation with the added loss of the fiber and the connectors.

Because the probe had to be operated close to the receiver, it was necessary to operate the receiver at the point where the bushing penetrated the wall. Coaxial (copper) extensions were used to bring the data from the receiver to the data acquisition system in the control room. While this arrangement was reasonably satisfactory, safety considerations made it impossible to change the range of the receiver during the tests. An estimate of the field values was made prior to energization, and the range switch set accordingly.

The actual field values experienced by the probe were somewhat higher than expected, and as a result the meter was operated in a non-linear region. The maximum value that can be measured by the meter is about 500 kV/m, which occurs part-way up the highest range. At this field value, the probe electronics become nonlinear. With this exception, the receiver of the meter system is designed to saturate when the reading reaches a multiple of 2: 200 kV/m, 20 kV/m and so on. The saturation is immaterial in ordinary use because the

panel meter will not display values greater than 1999. Since meter system saturation is therefore clearly evident, the dynamic range of the measurement system is maximized.

In the tests in Ludvika, the reading of the panel meters was not visible. Even if it had been observed that they were showing overload, the range of the meter could not have been changed without interrupting the test. Consequently, when the field values being recorded went above 200 kV/m, and the incoming waveform was observed to become distorted, we had no choice but to grin and bear it. On our return to Västerås, the meter nonlinearities were "calibrated out" by repeating the field values with the meter configured in the same way it had been in Ludvika, and then changing the range switch to obtain the "true" value of the field.<sup>6</sup> In this way, reasonable confidence in the final readings can be maintained. The calibration curve for this saturation is shown in Figure A-15. Since the worst-case nonlinearity experienced was evidently in the order of 10%, the corrected value is probably within the basic uncertainty of the instrument, about 2%. The relevant data, the field readings above about 180 kV/m, in Figure A-14, have been corrected in this way.

One other factor should be mentioned here. A layer of conducting paint was added to the nylon ring at the end of the probe, prior to the Ludvika tests. This paint increased the area of the electrodes, and certainly affected the calibration. It was not possible to establish a field cage that was as well-understood as the JPL cage while the equipment was in Sweden. After the equipment was returned to JPL, its calibration was checked. The readings were all about 9% high. This is very much in line with the increased electrode area due to the paint. Strictly speaking, it means that all the readings obtained since the paint was added should be scaled down by 9%.<sup>7</sup>

---

<sup>6</sup> On the subject of confidence in the data, it is worthwhile to mention one other test that was performed in Ludvika. The field was measured under the wire connecting the bushing to the supply. Conditions were dry, the conductor height was about 8 m, and the voltage was 800 kV. Considerable doubt was cast on the accuracy of the meter when it displayed a field of 96 kV/m. After all, a field of that magnitude would be expected in a parallel plate configuration. In the transmission line configuration, a higher field pertains near the conductor, and a much lower field is found near the ground.

In fact, the reading of 96 kV/m is almost certainly correct. Since the wire connecting the supply to the bushing is very small, it is certainly in corona. The region under it is no longer a Laplace region; Poisson's equation applies. The electric field is the sum of two components, one due to the applied voltage and the other to ion current. If the corona reaches space charge limiting (SCL) conditions, as it almost certainly did with 800 kV applied to it, the gradient at the conductor surface falls to zero (by definition), and a high value is found near the surface of the ground.

In the parallel plate geometry, the ground level field under SCL conditions is 50% higher than when there is no corona. In a cylindrical geometry, our simulations show an increase in the ground level field approaching a factor of 5. Presumably, the transmission line geometry is close to cylindrical. The ion current contribution to the field is significant, if not dominant.

<sup>7</sup> This has not been done; the information obtained about the bushing performance is contained in the relative values in rain and dry conditions. This correction would reduce the observed field under the HV supply conductor at Ludvika (discussed in the previous footnote) to 87 kV/m, a value still considerably above the expected field in the absence of space charge.

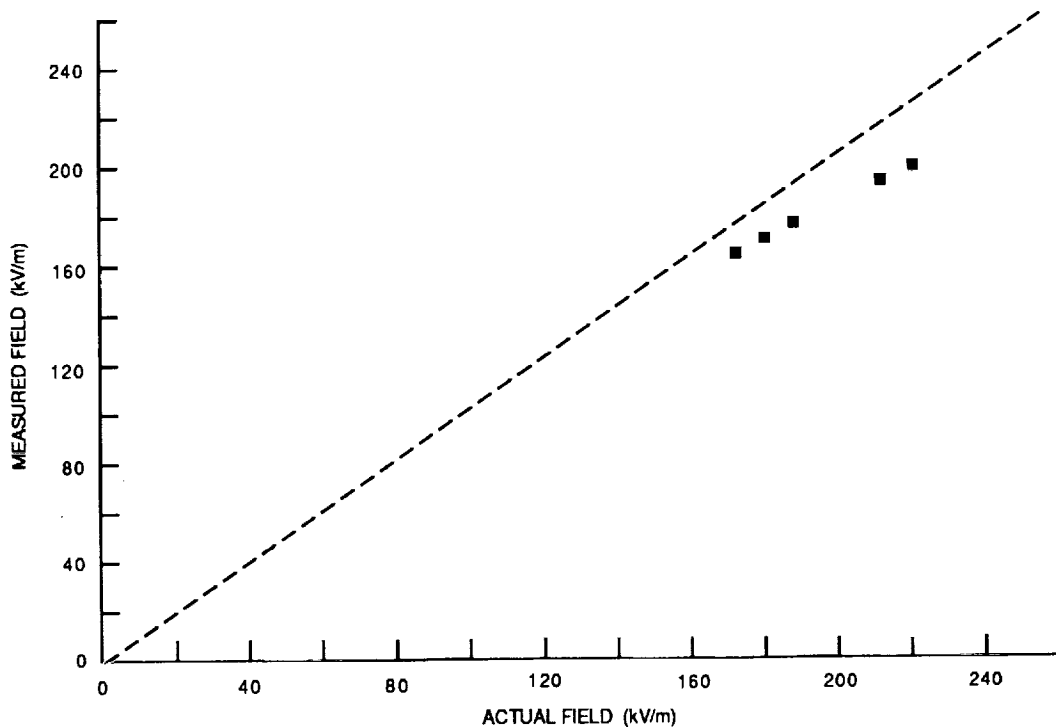


Figure A-15. Calibration curve for high-field saturation

#### A.6. Suggestions For Future Work

It is clear from the foregoing results that the DOE/JPL field meter is capable of making measurements in the hostile environment near a HVdc bushing in heavy rain conditions. While it is clear that the explanation for anomalous flashovers advanced by the engineers from ASEA is almost certainly correct, further experimental data would be very valuable.

There are two areas in particular for which further data would be most useful. First, a longitudinal scan of the electric field during rain conditions would provide unequivocal evidence of the redistribution of voltage after the onset of rain. A detailed description of the partially wetted voltage distribution would be very informative. There are several unanswered questions in this area; for example, just how far down the bushing does the wetted region bring the potential of the conductor? Is the voltage distribution in the nonwetted region reasonably uniform? What palliative measures can be applied to improve the situation?

Further data are also needed on the direction of the electric field, in both dry and wet conditions. In the tests in Ludvika only one component of the field was measured, and while it is reasonable to assume that there is no significant circumferential component, a radial component is inevitable, as indicated by Figures A-1 and A-2. How large is this component, compared to the axial component? It would increase the value of the dc field meter data significantly if arrangements were made to orient it to yield both axial and radial field components directly.

The use of more than one probe and the use of a multi-channel data acquisition system would be useful additions.

#### A.7. Conclusions

Experimental data have been obtained supporting a theoretical explanation of some of the anomalous flashovers that have occurred under wind and rain conditions on HVdc bushings. The explanation seems to lie in the significant redistribution of voltage along the surface of the bushing when only part of it is wet.

The experimental data were obtained with a DOE/JPL probe in a collaborative effort with ASEA of Sweden. There is at present no other dc field meter that could have made these measurements, and there may be no other HVdc test facility that could have staged such an elaborate test.

The results obtained with the field meter indicate a kind of behavior that has no counterpart in ac systems. Further experimentation of this kind may lead to an improved understanding of the behavior of insulation systems stressed with direct voltage.



APPENDIX B  
THE HELMHOLTZ COIL



## APPENDIX B

### THE HELMHOLTZ COIL

Uniform magnetic fields that are large enough and controllable enough to be of value in calibrating field meters are somewhat complicated to establish. An arrangement of two coils connected in series is frequently used. The configuration is attributed to von Helmholtz; Rayleigh used the same scheme in his Current Balance.

First consider the magnetic field of a circular wire carrying a current  $i$ , at a point  $P$  on the axis of the circle, as shown in Figure B-1.

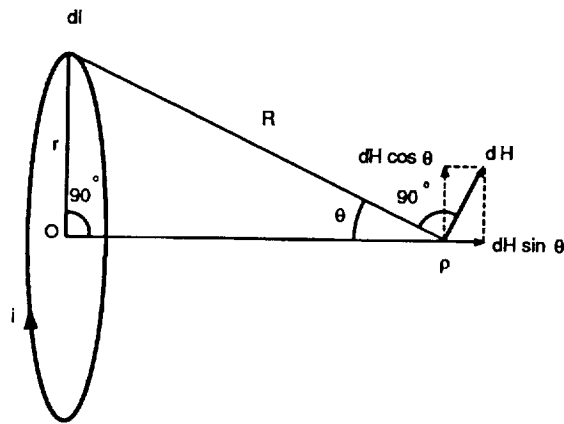


Figure B-1. Field due to a circular current-carrying wire

The field at  $P$  due to an element  $dl$  of the conductor is

$$dH = \frac{i \, dl}{4\pi R^2} \quad (\text{B.1})$$

in a direction perpendicular to the line joining  $P$  to the element  $dl$ . This field can be resolved into two directions — radial ( $dH \cos \theta$ ) and axial ( $dH \sin \theta$ ). Clearly, the radial components of the field cancel, so that the total field is in the axial direction, and is given by

$$H = \int dH \sin \theta \quad (\text{B.2})$$

$$= \int \frac{i \, dl}{4\pi R^2} \sin \theta \quad (\text{B.3})$$

$$= \frac{r^2}{2R^3} \quad (\text{B.5})$$

The field is thus seen to decrease as  $R$  increases. By arranging two coils along the same axis, the field between them can be made more uniform. Any arbitrary spacing of the coils will result in a stationary point in the magnitude of the field at the center; i.e., the first derivative of the field magnitude vanishes at the center of any symmetrical configuration. A more uniform field results if the arrangement is such that the second derivative also vanishes.

The diagram illustrates a magnetic circuit with two vertical coils, COIL A and COIL B, connected by a central magnetic core. The circuit is divided into sections A, B, R, and P. The total magnetic flux is labeled TOTAL. The dimensions are defined as follows:  $l$  is the length of the central core,  $r$  is the radius of the coils, and  $q$  is the distance from the center of the core to the center of the coils. The magnetic flux in section A is labeled  $\Phi_A$ , in section B is labeled  $\Phi_B$ , in section R is labeled  $\Phi_R$ , and in section P is labeled  $\Phi_P$ . The magnetic flux in the central core is labeled  $\Phi$ . The magnetic flux in the coils is labeled  $\Phi_A$  and  $\Phi_B$ .

**B-2**

The field at a point Q, distant x from coil A is given by adding the contributions from coils A and B:

$$H_Q = \frac{r^2 i}{2(r^2 + x^2)^{3/2}} + \frac{r^2 i}{2(r^2 + (1-x)^2)^{3/2}} \quad (\text{B.6})$$

since  $R_A^2 = r^2 + x^2$  and  $R_B^2 = r^2 + (1-x)^2$

Thus, for N turns in each coil, the field at Q is

$$H_Q = \frac{r^2 Ni}{2} \left[ \frac{1}{(r^2 + x^2)^{3/2}} + \frac{1}{(r^2 + (1-x)^2)^{3/2}} \right] \quad (\text{B.7})$$

The first derivative of H with respect to x is

$$\frac{dH_Q}{dx} = \frac{r^2 Ni}{2} \left[ -\frac{3}{2} \frac{2x}{(r^2 + x^2)^{5/2}} - \frac{3}{2} \frac{2(x-1)}{(r^2 + (1-x)^2)^{5/2}} \right] \quad (\text{B.8})$$

which vanishes at  $x = 1/2$  as expected. The second derivative with respect to x is

$$\begin{aligned} \frac{d^2 H_Q}{dx^2} = & -\frac{3r^2 Ni}{2} \left[ \frac{1}{(r^2 + x^2)^{5/2}} - \frac{5}{2} \frac{2x^2}{(r^2 + x^2)^{7/2}} \right. \\ & \left. + \frac{1}{((1-x)^2 + r^2)^{5/2}} - \frac{5}{2} \frac{2(x-1)^2}{((1-x)^2 + r^2)^{7/2}} \right] \end{aligned} \quad (\text{B.9})$$

At the center of the coil pair  $x = 1/2$  and the second derivative of the field is given by

$$\frac{d^2 H_C}{dx^2} = -\frac{3r^2 Ni}{2} \left[ \frac{(1/2)^2 + r^2 - 5(1/2)^2 + (1/2)^2 + r^2 - 5(1/2)^2}{((1/2)^2 + r^2)^{7/2}} \right] \quad (\text{B.10})$$

which vanishes if  $l = r$ .

The Helmholtz arrangement is therefore one where the coil separation l is the same as the radius r. A field of almost uniform strength is produced in the vicinity of the center.

At the center, each coil makes an equal contribution. The flux density in air can be found from  $B = \mu_o H$  and equation (B.7), where B is the flux density, and  $\mu_o$  is the permeability of air. Thus,

$$B = \mu_o r^2 Ni \left[ \frac{1}{(r^2 + (r^2/4))^{3/2}} \right] \quad (\text{B.11})$$

$$= \frac{8\mu_0 Ni}{r(5)^{3/2}} \quad (\text{B.12})$$

If we evaluate (B.12) explicitly, we obtain

$$B = 899.17 \frac{Ni}{r} \quad (\text{B.13})$$

where  $B$  is in nT,  $i$  is in Amps and  $r$  is in meters.

In our apparatus,  $r = 0.3\text{m}$ ,  $N = 10$ , so that  $B = 29.97 \mu\text{T}$  per Amp.

APPENDIX C  
GRAPHICAL PRESENTATION PROGRAM



## APPENDIX C

### GRAPHICAL PRESENTATION PROGRAM

#### C.1. Overview

This program is used to plot contour diagrams. It uses the data which is taken, for example, with the ac magnetic sensor, and plots contour lines on the computer screen. The program consists of three separate modules: TRANS.PAS, INTER.PAS, and GR.FOR. The purpose of the first module, TRANS.PAS, is to translate the coordinates that are used in taking the measurements into relative coordinates which the other two programs can use more efficiently. The second program, INTER.PAS, performs linear interpolation to obtain values for empty grid points. The third program, GR.FOR, uses the values to plot contour lines on the computer screen. A module-level flowchart for the program is shown in Figure C-1.

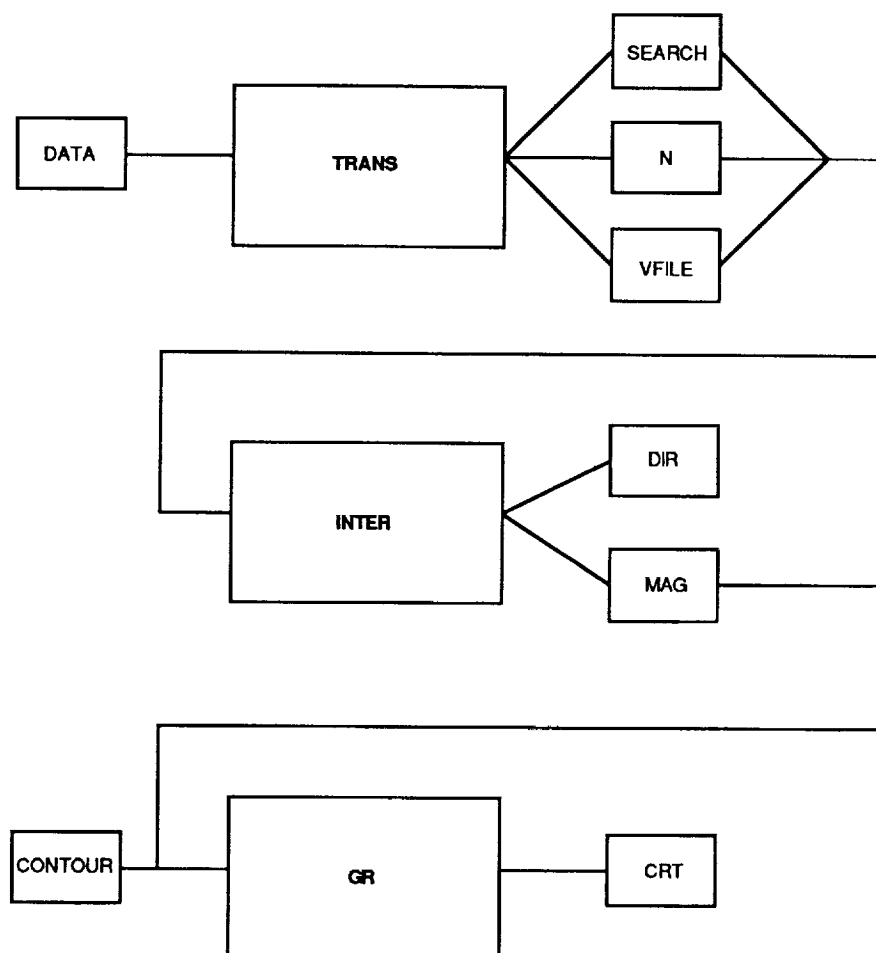


Figure C-1. Flowchart of graphical presentation routines

The measured data are assumed to be at regular intervals inside the region of interest. The data area should be a square matrix, although the program has worked when the number of rows is less than the number of columns. The reason for this is explained with GR.FOR, below.

## C.2. Program Description

### C.2.1. TRANS.PAS

TRANS.PAS uses one input file. This is the file containing the data taken with the sensor. The format of the file is described below. After the translation, up to three new files may be generated: SEARCH.DAT will contain starting points for interpolation; N.DAT will contain the values taken with the sensor; VFILE.DAT will contain vertices of boundary segments. If any of the data files is empty, it will be erased.

The values in each line of the input data file are separated by spaces. These values are parsed and stored in the array ARGV(). This array is then passed to Mapping procedure for the purpose of translating into relative coordinates. The following formulas are used to convert addresses to relative addresses:

$$\begin{aligned} \text{relative\_addr\_x} &= (\text{addr\_x} - \text{lower\_bound\_x}) / \text{psize} \\ \text{relative\_addr\_y} &= (\text{addr\_y} - \text{lower\_bound\_y}) / \text{psize} \end{aligned}$$

where *addr* is the position (x or y) to convert, *psize* is the spacing between grid points, and *lower\_bound* marks the lower bound on an axis (x or y).

The following formulas are used to compute the maximum number of grid points on each axis:

$$\begin{aligned} \text{max\_grid\_x} &= (\text{upper\_bound\_x} - \text{lower\_bound\_x}) / \text{psize} \\ \text{max\_grid\_y} &= (\text{upper\_bound\_y} - \text{lower\_bound\_y}) / \text{psize} \end{aligned}$$

where *upper\_bound* marks the upper bound of the data area on an axis and *psize* is as defined above. The maximum size of the data area is determined by the amount of memory available to the program. Each grid point requires about 32 bytes.

There are two constants in the program which may be modified: MAX\_X and MAX\_Y. They indicate, respectively, the maximum number of grid points on the X-axis and Y-axis.

### C.2.2. INTER.PAS

INTER.PAS will read data from the files created by TRANS.PAS. Interpolation of both magnitude and direction data will take place if SEARCH.DAT exists. The result of the interpolation is written to two files: OUTDAT.DAT will contain direction values; OUTMAG.DAT will contain magnitude values. The memory requirement for this program is identical to TRANS.PAS.

Magnitude and direction values are read from N.DAT, and are stored in the arrays MA() and N(). Boundary points between two vertices are calculated based

on the coordinates of the two vertices given for each boundary segment, using a linear equation,  $(y - y_1) = m(x - x_1) + b$ , in *Find\_Bound* procedure.

The interpolation process starts at a point defined in SEARCH.DAT, and it moves, row by row, first up and then down, to cover the entire data region. If a grid point contains no value, *Search* procedure is called to search outward in four directions: up, down, left, and right. The number of points in a search region must equal to that of the region on the opposite side. When this condition is met, the average value will be calculated and stored in the empty grid point. The shape of a search region is basically a trapezoid. The maximum displacement from the origin of search is set by LEN, and the maximum width of the search path is  $2 * MAX\_WIDTH + 1$ .

There are five constants in the program which may be modified: MAXI\_X, MAXI\_Y, LEN, MAX\_WIDTH, and MAX\_VERTICES. MAXI\_X and MAXI\_Y indicate, respectively, the maximum number of grid points on the X-axis and Y-axis. LEN and MAX\_WIDTH are used in the interpolation process. LEN is the maximum displacement from an empty grid point up to which a search for existing values may proceed. MAX\_WIDTH is equal to the smallest integer greater than or equal to  $LEN/2$ . MAX\_VERTICES defines the maximum number of boundary segments that is allowed.

The contour program, GR.FOR, uses magnitude values stored in OUTMAG.DAT. It sets up the screen for high-resolution graphics, and plots the contour lines specified in the file CONTOUR.DAT.

#### C.2.3. GR.FOR

GR.FOR is written in FORTRAN 77, which allows the use of Graphmatic™ graphics routines. The dimensions of three arrays in the program, X(), Y(), and VALUES(), must be modified to match the number of grid points calculated by the interpolation program. The number of rows should equal the number of columns. This is necessary because FORTRAN stores arrays linearly in column-major order, and because it does not offer type checking. If these restrictions are not met, the addresses of the arrays will not be mapped correctly.

To modify the dimensions of the arrays, first look at line two of N.DAT. The two numbers should be identical, although the program has worked when the first number is smaller than the second number. And then modify the dimensions of the arrays using the second number. Compile and link the modified program.

### C.3. Data File Format

The data file containing measured data must be in ASCII form. Comments and blank lines are allowed in the data file. The maximum length of a line is 80 characters, and it may be grouped into one of the following types:

1. Comments. If the first character of the line is a "C" or "\*", the entire line is treated as a comment line.
2. Blank lines.
3. Boundary data. Defines an artificial boundary segment in the drawing area. The maximum number of segments allowed is set in the program INTER.PAS. The format of the line is:

B x1 y1 x2 y2 boundary\_type direction magnitude

The character "B" identifies that the line is boundary data.

x1, y1, x2, and y2 are coordinates of the vertices of the boundary segment.

boundary\_type may be "CONDUCTIVE" or "UNSPECIFIED". Only the first three characters are significant. The values of direction and magnitude will be ignored if the boundary type is "UNSPECIFIED".

4. Data area. Defines the area in which the data points are taken. The format of the line is:

W x1 y1 x2 y2 psize

The character "W" identifies that the line defines the data area.

x1 and y1 are the coordinates of the upper left-hand corner of the area.

x2 and y2 are the coordinates of the lower right-hand corner of the area.

psize is a positive integer defining the spacing of the grid points.

5. Starting point for interpolation. If interpolation is desired, at least one point must be entered. This is the point at which the process will begin. The format of the line is:

S x y

The character "S" identifies that the line is a starting point for interpolation.

x and y are the starting coordinates.

6. Data point. A reading from the sensor is entered in the following format:

x y direction magnitude

x and y are the coordinates at which the measurement is taken.

direction is an integer.

magnitude is a real number.

#### C.4. Graphics Routines

QSMODE(n) is used to set graphics mode.

n = 3 sets 80x25 Color Text mode

n = 6 sets 640x200 B/W Graphics mode

QCMOV(col, row) moves the cursor to the position specified.

QXAXIS(start, finish, major\_tic, minor\_tic, label, dec)

draws x axis, including tic marks and labels.

start is the starting value of x on the axis

finish is the ending value of x on the axis

major is the distance between large tic marks

minor 0 for no minor tic marks

1 for halfway between major tic marks

-1 for logarithmic set of tic marks

label 0 for no labeling

1 to label major tic marks

dec number of decimal places for labels

QYAXIS similar to above, for y axis.

QCTRDEF(mode, l\_color, color, m\_color, legend)

is used to set parameters for QCNTOUR.

mode graphics mode

l\_color color of labeled contour lines

m\_color color of unlabeled contour lines

legend 0 for no legend; 1 for legend

QCNTOUR(aspect, x\_array, y\_array, data, contours,  
labels, nx, ny, num)

creates contour plot.

aspect aspect ratio of screen

x\_array array of x values at each grid point

y\_array array of y values at each grid point

data two dimensional array of data values

contours array of contour values to plot

labels array of boolean values. 0 for no labels; 1  
for labels.

nx number of grid points on x axis

ny number of grid points on y axis

num number of contour lines to plot

```

QPLOT(c1, c2, r1, r2, xmin, xmax, ymin, ymax,
      xorg, yorg, option, yoverx, aspect)
is a plot initialization routine.
c1, r1   marks upper left-hand corner of window
c2, r2   marks lower right-hand corner of window
xmin, ymin values correspond to c1 and r1
xmax, ymax values correspond to c2 and r2
xorg, yorg location of origin
option   scaling method option.  0 for automatic scaling to fit plot
      in window; 1 for manual.
yoverx   number of rows over number of columns in the graphics window
aspect   aspect ratio of the screen

```

## C.5. Program Listings

### C.5.1. TRANS.PAS Listing

```

(* This program translates user coordinates into program coordinates.
   For example, (35, 70) into (5, 9) *)
program trans;
const MAX_Y = 30;          (* Maximum number of grid points on Y-axis *)
      MIN_Y = 0;
      MAX_X = 30;          (* Maximum number of grid points on X-axis *)
      MIN_X = 0;

type filename_type = string[65];

(* this function converts an integer in Real format into an integer
   in Integer format *)
function r2i(real_num : real):integer;
var i, int_num, code:integer;
    temp : string[80];
begin
  str(real_num:12:0,temp);  (* Change it into a string first *)
  i := pos(' ',temp);      (* drop all spaces *)
  while i < 0 do
    begin
      temp := copy(temp,1,i-1)+copy(temp,i+1,length(temp)-i);
      i := pos(' ',temp);
    end;
  val(temp,int_num,code);  (* And convert it into an integer *)
  if code < 0 then writeln('>>>Error converting real to integer');
  r2i:=-int_num;
end;  (* r2i *)

(* open a textfile *)
function open(var fvar:text; fname:filename_type):boolean;
begin
  assign(fvar, fname);
  (*$i-*) reset(fvar); (*$i+*)
  if ioresult < 0

```

```

    then begin
        close(fvar);
        open := false;
    end
    else open := true;
end; (* open *)

procedure translate;
const C_LN = 'Cc'; (* comment line specifiers *)
      WINDOW_FLAG = 'W'; (* window info flag *)
      CONDUCTIVE_FLAG = 'CON'; (* boundary types *)
      UNSPECIFIED_FLAG = 'UNS';
      MAX_ARGV = 10; (* max number of arguments allowed per line *)
      SE_FILE = 'SEARCH.DAT'; (* search point filename *)
      DP_FILE = 'N.DAT'; (* data point filename *)
      VE_FILE = 'VFILE.DAT'; (* vertices filename *)
type line_type = string[80];
      argv_type = array[1..MAX_ARGV] of line_type;
var fvar, fse, fdp, fve : text; (* input, search, data, and vertices files *)
    fname, tempname : filename_type;
    ch : char;
    init_bound : boolean; (* true = boundary initialized *)
    revised_se, revised_dp, revised_ve : boolean; (* archive bit *)
    temp, data : line_type;
    line_count, argc : integer; (* file line and argument counter *)
    argv : argv_type;

procedure mapping(argc:integer; argv:argv_type);
var i, code, scode, x, y, xl, yl, tp, direction, psize : integer;
    x_bound, y_bound, x_dir, y_dir : integer; (* max_x and y *)
    low_x, low_y, delta_x, delta_y : integer;
    magnitude : real;
    wr_ok : boolean; (* write-ok flag *)
    ch : char;

procedure chk_arg(n:integer);
begin
    if scode <> 0 then (* error in conversion if not 0 *)
        begin
            writeln('Error converting data -- program halted. ');
            for i := 1 to length(fname) do
                fname[i] := upcase(fname[i]);
            writeln('Line #', line_count, ' in file: ', fname);
            close(fvar); (* close all files before exit *)
            close(fdp); erase(fdp); (* and erase all data files *)
            close(fve); erase(fve);
            close(fse); erase(fse);
            halt;
        end;
    if argc > n then
        writeln('Extra arguments ignored, line ', line_count);
    end; (* chk_arg *)

```

```

(* returns true if n is between 0..n_bound, inclusive *)
function in_bounds(n, n_bound:integer):boolean;
begin
  if (n >= 0) and (n <= n_bound)
  then in_bounds := true
  else in_bounds := false;
end; (* in_bounds *)

procedure p1; (* get user window information - corner & pixel size *)
begin
  if ch <> WINDOW_FLAG then
  begin
    writeln('Setup data must appear first');
    close(fvar); (* close all files before exit *)
    close(fdp); erase(fdp); (* erase all data files *)
    close(fve); erase(fve);
    close(fse); erase(fse);
    halt;
  end;
  scode := 0;
  val(argv[2],x,code);
  scode := scode + code;
  val(argv[3],y,code);
  scode := scode + code;
  write('Window (' ,x, ' , ' ,y,')-');
  val(argv[4],x1,code);
  scode := scode + code;
  val(argv[5],y1,code);
  scode := scode + code;
  val(argv[6],psize,code);
  scode := scode + code;
  writeln((' ',x1, ' , ' ,y1,') , pixel size: ',psize);
  writeln;
  chk_arg(6);

  if x < x1 then low_x := x (* find lower value for calculations *)
  else low_x := x1;
  if y < y1 then low_y := y
  else low_y := y1;
  delta_x := x - x1; (* find difference *)
  delta_y := y - y1;
  if (delta_x < 0) (* get direction *)
  then x_dir := 1
  else x_dir := -1;
  if (delta_y < 0)
  then y_dir := 1
  else y_dir := -1;
  delta_x := r2i(abs(delta_x)); (* abs *)
  delta_y := r2i(abs(delta_y));
  x_bound := delta_x div psize;
  y_bound := delta_y div psize;
  writeln(fdp,y, ' ',x, ' ',y1, ' ',x1, ' ',psize);

```

```

        writeln(fdp,y_bound,' ',x_bound);
        revised_dp := true;
        init_bound := true;
    end; (* p1 *)

    procedure p2; (* get boundary data *)
    var i : integer;
        temp : string[3]; (* for storing boundary type *)
    begin
        scode := 0;
        val(argv[2],x,code);
        scode := scode + code;
        val(argv[3],y,code);
        scode := scode + code;
        val(argv[4],x1,code);
        scode := scode + code;
        val(argv[5],y1,code);
        scode := scode + code;
        for i := 1 to length(argv[6]) do (* translate boundary type *)
            argv[6][i] := upcase(argv[6][i]);
            temp := copy(argv[6],1,3); (* get first 3 chars *)
            if temp = CONDUCTIVE_FLAG then tp := 100
            else if temp = UNSPECIFIED_FLAG then tp := 102
            else begin
                write('Unknown boundary type on line ',line_count);
                writeln(', 'Unspecified' assumed. ');
                tp := 102;
            end;
        val(argv[7],direction,code);
        scode := scode + code;
        val(argv[8],magnitude,code);
        scode := scode + code;
        chk_arg(8);

        x := (x - low_x) div psize; (* get prg coordinates *)
        y := (y - low_y) div psize;
        x1 := (x1 - low_x) div psize;
        y1 := (y1 - low_y) div psize;

        wr_ok := true;
        if not in_bounds(x,x_bound) then wr_ok := false;
        if not in_bounds(y,y_bound) then wr_ok := false;
        if not in_bounds(x1,x_bound) then wr_ok := false;
        if not in_bounds(y1,y_bound) then wr_ok := false;

        if wr_ok then begin
            if x_dir = -1
            then begin
                x := x_bound - x;
                x1 := x_bound - x1;
            end;
            if y_dir = -1
            then begin

```

```

        y := y_bound - y;
        y1 := y_bound - y1;
    end;
    writeln(fve,y,' ',x,' ',y1,' ',x1,' ',tp,' ',direction,' ',magnitude);
    revised_ve := true;
end
else begin
    write('Vertices out of bounds, line ',line_count);
    writeln(' -- ignored');
end;
end; (* p2 *)

procedure p3; (* get data points info *)
begin
    scode := 0;
    val(argv[1],x,code);
    scode := scode + code;
    val(argv[2],y,code);
    scode := scode + code;
    val(argv[3],direction,code);
    scode := scode + code;
    val(argv[4],magnitude,code);
    scode := scode + code;
    chk_arg(4);

    x := (x - low_x) div psize; (* get prg coordinates *)
    y := (y - low_y) div psize;

    if not (in_bounds(x,x_bound) and in_bounds(y,y_bound))
    then writeln('Data point out of bounds, line ',line_count,' -- ignore-
d')
    else begin
        if x_dir = -1 then x := x_bound - x;
        if y_dir = -1 then y := y_bound - y;
        writeln(fdp,y,' ',x,' ',direction,' ',magnitude);
    end;
end; (* p3 *)

procedure p4; (* get search points *)
begin
    scode := 0;
    val(argv[2],x,code);
    scode := scode + code;
    val(argv[3],y,code);
    scode := scode + code;
    chk_arg(3);

    x := (x - low_x) div psize; (* get prg coordinates *)
    y := (y - low_y) div psize;

    if not (in_bounds(x,x_bound) and in_bounds(y,y_bound))
    then
        writeln('Search point out of bounds, line ',line_count,' -- ignored')

```

```

        else begin
            if x_dir = -1 then x := x_bound - x;
            if y_dir = -1 then y := y_bound - y;
            writeln(fse,y,' ',x);
            revised_se := true;
        end;
    end; (* p4 *)

begin (* mapping *)
    if argc > 0
    then begin
        ch := upcase(copy(argv[1],1,1));
        if not init_bound (* must find window info first *)
        then p1
        else if (ch = 'B') (* B for boundary *)
        then p2
        else if (ch = 'S') (* S for search point *)
        then p4
        else p3; (* data points *)
    end; (* if argc *)
end; (* mapping *)

begin (* translate *)
    init_bound := false;
    repeat
        write('Translate datafile (Y/N)? N'#8);
        readln(ch);
        if ch = chr(26) then ch := 'N' (* if CR, use N as default *)
        else ch := upcase(ch);
        if (ch = 'Y')
        then begin
            repeat
                write('Enter name of file to translate: ');
                readln(fname);
            until (open(fvar,fname));

            revised_dp := false; (* not modified *)
            revised_ve := false;
            revised_se := false;
            assign(fdp,DP_FILE); rewrite(fdp); (* open data point file *)
            assign(fve,VE_FILE); rewrite(fve); (* vertices file *)
            assign(fse,SE_FILE); rewrite(fse); (* and search point file *)
            line_count := 0;

            while not eof(fvar) do
                begin
                    readln(fvar,data);
                    line_count := line_count+1;
                    argc := 0;

                    (* if not blank or comment line then parse *)
                    if (data <> '') and (pos(copy(data,1,1),C_LN)=0)

```

```

then begin
  repeat
    temp := '';
    while copy(data,1,1) = ' ' do (* skip spaces *)
      data := copy(data,2,length(data)-1);
    (* get first word *)
    while (copy(data,1,1) <> ' ') and (length(data) > 0)
    do begin
      temp := temp + copy(data,1,1);
      data := copy(data,2,length(data)-1);
    end;

    (* if argument not empty, store it. only MAX_ARGV
       number of arguments will be accepted. *)
    if temp <> ''
    then if argc = MAX_ARGV
        then begin
          write('Too many arguments on line ');
          writeln(line_count, ' -- ignored');
        end
        else begin
          argc := argc + 1;
          argv[argc] := temp;
        end;

    until length(data)=0;
    mapping(argc,argv);
  end; (* if *)

end; (* while *)
close(fvar);
close(fdp);
close(fve);
close(fse);
if not revised_dp then erase(fdp);
if not revised_ve then erase(fve);
if not revised_se then erase(fse);
end
else if (ch = 'N')
then begin
  writeln('No need to translate');
end;
until (ch = 'Y') or (ch = 'N');
end; (* translate *)

begin (* main program *)
  translate;
end.

```

### C.5.2. INTER.PAS Listing

```

program inter;

const LEN = 2;          (* distance to search *)
      MAX_WIDTH = 1;    (* max displacement to one side = UPPER(LEN/2) *)
      MAXI_Y = 30;
      MIN_Y = 0;
      MAXI_X = 30;
      MIN_X = 0;

      NO_DATA = -1;     (* n_type for blank data points *)
      DATA_START = 0;  (* lowest n_type value for a data point *)
      DATA_END = 100;  (* highest n_type value for a data point *)

      MAX_VERTICES = 25;
      VERTICES_FILE = 'VFILE.DAT';
      DP_FILE = 'N.DAT';
      SE_FILE = 'SEARCH.DAT';
      OUT_DIR = 'OUTDAT.DAT';
      OUT_MAG = 'OUTMAG.DAT';
      TO_RADIAN = 1.7453292520E-02; (* multiply by this to get radian *)
      TO_DEGREE = 5.7295779513E+01; (* to get degree *)

type filename_type = string[65];
   data_pt_type = array[MIN_Y..MAXI_Y, MIN_X..MAXI_X] of integer;
   found_type = record (* for captured data points *)
       x, y : integer;
       direction : integer;
       magnitude : real;
   end;
   window_type = record
       ux, uy, lx, ly, psize : integer;
   end;
   magnitude_rec = record
       mag : array[MIN_X..MAXI_X] of real;
   end;
   mag_type = ^magnitude_rec;

var n, n_type, show : data_pt_type;
    ma : array[MIN_Y..MAXI_Y] of mag_type;
    winfo : window_type; (* window info *)

    x_axis_dp, y_axis_dp : array[1..20] of found_type;
    x_dp_cnt, y_dp_cnt, x_balance, y_balance : integer;
    MAX_X, MAX_Y, i, i2, sp_x, sp_y : integer; (* general counters *)
    fse : text; (* for search points *)

(* *_dp_cnt : number of captured data points on each axis.
   *_balance : data points found on both sides of the specified
               search point? 0, 1 = no; 2 = yes.
   *_axis_dp : contains information about captured points.

```

```

n_type      : contains characteristic about the data point in n[.

n_type:
-1 : blank, to be calculated

    0 : normal data point
    1 : direction, user specified
    2 : direction, calculated
    100 : conductive boundary

    102 : unspecified boundary (graph, wood...)
*)

```

```

(* this function converts an integer in Real format into an integer
   in Integer format *)

```

```

function r2i(real_num : real):integer;
var i, int_num, code:integer;
    temp : string[80];
begin
    str(real_num:12:0,temp);  (* Change it into a string first *)
    i := pos(' ',temp);      (* drop all spaces *)
    while i < 0 do
        begin
            temp := copy(temp,1,i-1)+copy(temp,i+1,length(temp)-i);
            i := pos(' ',temp);
        end;
    val(temp,int_num,code);    (* And convert it into an integer *)
    if code<0 then writeln('>>>Error converting real to integer');
    r2i:=int_num;
end;  (* r2i *)

```

```

(* open a textfile *)
function open(var fvar:text; fname:filename):boolean;
begin
    assign(fvar, fname);
    (*$i-*) reset(fvar);  (*$i+*)
    if ioresult < 0
        then begin
            close(fvar);
            open := false;
        end
        else open := true;
end;  (* open *)

```

```

(* returns true if x is between 0..n, inclusive *)
function in_bounds(x, b:integer):boolean;
begin
    if (x >= 0) and (x <= b)
        then in_bounds := true
        else in_bounds := false;

```

```

end; (* in_bounds *)

(* for magnitude info *)
procedure st_mag(row, column:integer; value:real);
begin
    ma[row]^mag[column] := value;
end; (* st_mag *)

function rd_mag(row, column:integer):real;
begin
    rd_mag := ma[row]^mag[column];
end; (* rd_mag *)

procedure dump_mag;
var i, i2 : integer;
begin
    writeln; writeln('Magnitude Information'); write(' ');
    for i := MIN_X to MAX_X do
        write(' ', i:3, ' ');
        writeln;
        for i := MIN_Y to MAX_Y do
            begin
                write(i:3, ' ');
                for i2 := MIN_X to MAX_X do
                    write(ma[i]^mag[i2]:5:1, ' ');
                writeln;
            end;
        end;
    end; (* dump_mag *)

(* clear all data points to blank *)
procedure init;
var i, i2 : integer;
    fvar : text;
    x, y, d : integer; (* d: direction, mag: magnitude *)
    mag : real;
begin
    for i := MIN_Y to MAXI_Y do
        new(ma[i]);
    MAX_X := MAXI_X; (* initial boundary values set to maximum *)
    MAX_Y := MAXI_Y;
    for i := MIN_Y to MAX_Y do
        for i2 := MIN_X to MAX_X do
            begin
                show[i,i2] := 0;
                n[i,i2] := NO_DATA; (* blanks *)
                n_type[i,i2] := NO_DATA;
                st_mag(i,i2,NO_DATA);
            end;
        end;
    end;

    if open(fvar,DP_FILE) then

```

```

begin
  readln(fvar, winfo.uy, winfo.ux, winfo.ly, winfo.lx, winfo.psize);
  readln(fvar, MAX_Y, MAX_X); (* get boundary values set by translator *)
  write('Window (', winfo.ux, ', ', winfo.uy, ')-(', winfo.lx, ', ', winfo.ly);
  writeln('), pixel size: ', winfo.psize);
  if (MAX_X > MAXI_X) or (MAX_Y > MAXI_Y) then
    begin
      writeln('Not enough memory to handle information:');
      if (MAX_X > MAXI_X) then writeln('Too many columns');
      if (MAX_Y > MAXI_Y) then writeln('Too many rows');
      close(fvar);
      halt;
    end;
  while not eof(fvar) do
    begin
      readln(fvar, y, x, d, mag);
      if not (in_bounds(y, MAX_Y) and in_bounds(x, MAX_X)) then
        begin
          writeln('Invalid coordinates in ', DP_FILE, ', program halted');
          close(fvar);
          halt;
        end;
      n[y, x] := d;
      n_type[y, x] := 1;
      st_mag(y, x, mag);
    end;
  close(fvar);
end
else begin
  writeln('File ', DP_FILE, ' does not exist, program halted');
  halt;
end;
end; (* init *)

```

```

procedure search(y, x:integer);
var x1, y1: integer;
    ystart, ystop,
    xstart, xstop, disp, temp : integer;
    x_nobound, y_nobound : boolean;

```

(\* this procedure is called by "search" to verify and correct  
any out-of-bound variables for looping \*)

```

procedure chk_xy(var v1, v2:integer; t:char);
begin
  t := upcase(t);
  case t of
    'Y' : begin
      if v1 < MIN_Y then v1 := MIN_Y;
      if v2 < MIN_Y then v2 := MIN_Y;
      if v1 > MAX_Y then v1 := MAX_Y;
      if v2 > MAX_Y then v2 := MAX_Y;
    end;
  end;

```

```

        'X' : begin
            if v1 < MIN_X then v1 := MIN_X;
            if v2 < MIN_X then v2 := MIN_X;
            if v1 > MAX_X then v1 := MAX_X;
            if v2 > MAX_X then v2 := MAX_X;
        end;
    end; (* case *)
end; (* chk_xy *)

procedure find_x;
begin
    disp := abs(y1 - y);
    if (disp > MAX_WIDTH)
        then disp := MAX_WIDTH;
    x_nobound := true;
    xstart := x-disp;
    xstop := x+disp;
    chk_xy(xstart, xstop, 'x');
    x1 := xstart;
    while (x1 <= xstop) do
        begin
            (* if data pt exists, get value *)
            if (n_type[y1,x1] <> NO_DATA) then
                begin
                    if (n_type[y1,x1] >= DATA_START) and (n_type[y1,x1] <= DATA_END) then
                        begin
                            y_dp_cnt := y_dp_cnt + 1;
                            y_axis_dp[y_dp_cnt].x := x1;
                            y_axis_dp[y_dp_cnt].y := y1;
                            y_axis_dp[y_dp_cnt].direction := n[y1,x1];
                            y_axis_dp[y_dp_cnt].magnitude := rd_mag(y1,x1);
                        end;
                    y_nobound := false; (* tell to stop searching *)
                end;
                show[y1,x1] := show[y1,x1]+2;
                x1 := x1 + 1;
            end;
        end;
    end;

procedure find_y;
begin
    disp := abs(x1 - x);
    if (disp > (MAX_WIDTH+1)) (* see notes for reason *)
        then disp := (MAX_WIDTH+1);
    y_nobound := true;
    ystart := y-disp+1;
    ystop := y+disp-1;
    chk_xy(ystart, ystop, 'y');
    y1 := ystart;
    while (y1 <= ystop) do
        begin
            (* if data pt exists, get value *)

```

```

    if (n_type[y1,x1] <> NO_DATA) then
    begin
        if (n_type[y1,x1] >= DATA_START) and (n_type[y1,x1] <= DATA_END) then
        begin
            x_dp_cnt := x_dp_cnt + 1;
            x_axis_dp[x_dp_cnt].x := x1;
            x_axis_dp[x_dp_cnt].y := y1;
            x_axis_dp[x_dp_cnt].direction := n[y1,x1];
            x_axis_dp[x_dp_cnt].magnitude := rd_mag(y1,x1);
        end;
        x_nobound := false; (* tell to stop searching *)
    end;
    show[y1,x1] := show[y1,x1]+3;
    y1 := y1 + 1;
end;
end;

begin (* search *)
    temp := 0; (* to determine balances *)
    x_balance := 0;
    y_balance := 0;
    x_dp_cnt := 0;
    y_dp_cnt := 0;

    y_nobound := true; (* search region above the fixed point *)
    ystart := y-1;
    ystop := y-LEN;
    chk_xy(ystart, ystop, 'y');
    y1 := ystart;
    temp := y_dp_cnt; (* store old value of y_dp_cnt *)
    while ((y1 >= ystop) and (y_nobound)) do
    begin
        find_x;
        y1 := y1 - 1;
    end;
    if (y_dp_cnt > temp) then (* new data point(s) captured *)
        y_balance := y_balance + 1;

    y_nobound := true; (* search region below the fixed point *)
    ystart := y+1;
    ystop := y+LEN;
    chk_xy(ystart, ystop, 'y');
    y1 := ystart;
    temp := y_dp_cnt;
    while ((y1 <= ystop) and (y_nobound)) do
    begin
        find_x;
        y1 := y1 + 1;
    end;
    if (y_dp_cnt > temp) then (* new data point(s) captured *)
        y_balance := y_balance + 1;

    x_nobound := true; (* search region right of the fixed point *)

```

```

xstart := x+1;
xstop  := x+LEN;
chk_xy(xstart, xstop, 'x');
xl := xstart;
temp := x_dp_cnt;
while ((xl <= xstop) and (x_nobound)) do
begin
    find_y;
    xl := xl + 1;
end;
if (x_dp_cnt > temp) then (* new data point(s) captured *)
    x_balance := x_balance + 1;

x_nobound := true; (* search region left of the fixed point *)
xstart := x-1;
xstop  := x-LEN;
chk_xy(xstart, xstop, 'x');
xl := xstart;
temp := x_dp_cnt;
while ((xl >= xstop) and (x_nobound)) do
begin
    find_y;
    xl := xl - 1;
end;
if (x_dp_cnt > temp) then (* new data point(s) captured *)
    x_balance := x_balance + 1;
end; (* search *)

```

(\* reads boundary vertices from a data file VERTICES\_FILE, and  
computes all points between each pair of vertices \*)

procedure find\_bound;

type v\_type = record

    x, y, xl, yl, tp, direction : integer;  
    magnitude : real;

end;

var i, i2, j : integer; (\* general counter \*)

dx, dy : integer; (\* used to compute slope \*)

m, p4, p4t : real; (\* slope and y position \*)

vfile : text;

p1, p2, p3, horizontal, vertical : integer;

vertices : array[1..MAX\_VERTICES] of v\_type;

vertcount : integer;

procedure swap\_vertices(var v1, v2 : v\_type);

var t : v\_type; (\* temporary \*)

begin

    t := v1;

    v1 := v2;

    v2 := t;

end;

```

begin (* find_bound *)
  vertcount := 0; (* reads all vertices into array *)
  if open(vfile, VERTICES_FILE) then
    begin
      while (not eof(vfile)) and (vertcount < MAX_VERTICES) do
        begin
          vertcount := vertcount + 1;
          read(vfile, vertices[vertcount].y, vertices[vertcount].x);
          read(vfile, vertices[vertcount].y1, vertices[vertcount].x1);
          read(vfile, vertices[vertcount].tp, vertices[vertcount].direction);
          readln(vfile, vertices[vertcount].magnitude);
        end;
      if (not eof(vfile)) and (vertcount >= MAX_VERTICES) then
        writeln('Maximum of ', MAX_VERTICES, ' boundaries found, extra ignored');
      close(vfile);

      for i := 1 to vertcount do
        for i2 := i+1 to vertcount do
          if vertices[i].tp < vertices[i2].tp
            then swap_vertices(vertices[i], vertices[i2]);

      for i := 1 to vertcount do
        begin
          dx := vertices[i].x - vertices[i].x1;
          if (dx <= 0) then horizontal := 1
            else horizontal := -1;
          dy := vertices[i].y - vertices[i].y1;
          if (dy <= 0) then vertical := 1
            else vertical := -1;

          if (dx > 0) and (dy > 0) (* line, other than hori or vert *)
            then begin
              p4 := 0; (* initial last displacement *)
              j := 0;
              repeat
                m := (abs(dy)+1) / (abs(dx)+1);
                p4t := m*(j+1);
                repeat
                  p1 := j * horizontal + vertices[i].x;
                  p2 := r2i(p4 * vertical + vertices[i].y);
                  show[p2, p1] := 5;
                  if not (in_bounds(p2, MAX_Y) and in_bounds(p1, MAX_X)) then
                    begin
                      write('Invalid coordinates in ', VERTICES_FILE);
                      writeln(', line ', i, ', program halted');
                      halt;
                    end;
                  n[p2, p1] := vertices[i].direction;
                  n_type[p2, p1] := vertices[i].tp; (* assign type *)
                  st_mag[p2, p1, vertices[i].magnitude);
                  p4 := p4 + 1;
                until p4 >= p4t;
                j := j + 1; (* inc x position *)
            end;
        end;
    end;

```

```

        p4 := int(p4t);                                (* keep last value *)
        until j > abs(dx);
    end;

    if (dx = 0) and (dy <> 0) then (* vertical line *)
    begin
        p1 := vertices[i].x; (* x position *)
        p2 := vertices[i].y; (* starting point - y *)
        p3 := vertices[i].y1 + vertical; (* ending point - y *)
        while p2 <> p3 do
        begin
            show[p2,p1] := 3;
            if not (in_bounds(p2,MAX_Y) and in_bounds(p1,MAX_X)) then
            begin
                write('Invalid coordinates in ',VERTICES_FILE);
                writeln(' line ',i,', program halted');
                halt;
            end;
            n[p2,p1] := vertices[i].direction;
            n_type[p2,p1] := vertices[i].tp; (* assign type *)
            st_mag(p2, p1, vertices[i].magnitude);
            p2 := p2 + vertical;
        end;
    end;

    if (dx <> 0) and (dy = 0) then (* horizontal line *)
    begin
        p1 := vertices[i].y; (* y position *)
        p2 := vertices[i].x; (* starting point - x *)
        p3 := vertices[i].x1 + horizontal; (* ending point - x *)
        while p2 <> p3 do
        begin
            show[p1,p2] := 2;
            if not (in_bounds(p1,MAX_Y) and in_bounds(p2,MAX_X)) then
            begin
                write('Invalid coordinates in ',VERTICES_FILE);
                writeln(' line ',i,', program halted');
                halt;
            end;
            n[p1,p2] := vertices[i].direction;
            n_type[p1,p2] := vertices[i].tp; (* assign type *)
            st_mag(p1, p2, vertices[i].magnitude);
            p2 := p2 + horizontal;
        end;
    end;

    end; (* open *)
end; (* find_bound *)

(* this procedure accepts the coordinates of the starting point and
   does interpolating. *)
procedure inter(py, px:integer);

```

```

var i, x, y, px1, py1, search_dir : integer;
    sum_direction, total_dp_cnt : integer;
    hit_edge, all_done : boolean;
    b, a, magnitude : real; (* Cartesian coord *)
begin
    search_dir := -1; (* search upwards *)
    x := px; (* current element position *)
    y := py;

    if n_type[y,x] >= DATA_END then
        begin
            writeln;
            writeln('Starting point defined as boundary - program halted.');
            halt;
        end;

    repeat
        hit_edge := false;
        if x+1 > MAX_X then hit_edge := true;
        (* after loop X will be at left of a boundary *)
        while (not hit_edge) and (n_type[y,x+1] < DATA_END) do
            begin
                x := x + 1;
                if x+1 > MAX_X then hit_edge := true;
            end;
            px1 := x;
            py1 := y;

            repeat
                if (n_type[y,x] = NO_DATA) or (n_type[y,x] = 2) then
                    begin
                        search(y, x);

                        sum_direction := 0; (* interpolation *)
                        total_dp_cnt := 0;
                        b := 0; a := 0; magnitude := 0;

                        if x_balance = 2 then (* if balanced, get values *)
                            begin
                                for i:= 1 to x_dp_cnt do
                                    begin
                                        b := b + sin(x_axis_dp[i].direction*TO_RADIAN);
                                        a := a + cos(x_axis_dp[i].direction*TO_RADIAN);
                                        magnitude := magnitude + x_axis_dp[i].magnitude;
                                    end;
                                total_dp_cnt := total_dp_cnt + x_dp_cnt;
                            end;

                        if y_balance = 2 then (* if balanced, get values *)
                            begin
                                for i:= 1 to y_dp_cnt do
                                    begin
                                        b := b + sin(y_axis_dp[i].direction*TO_RADIAN);

```

```

        a := a + cos(y_axis_dp[i].direction*TO_RADIAN);
        magnitude := magnitude + y_axis_dp[i].magnitude;
    end;
    total_dp_cnt := total_dp_cnt + y_dp_cnt;
end;

if total_dp_cnt > 0 then (* write data point *)
begin
    n[y,x] := r2i(arctan(b/a)*TO_DEGREE);
    if (a<0) and (b<0) then n[y,x] := n[y,x] + 180;
    if (a<0) and (b>0) then n[y,x] := n[y,x] + 180;
    if n[y,x] < 0 then n[y,x] := n[y,x] + 360;
    n_type[y,x] := 2;
    magnitude := magnitude / total_dp_cnt;
    st_mag(y,x,magnitude);
end;
end;
x := x - 1;
until (n_type[y,x] >= DATA_END) or (x < MIN_X);

all_done := false;
x := px1;
y := py1;
if (y+search_dir > MAX_Y) or (y+search_dir < MIN_Y) then
    all_done := true;
while (not all_done) and (n_type[y+search_dir,x] >= DATA_END) do
begin
    x := x - 1;
    if (x < MIN_X) or (n_type[y,x] >= DATA_END)
        then all_done := true;
end;
y := y + search_dir;

if (search_dir < 0) and (all_done)
    then begin
        search_dir := 1; (* reverse direction and search downwards *)
        x := px;
        y := py;
        hit_edge := false;
        if x+1 > MAX_X then hit_edge := true;
        while (not hit_edge) and (n_type[y,x+1] < DATA_END) do
            begin
                x := x + 1;
                if x+1 > MAX_X then hit_edge := true;
            end;
        px1 := x;
        py1 := y;

        all_done := false;
        if (y+search_dir > MAX_Y) or (y+search_dir < MIN_Y) then
            all_done := true;
        while (not all_done) and (n_type[y+search_dir,x] >= DATA_END) do
            begin

```

```

        x := x - 1;
        if (x < MIN_X) or (n_type[y,x] >= DATA_END)
            then all_done := true;
        end;
        y := y + search_dir;
    end;
until all_done;
end; (* inter *)

(* write all values to files *)
procedure write_file;
var fmag, fdir : text;
    i, i2 : integer;
begin
    assign(fmag,OUT_MAG); rewrite(fmag);
    assign(fdir,OUT_DIR); rewrite(fdir);
    writeln(fdir,winfo.uy:5,winfo.ux:5,winfo.ly:5,winfo.lx:5,MAX_Y:5,MAX_X:5);
    writeln(fmag,winfo.uy:5,winfo.ux:5,winfo.ly:5,winfo.lx:5,MAX_Y:5,MAX_X:5);
    for i := MAX_Y downto MIN_Y do
        for i2 := MIN_X to MAX_X do
            begin
                writeln(fdir,n[i,i2]:5,n_type[i,i2]:5);
                writeln(fmag,rd_mag(i,i2):8:2);
            end;
        close(fmag);
        close(fdir);
    end; (* write_file *)

begin (* main program *)
    init;
    find_bound;

    if not open(fse,SE_FILE)
        then begin
            writeln('File not found: ',SE_FILE);
            halt;
        end
    else begin
        while not eof(fse) do
            begin
                (*$i-*) readln(fse,sp_y,sp_x); (*$i+*)
                if ioresult <> 0
                    then begin
                        writeln('Invalid search coordinates in ',SE_FILE);
                        close(fse);
                        halt;
                    end;
                if not (in_bounds(sp_y,MAX_Y) and in_bounds(sp_x,MAX_X))
                    then writeln('Search position out of bounds -- ignored')
                    else inter(sp_y,sp_x);
            end; (* while *)
        end;
    end;
end;

```

```

        dump_mag;
        close(fse);
    end;
    write_file; (* write all values to files *)
end.

```

### C.5.3. GR.FOR Listing

```

$STORAGE:2
$NODEBUG
$NOFLOATCALLS

```

```

    PROGRAM GR

```

c The number of columns must be greater than the number of rows.

```

    DIMENSION X(13),Y(13),CONS(10),LABELS(10),VALUES(13,13)
    INTEGER MAXX, MAXY, UY, UX, LY, LX

```

```

    data x1,y1/0.,0./

```

```

    open(2,file='contour.dat',status='old')
    read(2,'(I2)') nc
    do 70 i=1,10
    read(2,'(F8.2,I1)') cons(i), LABELS(i)
70    continue
    close(2)

```

```

    open(1,file='outmag.dat',status='old')
    read(1,1000) UY, UX, LY, LX, MAXY, MAXX
1000    FORMAT(6I5)
    X2 = MAXX
    Y2 = MAXY
    n = MAXX+1
    NY = MAXY+1
    DX=(X2-X1)/(n-1.)
    DY=(Y2-Y1)/(NY-1.)
    XX=X1
    YY=Y1
    DO 10 I=1,N
    X(I)=XX
    XX=XX+DX
10    continue
    DO 20 I=1,NY
    Y(I)=YY
    YY=YY+DY
20    continue

```

C Read values from data file

```

    DO 30 J=1,NY
    DO 30 I=1,N

```

```

      READ(1,1001) VALUES(I,J)
1001  FORMAT(F5.0)
30    CONTINUE
      CLOSE(1)

c   Scaling factor
      XSCALE=1.0

c   Define plot area
      ideo = 2
      jcl=50
      jc2=350
      jrl=30
      jr2=180
      klr=1
      ilegnd=1
      call qctrdef(modec,klr,klr,klr,ilegnd)

      xorg = x1
      yorg = y1

c   Set graphics mode
      modec = 6
      call qsmode(modec)

c
c   qplot will change the value of ymax, when iopt=1 is used.
c   so we use a dummy ymax value here as input.
c
      ymax2=y2
      iopt=1
      yoverx=1.0
      aspect=1.5

      call qplot(jcl,jc2,jrl,jr2,x1,x2,y1,ymax2,xorg,yorg,
1iopt,yoverx,aspect)
      CALL QCNTOUR(XSCALE,X,Y,VALUES,CONS,LABELS,N,NY,NC,IDEO)

      call qxaxis(x1,x2,2.0,1,-1,0)
      call qyaxis(y1,y2,2.0,1,-1,0)
      call qcmov(0,24)
      read(*,*)
      call qsmode(3)
      END

```

## APPENDIX D

## REFERENCES

KAUF  
KLEINER KLEINER KLEINER KLEINER

## APPENDIX D

### REFERENCES

- Ahlbom, A., Albert, E.N., Fraser-Smith, A.C., Grodzinsky, A.J., Marron, M.T., Martin, A.O., Persinger, M.A., Shelanski, M.L., & Wolpow, E.R. (1987). Biological effects of power line fields, Scientific Advisory Panel Final Report of the New York State Powerlines Project.
- Deno, D.W. (1977). Currents induced in the human body by high voltage transmission line electric field -- measurement and calculation of distribution and dose. IEEE Transactions on Power Apparatus and Systems, 96, 1517-1527.
- Deno, D. W. and Zaffanella, L.E. Electrostatic effects of overhead transmission lines and stations. In Transmission line reference book, 345 kV and above, 1975, Electric Power Research Institute, Palo Alto, California.
- Gardner, F.M. (1966) Phaselock Techniques, New York, Wiley & Sons.
- Kaune, W.T. (1986). Physical interaction of humans and animals with power-frequency Electric and Magnetic fields. In W.E. Feero (Chair), Panel session on biological effects of power frequency electric and magnetic fields IEEE Publication 86TH0139-6-PWR.
- Kirkham, H., Johnston, A.R., Jackson, S., and Sheu, K., (1987). AC and DC electric field meters developed for the U.S Department of Energy, JPL Publication 87-20, Jet Propulsion Laboratory, Pasadena, California.
- Lampe, W., Eriksson, K.A., and Peixoto, C.A.O., (1984). Operating experience of HVDC stations with regard to natural pollution. CIGRE Paper No. 33-01.
- Leeper, E. (1987, April) Specifications for an exploratory ac milligaussmeter. Available from Monitor Industries, Boulder, CO.
- Naito, K., Matsuoka, R., Ito, S., and Morikawa, S. (1988). An investigation of the horizontally mounted insulators for HVDC stations. Paper 88 WM 089-5, presented at the IEEE Power Engineering Society Winter Meeting New York, NY, January 31 -February 5, 1988 (to be published in IEEE Transactions on Power Delivery).

